1 2  9 0

UNIVERSIDADE D
COIMBRA

Mário Pedro da Silva Marques

Monitoring of ripening-derived composition and morphology modifications in *Arbutus unedo* L. fruits, and characterization of vitrified tissues

Dissertação no âmbito do Mestrado em Biodiversidade e Biotecnologia Vegetal,
orientada pelo Doutor Ricardo Manuel Fernandes da Costa
e pelo Professor Doutor Jorge Manuel Pataca Leal Canhoto
e apresentada ao Departamento de Ciências da Vida da Faculdade de Ciências e Tecnologia
da Universidade de Coimbra

Agosto de 2019

Faculdade de Ciências e Tecnologia da Universidade de Coimbra

Monitoring of ripening-derived composition and morphology modifications in *Arbutus unedo* L. fruits, and characterization of vitrified tissues

Mário Pedro da Silva Marques

Dissertação no âmbito do Mestrado em Biodiversidade e Biotecnologia Vegetal, orientada pelo Doutor Ricardo Manuel Fernandes da Costa e Professor Doutor Jorge Manuel Pataca Leal Canhoto e apresentada ao Departamento de Ciências da Vida da Faculdade de Ciências e Tecnologia da Universidade de Coimbra.

Agosto de 2019

UNIVERSIDADE D
COIMBRA

Valeu a pena? Tudo vale a pena
Se a alma não é pequena.

Fernando Pessoa, A Mensagem.

This master thesis was supported by the Project “RENATURE – Valorization of the Natural Endogenous Resources of the Centro Region” (CENTRO-01-0145-FEDER-000007), funded by the Comissão de Coordenação da Região Centro (CCDR-C) and subsidized by the European Regional Developmental Fund (FEDER)

ACKNOWLEDGEMENTS

No fim desta longa jornada académica gostaria de começar por agradecer a todas as pessoas que cruzaram o meu caminho e que de alguma forma contribuíram para a concretização deste projeto, transmitindo força e coragem.

O mais profundo agradecimento só poderia ser em primeiro lugar, aos meus pais, porque sem eles este sonho não teria sido possível! Obrigado Mãe! Obrigado Pai! Vocês foram, são e serão o meu pilar.

Agradeço também aos meus irmãos, Sónia, Carla, Miguel, aos meus tios e toda a família que sempre me acompanhou. Gi, um especial obrigado também a ti.

Seria impossível esquecer-me de vocês os quatro! Obrigado Eduard's, obrigado Lena, obrigado Primo, obrigado Só, por terem sido os meus confidentes, o meu refúgio, por me ouvirem e incentivarem a lutar quando tudo pareceu estar perdido. Apesar de hoje separados, estaremos sempre unidos pelos laços de companheirismo e amizade.

Um especial agradecimento aos meus orientadores, Professor Doutor Jorge Canhoto e o Doutor Ricardo Costa, pela confiança que depositaram em mim, pelas opiniões, pela experiência e conhecimento que me transmitiram, porque foram essenciais para que este trabalho tivesse o corpo que tem agora.

Agradeço também a todos os meus colegas de mestrado e laboratório, por partilharmos juntos momentos de alegria, diversão, e alguns de angústia, e pelos passos que fomos dando em conjunto até concretizarmos agora esta nossa jornada. Obrigado a todos! Um especial obrigado ao João por todo o conhecimento que me transmitiu acerca da cultura *in vitro* do medronheiro e pela preciosa ajuda na obtenção dos cortes histológicos.

Um agradecimento ao projeto ReNATURE (Centro-01-0145-FEDER-000007) e a todos os envolvidos, através do qual me foi facultado o indispensável material para a execução deste trabalho. Um especial agradecimento ao Professor Doutor Luís Baptista de Carvalho (QFM-UC), também envolvido neste projeto, e aos restantes investigadores, do Laboratório de Espetroscopia Vibracional para Bioanálise, por tão bem me receberem e serem sempre tão prestáveis e atenciosos. Em especial, obrigado Ana Lúcia e Adriana por toda a ajuda durante a execução do FTIR.

Agradeço também, à Professora Doutora Maria da Graça de Carvalho do Departamento de Engenharia Química, por nos facultar o uso do HPLC-PDA para o perfil fenólico dos frutos.

Por fim, um sincero agradecimento à Doutora Mónica Zuzarte pelo tempo dispensado comigo na análise histológica através de microscopia de varrimento.

INDEX

FIGURES INDEX

TABLES INDEX

ACRONYM ABBREVIATIONS LIST

ab ep - abaxial epidermis

ABSL - Acetyl Bromide Soluble Lignin

ad ep - adaxial epidermis

AIR - Alcohol Insoluble Residue

ANOVA - Analysis of Variance

ATR - Attenuated Total Reflectance

CH_2 - Methylene group

CH_3 - Methyl group

COOH - Carboxylic acid

COO^- - Carboxylate

CWM - Cell Wall Material

ct - cortex

cu - cuticle

ep - epidermis

FTIR - Fourier transform mid-infrared spectroscopy

G lignin - Guaiacyl phenylpropanoid lignin unit

gr - growth ring

hd - glandular head of the trichome

HPLC-RI - High-Performance Liquid Chromatography coupled to Refractive Index detector

RP-HPLC-PDA - Reversed-Phase High-Performance Liquid Chromatography coupled to Photo Diode Array detector

INT - Intact Biomass

lc - lacunae

LMO - Liquid Medium Organogenesis

mp - mesophyll

mr - midrib

ngt - non-glandular trichome

NH_2 - Amide II

OH - Hydroxyl

pc - peduncle of the glandular trichome

PC - Principal Component

PCA - Principal Component Analysis

pd - periderm

pe - phellem

ph - phloem

pl - phellogen

pp - palisade parenchyma

pt - pith

RG-I - Rhamnogalacturonan I

RG-II - Rhamnogalacturonan II

RI - Refractive index

RT - Retention time

sc - sclerenchyma

SEM - Scanning Electron Microscopy

S lignin - Syringyl phenylpropanoid lignin unit

sp - spongy parenchyma

st - stomata

TFA - Trifluoroacetic acid (CF_3CO_2H)

TSS - Total Soluble Solids

vb - vascular bundle

vc - vascular cambium

xv - xylem vessels

xy - xylem

ABSTRACT

The Ericaceae family comprises a wide number of economic relevant species, such as the plants belonging to the *Rhododendron* and *Vaccinium* genera. Among them, the Mediterranean evergreen shrub *Arbutus unedo* L. outstands from the pomological and ornamental point of view. For an in-depth knowledge of this plant, the ripening-derived composition and morphology was monitored, aiming at identifying factors and events related with fruit maturation. Accordingly, to explore the ripening-derived compositional differences, FTIR spectroscopy was performed, founding chemical variations related to the structural polysaccharides of the cell wall, between immature and fully ripen fruits. Further spectroscopic investigations using the fruits intact biomass, revealed more variations, mainly due to matrix polysaccharides like pectins and hemicelluloses, and cellulose. The process of maturation was also found to be related to an increase of total soluble solids content (˚Brix), and a decrease in fruits acidity. Notwithstanding, the hydrolysis and/or oxidative derived-degradation of structural sugars, results in an extreme decline of fruit firmness, leading to fruit softening, and variations in the polar and equatorial diameters. Furthermore, a preliminary phenolic profile of the fruits was also investigated by RP-HPLC-PDA, and only slight variations of the phenolic compounds were observed during fruit maturation. On the other hand, concerning the vitrification (hyperhydricity) phenomenon that outcomes through the culture of axillary shoots in liquid medium, the cell wall of non-vitrified and vitrified *in vitro* shoots of *A. unedo* was evaluated, comparing leaves and stems. Regarding on the differences in the amounts of cellulose, matrix polysaccharides and lignin, compositional differences were uncovered in leaves and stems from *in vitro* shoots, using FTIR-ATR spectroscopy, acetyl-bromide soluble lignin method and total carbohydrates estimation. Unexpectedly, our results showed higher amounts of lignin in leaves, comparing to stems. Additionally, meticulous information about the *A unedo* anatomy was assessed by light, fluorescence and scanning electron microscopy, making comparisons between leaves and stems of non-vitrified and vitrified *in vitro* shoots, and tissues from a strawberry tree. Comparing with normal leaves, the vitrified ones showed to have a delicate and disorganized epidermis, with many abnormal stomata present in the abaxial surface. The mesophyll has wide lacunar spaces, and lack of palisade parenchyma. Concerning vitrified stems, the major differences relied on the the broad-spaced cortical cells. In the end, the present dissertation contributed to better characterization of this economic relevant species

but largely unknown, not only for a better understanding on the fruits ripening events, but also by helping to unveil the chemical and anatomy-related factors of the vitrified phenotype.

Keywords: cell wall; leaves; lignin; polysaccharides; stems.

RESUMO

A família Ericaceae é constituida por várias espécies economicamente importantes, tais como as pertencentes ao género *Rhododendron* and *Vaccinium*. Entre elas, o arbusto mediterrânico *Arbutus unedo* L. destaca-se do ponto de vista pomológico e ornamental. Para aprofundar o conhecimento sobre esta espécie, analisaram-se as alterações morfológicas e composicionais que ocorrem na ontogenia dos frutos, com o objetivo de identificar fatores e eventos relacionados com a sua maturação. Deste modo, os resultados das análises espetroscópicas revelaram alterações ao nível dos polissacarídeos estruturais da parede celular, entre frutos imaturos e maduros. Investigações espetroscópicas adicionais com biomassa intacta dos frutos, revelaram que existem variações composicionais, principalmente decorrentes de polissacarídeos da matriz, tais como as pectinas e hemicelulloses, e também celulose. No decorrer da maturação verificou-se também um aumento no teor de sólidos solúveis totais (˚Brix), e um decréscimo na acidez dos frutos. Por outro lado, a degradação de açúcares estruturais que advém da hidrólise e/ou do processo oxidativo, resulta num decréscimo acentuado da firmeza dos frutos, que leva ao seu amolecimento, e também a variações do seu diâmetro polar e equatorial. Além disso, traçou-se um perfil fenólico preliminar dos frutos recorrendo a RP-HPLC-PDA, concluindo-se que ocorrem poucas variações desses compostos durante a maturação. Por sua vez, no que diz respeito à vitrificação de tecidos, decorrente da sua cultura em meio líquido, investigou-se a parede celular de folhas e caules vitrificados, comparando depois com tecidos não vitrificados. As diferenças nos teores de polissacarídeos e lenhina, entre material *in vitro* não vitrificado e vitrificado, foram reveladas através de FTIR-ATR, lenhina solúvel em brometo de acetil e quantificação de carbohidratos totais. Contrariamente ao que poderia ser expectável e ao que é normalmente indicado na literatura, os resultados obtidos mostraram, de forma consistente, um teor de lenhina mais elevado nas folhas do que nos caules. Por outro lado, através de microscopia ótica de campo claro, fluorescência e varrimento, revelaram-se informações meticulosas sobre a anatomia de *A. unedo*, através de comparações entre folhas e caules de um arbusto e de material *in vitro*, vitrificado e não vitrificado. Em comparação com folhas normais, as vitrificadas evidenciaram uma epiderme desorganizada e fina, com imensos complexos estomáticos anormais presentes na página inferior da folha. O mesófilo apresentava grandes espaços lacunares e não existia um parênquima em paliçada bem definido. No que diz respeito aos caules, as principais diferenças estão relacionadas com as células corticais muito espaçadas devido à presença de pronunciados

espaços intercelulares. A presente dissertação contribui para um melhor conhecimento desta espécie economicamente importante, mas pouco conhecida, não só pelo melhor conhecimento do processo de maturação dos frutos, mas também por ajudar a perceber as alterações morfológicas e químicas num fenótipo vitrificado.

Palavras-chave: caules; folhas; lenhina; parede celular; polissacarídeos.

1. Introduction

1.1 Theorical framework

In a world facing many economic and environmental challenges, the demand for the valorization of renewable and endogenous resources is increasing. Henceforward, the typical Mediterranean shrub *Arbutus unedo* (strawberry tree), has revealed to be a potential source of phytochemical compounds, with a wide range of interest for food and the pharmaceutical industries. Moreover, sustainable ways of exploring its economic potentialities have been developed, for example by means of micropropagation of selected plants with desired characteristics, avoiding the dilapidation of the natural sources of *A. unedo*.

Micropropagation assays of *A. unedo*, carried out at the Laboratory of Plant Biotechnology of the Centre for Functional Ecology of the Department of Life Sciences of the University of Coimbra, revealed that the shoot proliferation in liquid medium, is a quick-efficient method to the propagation of this species. However, quite often, the obtained plants exhibit vitrification-derived abnormalities that slow down the rates of micropropagation in this species, and its ability to survive during the acclimatization period (Martins *et al*., 2018). The vitrification-derived phenotype was described for the first time by Quoirin and Lepoivre, (1977), in *Prunus* sp. leaves, and since then several studies have been carried out (Kevers *et al*., 1984; Ziv, 1991; Apostolo and Llorente, 2000; Jausoro *et al*., 2010; van des Dries *et al*., 2013; de Klerk *et al*., 2017). However, in account of the fragile nature of vitrified plants, that is mostly correlated with altered polysaccharide and lignin structures, few studies have focused on the cell wall, and on the chemical-derived differences between normal and vitrified plants. Henceforward, arises the need to investigate some aspects related to this problem, using *A. unedo* as a model plant.

In turn, the fruits of strawberry tree have been proved to have many applications, such as in tanning manufactures by its richness in tannins, production of honey, jellies and spirits, and recently a rising interest of small farmers in exploring its commercial potential as a pomological species. Several studies have focused their attention in the chemical characterization of fruits, concerning the phenolic compounds, polysaccharides, vitamins, fatty acids, minerals and proteins (Alarcão-e-Silva *et al*., 2001; Oliveira *et al*., 2011; Ruiz-Rodriguez *et al*., 2011; Guerreiro *et al*., 2013; Miguel *et al*., 2014; Salem *et al*., 2018). However, none of these works have focused on the variation of these compounds during maturation in fruits of *A. unedo*, and lack information about consistent and independent ripening stages. In account of these facts, arises the need for in-depth studies about the maturation of *A. unedo* fruits, and the related chemical differences.

1.2 *Arbutus unedo* L.

1.2.1 Taxonomy

The genus *Arbutus* is part of the class Magnoliopsida, order Ericales, and family Ericaceae (Hileman *et al*., 2001). The genus *Arbutus* includes about twenty species spread out over the Mediterranean Region, Macaronesia Islands and North America (Heywood, 1993). However, the strawberry tree or madrone in English, and *medronheiro* or *ervedeiro* in Portuguese, as it is commonly known, revealed to be the most interesting species from an economic point of view (Gomes *et al*., 2010). Concerning the phylogeny, the subfamily Arbutoideae is related to the subfamily Vaccinioideae, which includes relevant pomological species such as the blueberries (*Vaccinium corymbosum* L.). Additionally, the Arbutoideae members are also related to the subfamily Ericoideae, that in turn comprises important ornamental species such as *Rhododendron ponticum* L. (Gomes, 2011).

1.2.2 Geographic distribution

The strawberry tree is frequently found in various regions around the Mediterranean Sea (Fig. 1), such as the Iberian Peninsula, in the South of France, Italy or Croatia. This plant is also present in several islands of the Mediterranean Basin (Balearic Islands, Sardinia, Corsica) (Torres *et al*., 2002; Prada and Arizpe, 2008). In addition to its circum-Mediterranean distribution, *A. unedo* arises also in Atlantic areas particularly in Portugal and on the western shores of Ireland and France (Fig. 1), and further South in the Macaronesia Region, especially in the Canary Islands (Torres *et al*., 2002).

Strawberry tree is rarely dominant, despite its importance in Mediterranean forests (Quevedo *et al*., 2013). In Portugal, this spontaneous evergreen shrub, occurs in fragmented populations North to Tagus River, by virtue of intensive forestation campaigns and lower temperatures in those regions. On the contrary, in the South it occupies largest areas, with special focus on the populations of Serra do Caldeirão, Monchique granitic soils, and limestone shores in Serra da Arrábida (Pedro, 1994; Silva, 2007; Gomes, 2011). Strawberry tree forest-like, known as *medronhal*, occupied in 2005 about 0,5% of Portuguese forest, that corresponds to approximately 1500 hectares (Godinho-Ferreira *et al*., 2005).

Figure 1 Geographic distribution of *A. unedo* in the Mediterranean Sea and Atlantic Shores. (Oliveira, 2010).

1.2.3 Botanic characterization

Depending on the environmental conditions, strawberry tree could reach three meters high being classified as a shrub, or instead considered a tree reaching twelve meters high (Prada and Arizpe, 2008). The root system of this species is very superficial, and the bark of its stem is fissured, grey or red-brownish (Castroviejo *et al*., 1993; Pedro, 1994). The leaves are petiolate and oblong-lanceolated, with serrate margins, and a coriaceous surface. The young leaves have a light green color and the older ones are olivaceous green, with the first appearing mostly in springtime exhibiting a shape that seems like laurel leaves, a feature inherited from their *laurissilva* ancestors (Fig. 2B; Martins, 2012). In the mesophyll of the adaxial face there are one or two regular palisade layers, whereas the spongy parenchyma in the abaxial face is full of large air spaces, the lacunae (Gomes, 2011).

This species has a long reproductive cycle that extends for more than one year. Therefore, flowers and fruits occur simultaneously in the same plant (Martins, 2012). The peculiar hermaphrodite flowers of strawberry tree have five petals, gathered into an urceolated corolla. Either white, slightly pink or green colored, the flowers appear in outstanding terminal

panicles in a maximum of forty per inflorescence, during the autumn and spring (Fig. 2B; Castroviejo *et al*., 1993; González, 2007).

The edible berries of strawberry tree are covered by numerous and distinctive conic structures, the papillae (Fig. 2A and 2C; Castroviejo *et al*., 1993; González, 2007). When completely ripen, fruits acquire a dark red color and a yellow pulp, each one carrying several little brown seeds dispersed by endozoochoric birds (Castroviejo *et al*., 1993; Piotto *et al*., 2001; Martins, 2012).

Figure 2. Different aspects related to the strawberry tree. (A) Fruiting strawberry tree. (B) Flowering strawberry tree. (C) Two different aspects of strawberry tree fruits, the cleaned green and the brownish ones.

1.2.4 Ecologic aspects

The strawberry tree is a drought tolerant species that thrives in poor, thin, acidic soils where other species, particularly trees or shrubs, can hardly grow (Piotto *et al*., 2001). The species has the capacity to promote seed dispersal out of wildfires season, and also sprouts easily after fire damage (Konstantinidis *et al*., 2006). Furthermore, it promotes faunistic diversity and detains soil deterioration (Gomes and Canhoto, 2009), henceforth proving its ecologic importance and the use of this species in reforestation programs in South Europe (Gomes *et al*., 2010).

According to its edaphic features, *A. unedo* is highly adaptable to vary types of soil, either growing in alkaline, acidic or silicic rich soils (Takrouni and Boussaid, 2010). This

evergreen shrub can be found since sea level until 1200m high (Blanco *et al*., 2005), growing especially in sclerophyllous shrublands (Celikel *et al*., 2008; Molina *et al*., 2011). Considered part of the Mediterranean macchia, *A. unedo* coexists with both Pinaceae, and Fagaceae species like *Quercus ilex* L. and *Quercus suber* L. (Molina *et al*., 2011), and other typical dryness resisting plants like *Myrtus communis* L., *Olea europaea* L., and *Erica arborea* L. (Takrouni and Boussaid, 2010), as well as *Cistus* sp. , *Spartium* sp. and *Ulex* sp. bushes (Godinho-Ferreira *et al*., 2005).

1.2.5 Economic relevance and ethnobotany

Human consumption of strawberry tree fruits is widely spread around the Mediterranean basin (Molina *et al*., 2011). The phenolic composition and sweet taste of fruits when mature, provide unique features to the distilled spirit, known as *aguardente de medronho* or *medronheira*. This traditional liquor is produced in small factories or as a homemade product for own consumption. However, the production of this alcoholic beverage is the most economic value of the strawberry tree in Portugal (Gomes *et al*., 2010; Botelho *et al*., 2015). Nevertheless, the pollen and nectar of this species make this an important melliferous species for honey production, with bitter taste and ancient therapeutic uses (Tuberoso *et al*., 2010). Fruits instead, could be converted in marmalades and jellies, then conserving and consume this fruit after its harvest season (Molina *et al*., 2011). Concerning tanning manufactures, mostly the leaves and the cork, have been employed given the abundance of phenolic compounds like tannins, responsible for leather softening (Gomes *et al*., 2010).

Despite the proven value and the wide range of applicability of this plant, *A. unedo* has been considered a NUC (Neglected or Underutilized Crop) species (Rui-Rodríguez *et al*., 2011). Nonetheless, many assays have been focused on the importance of this plant to the food and pharmaceutical industries, as well its ornamental and ecologic relevance (Celikel *et al*., 2008).

1.3 Plant biotechnology and *in vitro* culture

1.3.1 Conventional methods and *in vitro* techniques

Conventional methods like grafting and cutting are frequently used in the propagation of *A. unedo* (Prada and Arizpe, 2008). Seed germination is another advantageous conventional

method since it promotes genetic diversity, whereas seed dormancy comprises the principal barrier to the application of this method successfully in this species (Gomes, 2011; Vásquez *et al*., 2014).

Micropropagation is a technique of *in vitro* culture, alternative to conventional methods like grafting or cutting, and consists in the obtention of individuals genetically equal to the mother plant (George *et al*., 2008). This method of *in vitro* multiplication has other advantages. Continuous production is assured, it is set the acquisition of phenotypes with interesting characteristics from the agroeconomic point of view, and also turns out possible the propagation of recalcitrant plants to the conventional methods (Chawla, 2009; Canhoto, 2010; Gomes, 2011).

Regarding *in vitro* techniques used in *A. unedo* propagation, shoot proliferation has been applied (Gomes and Canhoto, 2009). This approach consists in the development of preexistent shoot meristems (apical or axillary), into shoots demanding no induction of new meristematic zones, being the simplest way of micropropagation. Axillary shoot proliferation is most efficient when these meristematic tissues are out of inhibitory influence of the apical meristem, and regenerated plants are expected to be genetically uniform between them and equal to the mother plant (Canhoto, 2010).

Organogenesis is another technique that has been applied on *A. unedo* propagation (Martins *et al*., 2018). It consists on the induction of new meristems, resulting in the formation of an unipolar structure such as radicular or stem primordia. Organogenesis could lead directly to the formation of adventitious meristems or, more frequently lead indirectly to callus formation from which meristems arise (Canhoto, 2010). Different factors can influence regeneration through organogenesis, being the most important the balance between auxins and cytokinins present in the culture medium, since these phytohormones are known to control cell growth and elongation (Moubayidin *et al*., 2009). However, liquid medium organogenesis of *A. unedo* shoots leads frequently to vitrification of stems and leaves (Martins *et al*., 2018).

1.3.2 Vitrification

Different techniques of tissue culture have been applied for vegetative propagation, plant breeding and to protect plants from pathogens in agriculture (Canhoto, 2010). However, tissue culture in liquid and solid media based on gelrite, could lead to the accumulation of water in the apoplast, causing vitrification that has serious consequences, reducing the quality and multiplication rates of plants (van des Dries *et al*., 2013). Vitrification was described for the

first time in leaves of *Prunus* sp., that were underdeveloped and had a succulent appearance (Quoirin and Lepoivre, 1977).The phenomenon of vitrification has been defined based on morphological alterations easily visualized, like atypical growth, and hyperhydrated and brittle aspect (Ziv, 1991). Although, this condition also known as hyperhydricity, translucency, succulency or glassiness, is a broader anomaly arising in micropropagated plants that includes previous physiological and biochemical events, before visual symptoms could be observed (Ziv, 1991; Kevers *et al*., 1984).

Vitrified shoots exhibit common symptoms like thick, brittle, curled and crystalline leaves (Saher *et al*., 2005). Additionally, leaves lack epicuticular waxes, the mesophyll has a disorganized palisade parenchyma, while the spongy parenchyma has large lacunae (Picolli *et al*., 2001; Jausoro *et al*., 2010). In turn, stomatic cells have irregular orientation of cellulose microfibrils and deficiencies in sodium/potassium ratios, causing the absence of response to stimulus like carbon dioxide, abscisic acid, luminosity, hypertonic solutions and water stress (Apóstolo and Llorente, 2000; Canhoto, 2010). Moreover, guard cells are convex instead oval-shaped with delicate cell walls marked by the presence of high amounts of callose, and deficient chloroplasts with faulty grana and stroma. Concerning the stems, there is no sclerenchyma cells, the vascular bundles are disorganized, and the cortex area has broad spaces between cells, thus leading to reduced diameter (Ziv, 1991).

Since cellulose and lignin control the cell wall turgor pressure, the increase in transpiration and capacity for water absorption is highly related to conformational and structure of the cell wall polymers (Canhoto, 2010). Several enzymes had been related with vitrification (Kevers *et al*., 1984), and among them phenylalanine ammonia-lyase (PAL) revealed to be present in much lower concentrations in vitreous tissues, causing reduced synthesis of phenolic compounds like lignin and so its lack in cell walls. Likewise, membrane peroxidases and hydroxy cinnamic CoA-ligase, were found to have reduced activities in vitreous shoots (Ziv, 1991). In addition to lignin, cell wall polysaccharides (e.g. cellulose) are apparently converted into amino acids by glutamate dehydrogenase, explaining the reduced rigidity of vitrified cell walls (Kevers *et al*., 1984). The control of some factors like the relative humidity in the *in vitro* air, the choice of the gelling agent, the type of explant, cytokinins in the culture medium, and the accumulation of ethylene had been reported as some of the causes leading to vitrification (de Klerk *et al*., 2017).

The latest mechanism proposed, reports that vitrified plants are not able to balance the absorption of water with its evapotranspiration, causing water accumulation in the apoplast (Fig. 3; van den Dries *et al*., 2013). According to these authors the apoplast of non-vitrified

plants contains 15% water, while in hyperhydric plants this value raises to 85%. Henceforward, accumulation of water in the apoplast leads to slow diffusion of gases in the water, and subsequently hypoxia appears as an undesirable consequence, what brings several anatomical and physiological consequences for vitrified plants. Several assays have explored the anatomical, molecular, and biochemical features of hyperhydric plants, however the true mechanisms leading to vitrification dilemma remains to be solved (de Klerk *et al*., 2017).

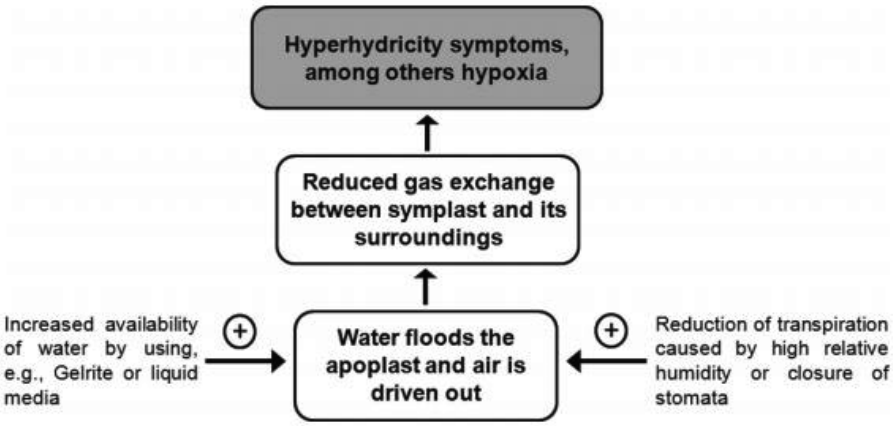

Figure 3. The role of water present in the apoplast leading to vitrification. (van den Dries *et al*., 2013).

1.4 Phytochemistry of the fruits

The fruits of *A. unedo* have been assayed in the last years to fulfill the entire chemical profile of this species, and numerous bioactive compounds have been reported, such as vitamins, minerals, polyunsaturated fatty acids, phenolic compounds (Fig. 4) and carbohydrates, justifying so its medicinal properties and nutritive potential (Alarcão-e-Silva *et al*., 2001; Barros *et al*., 2010; Ruiz-Rodriguez *et al*., 2011; Salem *et al*., 2018).

1.4.1 Phenolic compounds

Phenolic compounds are the largest and most heterogeneous group of secondary metabolites founded in plants, including thousands of known molecules, separated in a dozen families according to their chemical structure (Harnly *et al*., 2007; Garcia-Salas *et al*., 2010). This group of molecules has critical roles in plant development, providing protection against

UV radiation, signaling in the immunity response against pathogens and protection after wounding (Khodami *et al*., 2013).

This polymorphic group of molecules is mainly synthesized through the shikimic acid pathway that ends in the synthesis of the aromatic amino acids tyrosine, phenylalanine, and tryptophan, the precursors of phenolic compounds of very important signaling and structural molecules such as auxins and lignin, respectively (Taiz *et al*., 2015).

Phenolic compounds could be grouped in different families according to their structure: phenols and benzoquinones (C_6); phenolic acids (C_6-C_1), acetophenones, phenylacetic acid (C_6-C_2), cinnamic acids, phenylpropene, coumarins, chromones (C_6-C_3), naphthoquinones (C_6-C_4), xanthones (C_6-C_1-C_6), stilbenes, anthraquinones (C_6-C_2-C_6), flavonoids (C_6-C_3-C_6), lignans, neolignans ($[C_6$-$C_2]_2$), tannins ($[C_6$-$C_1]_n$) and lignins ($[C_6$-$C_3]_n$) (Harnly *et al*., 2007; Garcia-Salas *et al*., 2010). Regardless of the diversity of these metabolites, they can be used as botanical fingerprints in result of their restricted distribution to specific taxa (Harnly *et al*., 2007).

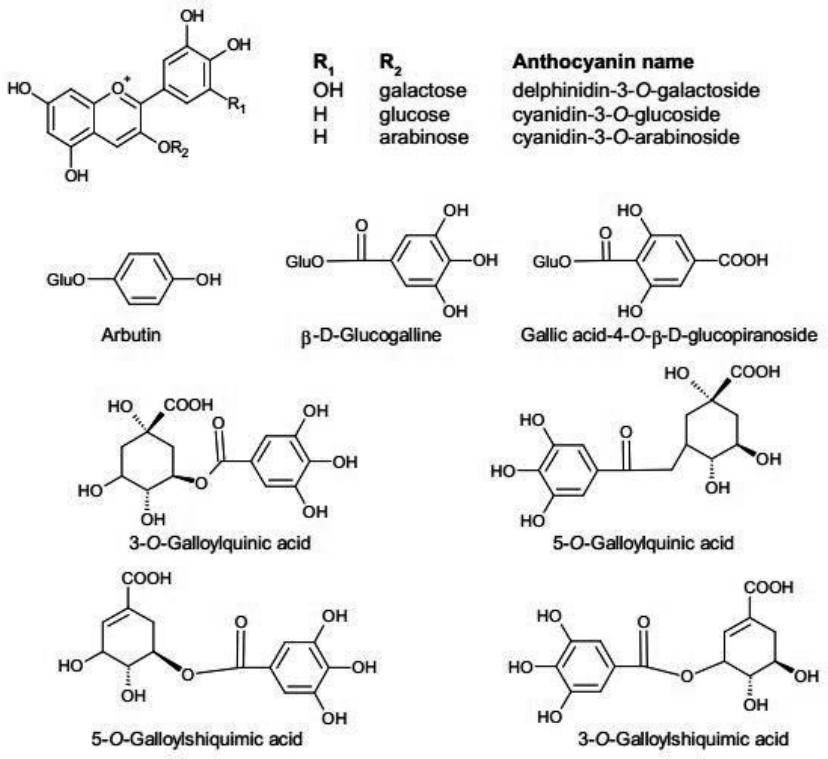

Figure 4. Chemical structures of some phenolic compounds, including anthocyanins, identified in *A. unedo* fruits collected in Italy (Miguel *et al*., 2014).

1.5 The plant cell wall

The plant cell wall has a complex dynamic architecture. This extracellular strong structure is composed by cellulose inserted in a matrix of non-cellulosic polysaccharides, namely hemicelluloses and pectins (Fig. 5; Srivastava *et al*., 2017). Frequently, these carbohydrates form covalent and non-covalent linkages with molecules composed by aromatic and aliphatic domains like lignin, cutin, suberin and highly glycosylated proteins (Harris and Stone, 2009; Taiz *et al*., 2015; Srivastava *et al*., 2017).

The cell wall controls cell growth and development by determining its size and shape. Moreover, broader biological functions may depend on the cell wall such as support to xylem vessels, frontier controlling the uptake or runoff of molecules in and out the cell, the development of turgor pressure, and control of cell expansion. Furthermore, several signaling pathways depend on cell wall components, including somatic embryogenesis in which arabinogalactan proteins have been referred as playing a central role, or the response to biotic stresses when enzymes degrade polysaccharides into smaller sugars that act as messengers for the plant immunity system (Taiz *et al*., 2015).

In respect to chemical composition and morphology, cell walls can differ between species, genotype, tissue and developmental stage (Srivastava *et al*., 2017). Despite great variation, cell walls are classified as primary and secondary, according to their chemical composition, structure and cell developmental phase in which they are built up (Taiz *et al*., 2015).

The primary cell wall has a simple and slim arrangement, around cells that are actively growing and developing (Taiz *et al*., 2015; Srivastava *et al*., 2017). Afterwards, the cell concludes its growth stage, no more cellulose microfibrils will be added to the wall (Fry, 2010; Srivastava *et al*., 2017). Not frequent but possible, is the insertion of other polymers, such as lignin and cutin, in specific cell types but it won't change its category as primary cell walls (Harris and Stone, 2009; Fry, 2010). Likewise, the width of primary walls is also dependent on the developmental stage, hence parenchyma walls are particularly thin, whereas collenchyma cells have thicker primary walls (Harris and Stone 2009; Taiz *et al*., 2015).

Secondary cell walls are formed internally to the primary walls after cell elongation stops (Taiz *et al*., 2015). This structure tends to be present in specific cell types, such as sclerenchyma and xylem and confers resistance to the cells, being generally thicker than primary walls (Lee *et al*., 2011; Srivastava *et al*., 2017). In secondary walls, cellulose deposition occurs in different orientations producing a three-layered (S_1, S_2, S_3) structure (Srivastava *et*

al., 2017). Moreover, this wall type has low or no pectin, while xylans and distinct hemicelluloses assortments are particularly abundant, therefore the polysaccharides present in this layer are different than the ones found in primary walls (Knox, 2008; Srivastava *et al*., 2017).

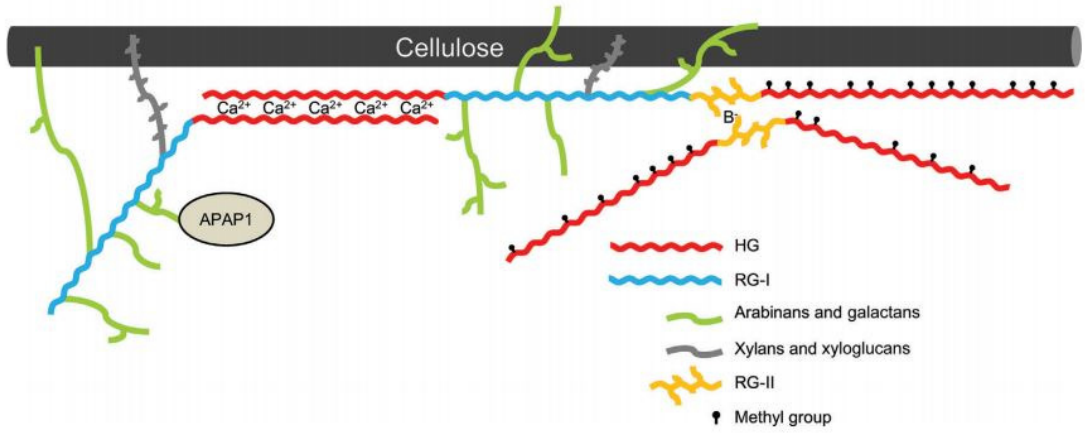

Figure 5. Hypothetical interactions and organization of the cellulose and matrix polysaccharides (pectin and hemicelluloses) in the primary cell walls of plants (Saffer, 2018).

1.5.1 Cellulose

Cellulose is a polysaccharide widely distributed, not just among higher plants but also present in non-vascular plants, algae, oomycetes and several bacteria (Kumar and Turner, 2015). This polymer is composed by β-D-glucopyranose residues linked by glyosidic bonds, forming linear and heavy chains of β-1,4-glucan. The cellulose microfibrils form a semi-crystalline structure that is interrupted by amorphous gaps in its structure at each 150 to 300 nm (Harris and Stone, 2009). These fibrils could be stabilized by Van der Walls interactions and hydrogen bonds. The microfibrillar phase of cell wall, can carry up until 25 000 glucose residues, extends until 13 µm length, with diameters of 3 nm in primary walls that could range until 23 nm in aggregated macrofibrils of secondary walls (Harris and Stone, 2009; Taiz *et al*., 2015).The dry mass of primary cell walls is constituted by 20% cellulose whereas in the lignified secondary walls, this value can reach 40%, representing almost half of the wall's dry mass (Harris and Stone, 2009; Fry, 2010).Synthesis of cellulose microfibrils, occurs at the plasma membrane, being carried out by highly complex proteins called rosette terminal complexes formed by subunits cellulose synthase A (Kumar and Turner, 2015; Taiz *et al*., 2015).

1.5.2 Pectins

Pectins are matrix polysaccharides present in the primary walls of spermatophyte (seed plants) with exception for grasses and commelinide monocotyledons (Harris and Stone, 2009). Pectic polysaccharides are highly soluble, strong and flexible forming an extensive gel structure in the middle lamella where they perform important adhesive functions between adjacent cells (Srivastava *et al*., 2017). The wide network of cross-linkages promoted by these sugars, allows the cellulose and hemicelluloses to merge in together (Fig. 5; Taiz *et al*., 2015).

Pectins are mainly built up of monomeric units like galacturonic acids and neutral sugars (rhamnose, galactose and arabinose), and so could be classified according to three principal domains, the homogalacturonan (HG), the rhamnogalacturonan I (RGI) and the rhamnogalacturonan II (RGII) (Fig. 5; Taiz *et al*., 2015; Srivastava *et al*., 2017). However, according to Harris and Stone (2009), and Fry (2010) there is a minor fourth domain composed by xylogalacturonans.

Homogalacturonan is a widely pectic sugar expressed among plants, representing more than 65% within the pectins, consisting of a linear chain of α-1,4-linked galacturonic acid (Mohnen, 2008). This homopolymer is frequently ornamented by methyl-esterification and acetylation (Fig. 5; Harris and Stone, 2009). Also abundant is the RGI domain that represents around 20-35% of pectins and has a repeated structure based on disaccharides (α-1,4-D-GalA-α-1,2-L-Rha), contrary to other pectins that have galacturonan backbones (Mohnen, 2008; Harholt *et al*., 2010). The scaffold of RGI is frequently adorned by rhamnose residues, arabinan, galactan, arabinogalactan, and acetyl groups (Fig. 5; Mohnen, 2008; Srivastava *et al*., 2017). The RGII represents around 10% of pectic sugars and its structure has less variation between different species. Consists of a linear chain composed by eight 1,4-linked α-D-GalA residues or even more, which have attached until twelve types of oligosaccharides cross-linked by 20 to 22 different ways (Harholt *et al*., 2010). Xylogalacturonan domains consist of an homogalacturonan backbone with β-linked xylose attached to the *O*-3 or *O*-4 positions (Mhonen, 2008; Harris and Stone, 2009; Harholt *et al*., 2010).

1.5.3 Hemicelluloses

The Hemicelluloses consist of a group of carbohydrates found in both primary and secondary walls, comprising structures of β-1,4-linked glucose, xylose and mannose, all sharing identical structures with the same equatorial disposition at C_1 and C_4 (Scheller and Ulskov,

2010; Srivastava *et al*., 2017). These polysaccharides are known as cross-linking glucans and can form a core with cellulose trough hydrogen bonds. Complex and diverse, these matrix polysaccharides show a high range of substitution patterns in the backbones namely on the xyloglucan, xylan, and mannan residues (Lee *et al*., 2011; Zhang *et al*., 2012).

Xyloglucan is an ubiquitous hemicellulose among vascular and non-vascular plants, and it is found in high amounts in the primary walls of dicots (20-25%) with exception for monocots (1-5%) (Scheller and Ulskov, 2010). Xyloglucan consist of a β-1,4 glucan polymer with linked xylose residues, that in turn can link other residues like galactose or fucose, depending on the taxonomic group (Taiz *et al*., 2015). For instance, xylans consist of a backbone of xylose residues linked in β-1,4 position, usually decorated with glucuronosyl and methyl-glucuronosyl groups. This type of pattern substitution gives rise to glucuronoxylans, abundant in secondary walls of dicots (20-25%) and in the primary walls of grasses (20%). In order, arabinoxylans and glucuronoarabinoxylans (GAX) are hemicelluloses characterized by arabinose linked to the xylan backbone (Scheller and Ulskov, 2010; Taiz *et al*., 2015). Other important hemicellulosic polymers are mannans and glucomannans, despite less abundant in cell walls, they consist of β-1,4 backbones mainly constituted by mannose, such as mannans frequently found in seeds, non-vascular plants and ferns (Scheller and Ulskov, 2010). The mixed-linkage glucans (MLG) are hemicelulloses well known in grasses, however they are not present in dicots cell walls. (Scheller and Ulskov, 2010).

1.5.4 Lignin

Lignin is a polyphenolic compound with heavy molecular weight and complex organization, produced by the phenylalanine-tyrosine pathway in higher plants (Fig. 6; Liu *et al*., 2018). This polymer is highly recalcitrant to deconstruction and gives strength for plant stems, preventing them to break or flexing, and contributing for plants to grow higher and develop multiple structures. Due to its hydrophobic nature, lignin limits water evaporation or penetration, being important in plant resistance to drought and salt stress (Taiz *et al*., 2015). Moreover, lignin has been found to increase its synthesis in infected tissues, being important in disease resistance, since its complex structure constitute an obstacle for the enzymes and toxins produced by pathogens (Bonawitz and Chapple, 2010). The wood of vascular plants is particularly impregnated by lignin mostly in secondary walls of specific cells and tissues, like sclerenchyma, Casparian strips in the endoderm and xylem vessels (Bonawitz and Chapple, 2010; Liu *et al*., 2018).

Lignin biosynthesis begins with the synthesis of the constituting monomers in the cytosol, known as monolignols, such as *p*-hydroxyphenyl (H), guaiacyl (G) and syringyl (S), which in turn had origin in the *p*-coumaryl, coniferyl and sinapyl alcohols. These molecules are formed after a sequence of deaminations, hydroxylations, methylations and reductions (Fig. 6; Liu *et al*., 2018). Moreover, other small molecules like hydroxycinnamic acids and ferulate monolignols could be inserted in the lignin scaffold, even though in small portions (Zhao, 2016; Liu *et al*., 2018). Afterall, the monolignols in the cytosol are driven to the secondary cell wall by the ABC transporters, and finally they are polymerized in complex lignin molecules, by peroxidases and laccases (Fig. 6). Several studies have been pointing that after monolignol synthesis certain steps of lignin biosynthesis are related to the primary wall and middle lamella (Taiz *et al*., 2015).

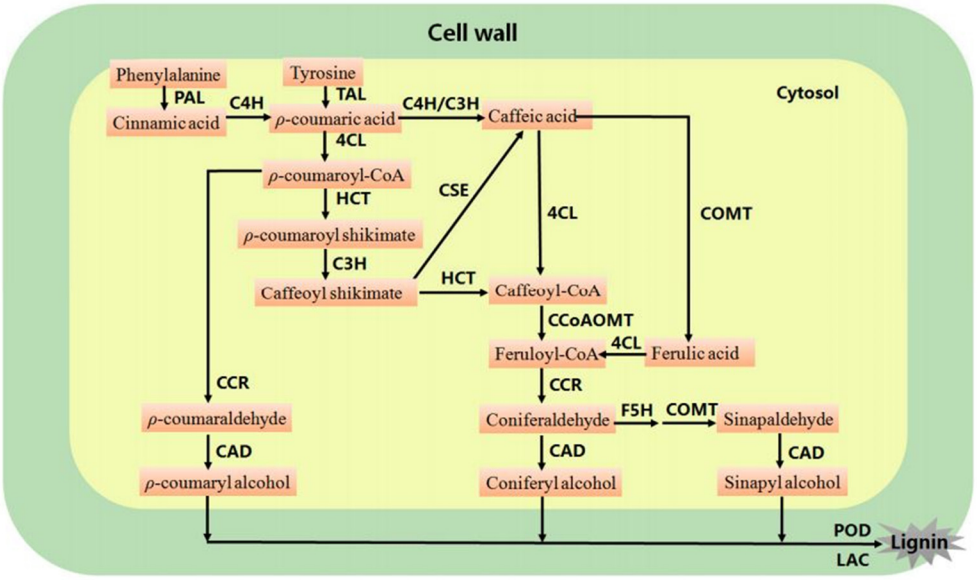

Figure 6. General biosynthetic pathway for lignin (Liu *et al*., 2018).

1.6 Dissertation objectives

Concerning the hyperhydricity affecting the plants propagated through liquid medium, the present work aims to unveil many vitrification-derived anatomic and compositional differences, by means of comparison between vitrified tissues with normal tissues. For this purpose, various sophisticated techniques will be applied, such as FTIR-ATR spectroscopy, ABSL lignin, and anatomical studies using light, fluorescence and SEM microscopy.

Regarding fruits, to contribute for an in-depth knowledge of their maturation, the present dissertation will monitor the ripening-derived morphology and compositional differences

across four distinct ripening stages, green, yellow, orange and red. To explore the entire events and factors related with the maturation of the fruits, several preliminary parameters here assayed, such as the ˚Brix, acidity, ˚Brix/acid ratio, firmness, water content, weight and size variations, have been previously explored by other authors. However, until now, sophisticated and more reliable techniques, that could be applied for the quality control of the fruits, have been neglected. Henceforward, these preliminary parameters will be complemented with FTIR spectroscopy, here performed to provide a broad image of compositional differences in intact and cell wall biomasses of fruits during maturation.

At the end, the present dissertation will contribute, not just to the improvement of the exploration of this plant in fruit production, and its industrial application for the development of derived-manufactured products with assured quality, but also to its entire economic and ecologic valorization, thus contributing to take out the strawberry tree from the list of Neglected and Underutilized Crops (NUC) species (www.nuscommunity.org).

2. Materials and Methods

2.1 Plant material

In all the assays plants from the genotype C1 previously established *in vitro*, through axillary shoot proliferation, were cultured in both solid and liquid media. Leaves and stems of an *A. unedo* tree growing in a greenhouse were also included. Fruits were collected at a location in Pampilhosa da Serra, close to Signo Samo village, on Lenda da Beira, aguardente de medronho Unipessoal Lda strawberry-tree orchard (40.0291055, -7.9238143; Fig. 7). The orchard is composed of rocky soils, arranged from north to southeast in a successively series of terraces and all the plants there, were obtained from seeds.

Figure 7. Location of the Lenda da Beira strawberry tree orchard next to Signo Samo village.

2.2 Ripening-derived quality and morphology parameters

Fruits were collected at Lenda da Beira orchard, transported to the laboratory in freezer containers and sampled (3 trees × 4 ripening stages × 5 fruit replicates). In the same day, the fruits were submitted to different evaluation processes by the order described beneath.

2.2.1 Fresh and dry weight - water content

Each sampled fresh fruit was weighed (mg) using a digital balance (ABJ 80-4NM, KERN & Sohn GmbH). Then, the fruits were freeze-dried by an excess of 5 days ensuring its

complete dryness. By the end of this period, fruits were weighed again (mg) in order to measure their dry weight. Between those different measurement points other morphologic quality parameters were assayed, as described below. The following equation was used to calculate the water content in the fresh fruits:

$$W_c = \frac{(F_w - D_w)}{F_w} \times 100\%$$

where W_c is the fresh fruit water content expressed as means of percentage (%); F_w is the fresh weight of each sampled fruit (mg); and D_w is the dry weight of each sampled fruit (mg).

2.2.2 Polar and equatorial diameter

The fresh fruits (3 trees × 4 ripening stages × 5 fruit replicates) were measured in order to obtain their polar and equatorial diameters (mm) using a digital caliper.

2.2.3 Firmness measurement

The same sampled fruits used to measure the polar and equatorial diameters, were submitted to a firmness test, using an hand-held tester (Fruit Hardness Tester FR-5120). The test was performed by compressing the fruits against the Fruit Hardness Tester accessory. The maximum force was recorded, by the moment that fruit started to be smashed, and expressed as Newtons (N) (Chea *et al*., 2019).

2.3 Ripening-derived quality and chemical parameters

After the collection, the fruits were kept at -80 ˚C until further analyses were carried out, and then pooled (3 trees × 4 ripening stages × 7 fruit replicates) for total soluble solids (°Brix) determination and acidity analysis.

2.3.1 Total soluble solids (°Brix) determination

Following the procedures described by Castrejón *et al*. (2008), using a mortar and a pestle, the pooled fruits were crushed until enough juice was obtained to perform

measurements. The °Brix was measured directly with the obtained juice using an operating manual digital refractometer (KERN optics, ORD 85BM, °Brix 0-85%, RI 1.3330-1.5100).

2.3.2 Acidity analysis

Concerning the acidity, the juice obtained as described above (section 2.3.1), was diluted and homogenized 1/100 (w/v) in deionized water. The acidity level of fruits (%) was measured using a hand-held (Atago Easy-ACID F5) set to blueberries, a typical Ericaceae fruit.

2.3.3 °Brix /acid ratio

The obtained values for °Brix (%) and acidity (%) were used to calculate the sugar/acid ratio, using the following equation:

$$Sugar/Acid\ ratio = \frac{Brix}{Acidity}$$

2.4 *In vitro* propagation of *A. unedo*

2.4.1 Shoot proliferation in solid medium

Single explants were cultured in test tubes containing Anderson's gellified medium. The medium was prepared by adding the components, as following described. First, in an Erlenmeyer containing deionized water it was added the sucrose (30 g/L) as carbon source and the cytokinin BAP (8.8 μM) included to promote shoot formation. The pH of the medium (6.5-6.7) was adjusted using HCl and KOH solutions of three different concentrations (1.0 M, 0.1 M and 0.01 M). After the pH adjustment, the agar (7 g/L) was added as gelling agent, heating while stirring at 150-200 ˚C until it is completely dissolved. The test tubes (15 x 2.2 cm) were filled with 10 mL of medium, capped and placed in an autoclave at 121 ˚C for 60 min. Cultures were kept in a growth chamber, at 25 ˚C, under a photoperiod of 16 hours light and 8 hours dark. This plant material was subcultured after approximately two months in the same conditions.

2.4.2 Liquid medium organogenesis (LMO)

Vitrified shoots were obtained through LMO following the procedures described by Martins *et al*. (2018). In order to promote vitrification, using nodal segments, selected shoots cultured in solid medium had their leaves cut and freed from the influence of the apical meristem. Each nodal segment (4±1 cm) had approximately 4 phytomeres. Five nodal segments were placed per Erlenmeyer flask (100 mL maximum capacity), each one containing 25 mL of Anderson's liquid medium. The medium preparation and composition were the same followed for gellified medium (section 2.4.1), with the exception that here the agar was not included. The flasks were placed in an orbital shaker (100 rpm) inside a growth chamber at 25 ˚C, under a photoperiod of 16 hours light and 8 hours dark. After two months of culture, the vitrified shoots were collected to further analysis.

2.5 Cell wall biomass preparation

A procedure based on a protocol reported by da Costa *et al*. (2015), was performed to produce purified cell wall, the alcohol insoluble residue (AIR), used in subsequent analyses. Freeze-dried fruits of the four ripening stages (Fig. 8A), were ground to powder using an analytical mill. An average of 5 g of plant intact ground material was weighed to 50 mL plastic centrifuge tubes. Subsequently, 10 mL of ethanol 70% (v/v) was added and left first for 12 h (overnight) in a shaking incubator (110 rpm) at room temperature 22 ˚C. Then twice more for 30min. in a shaking incubator set at 22 ºC/120 rpm with 10 mL of ethanol 70% (v/v). Twice for 30min. in a shaking incubator set at 22 ºC/120 rpm, with 10 mL of chloroform/methanol (1:1) (v/v), followed by 30 min. of incubation at 22 ˚C and 110 rpm. Lastly, twice with 10 mL of acetone, for 30 min., at 22 ˚C/110 rpm. Between each step of fruits biomass washing, the ground biomass was collected by centrifugation at 22 ˚C/2500 rpm for 10 min. and the supernatants were discarded by decantation. In the end, the alcohol insoluble residue (AIR) was left in an oven set to 35 °C, for an excess of approximately 72 h, to ensure its complete dryness. A similar procedure was adopted for the preparation of AIR from the *in vitro* shoots (Fig. 8B, 8C and 8D), following separation in leaves and stems and subsequently lyophilization. Leaves and stems of an *A. unedo* tree growing in a greenhouse, were collected and also submitted to the same treatment.

Additionally, following the first washing step with ethanol 70%, the tubes were centrifuged at 22 ˚C/2500 rpm for 10 min. and the supernatant ethanol extract was collected to

further analysis on RP-HPLC-PDA (Reversed-Phase High-Performance Liquid Chromatography coupled to Photo Diode Array detector).

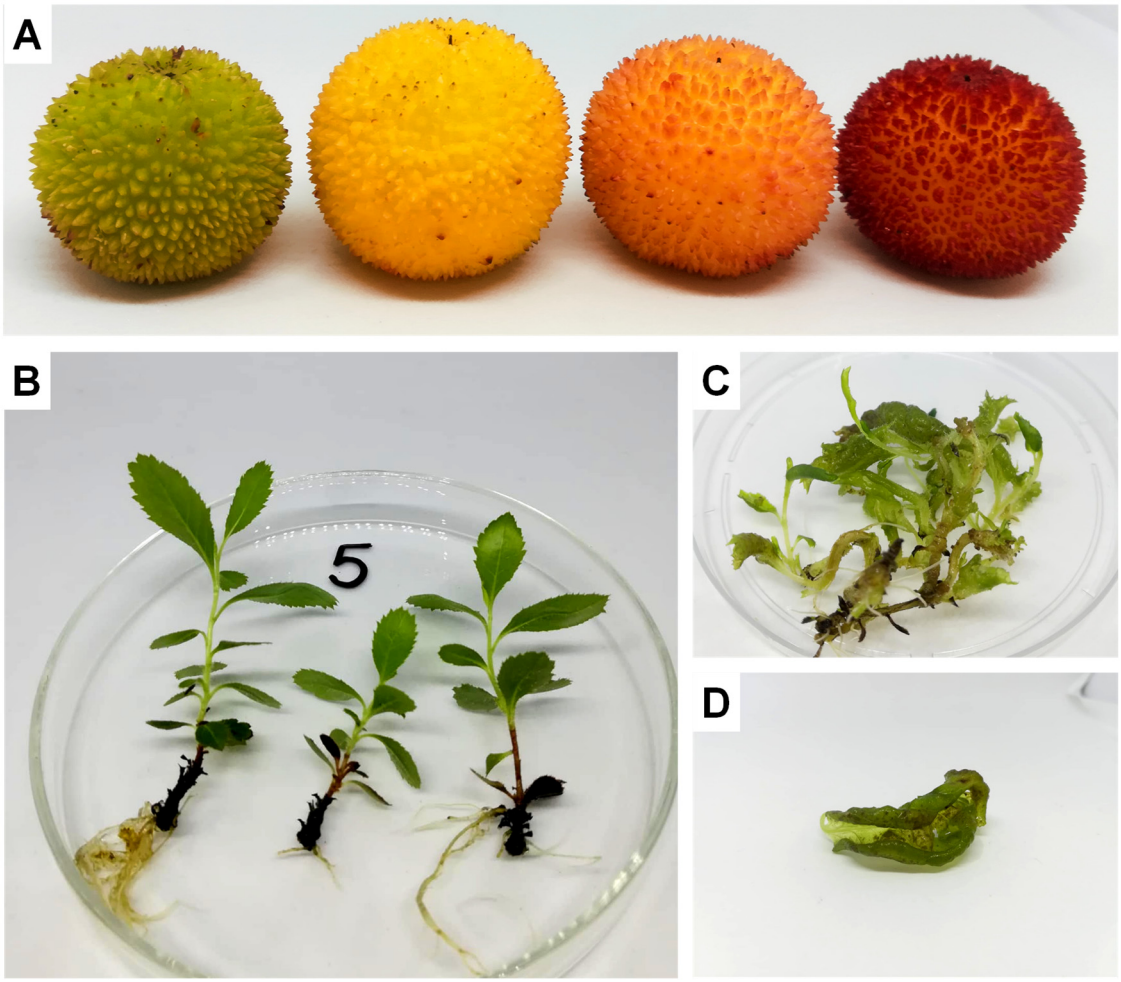

Figure 8. Fruits and shoots used in the experiments. (A) The four ripening stages considered, green, yellow, orange and red. (B) Non-vitrified shoots cultured in solid medium. (C) Vitrified shoots cultured in liquid medium. (D) Detail of a glassy and curled vitrified leaf.

2.6 Qualitative analysis of the phenolic profile of fruits by RP-HPLC-PDA

A 70% (v/v) aqueous ethanol extract derived of the first organic solvent washing, from the fruit's raw biomass, was transferred to 1mL Eppendorf tubes and stored at -80 ˚C. Following the procedures of Guimarães *et al*. (2013) and modified as described below, the aqueous ethanol extract was used to assess the ripening-derived phenolic profile of the fruits by Reversed-Phase High-Performance Liquid Chromatography coupled to a Photo Diode Array detector (RP-HPLC-PDA).

The ethanolic extract was concentrated under vacuum at 62 ˚C/1010 rpm for 48 h, re-dissolved in 1 mL of methanol, centrifuged at 22 ˚C/1000 rpm for 5 min., and submitted to

ultrasounds to remove the particles interference. The extract was then filtered before injection, through a disposable syringe (Labbox, SYRI-005-100) equipped with a disposable filter disk (CHROMAFIL, Xtra PTFE-45/25 0.45 μm), and 80 μL were placed into HPLC vials for analysis. Separation was performed using a Shimadzu Apparatus coupled to a Kromasil C_{18} (octadecyl) reverse-phase column (Sigma-Aldrich, Merck 250 mm × 4.6 mm, 5 μm, 100 Å), thermostatted at 35 ˚C. The mobile phase employed was a mixture of methanol and water, acidified with 0.1% of formic acid and the injection volume was 15 μL. A low pressure gradient was employed as follows from 5% to 60% for 30 min., rising from 60% to 100% for 5 min., and finally descending from 100% to 5% for 10 min., at a rate flow of 0.5 mL/min. Double detection was carried out by the PDA detector, at 280 nm and 340 nm. The examination of phenolic compounds across different ripening stages was assessed by a comparison of their spectra and retention times.

2.7 Biomass examination by Fourier-transformed infrared spectroscopy

The FTIR-ATR (Fourier-transformed infrared spectroscopy–attenuated total reflection) spectra were acquired in duplicate, in the mid-infrared range of 4.000-600 cm^{-1}, consisting of an average over 32 scans at a resolution of 4 cm^{-1}, using a Bruker Optics Vertex 70 FTIR spectrometer purged by CO_2-free dry air and a Bruker Platinum ATR single reflection diamond accessory. Without further preparation, approximately 10 mg of AIR of each fruit sample was placed in the ATR crystal. The sample was clamped against the ATR diamond window using the anvil of the ATR accessory, ensuring that the crystal remained completely covered by the sample, leading to an optimal reflectance spectra acquisition. Since FTIR is a non-destructive technique, between measurements each sample was recovered using a spatula. After each spectrum acquisition, the contact areas in the ATR accessory were cleaned with isopropyl alcohol, to prevent mistakes or contaminations between spectra acquisition. Likewise, every six consecutive measurements, spectra were corrected for background absorbance by subtraction of the spectrum of the empty ATR crystal, improving the acquired spectra and the absence of noise.

Using Opus 7.2 spectroscopy software spectra were corrected applying H_2O and CO_2 compensations, and smoothed according to the Savitzky-Golay algorithm (window: 17 pt). Afterwards, each spectrum was converted into an individual text file, containing the spectral two-dimensional Cartesian coordinates (x,y) in two separate columns. Matrices containing the raw data were created using EXCEL and the underlying relationships between the spectra were

investigated in the spectral fingerprint region (1900-800 cm^{-1}) using an R-based data analysis platform (Chong *et al*., 2018).

2.8 H_2SO_4 hydrolysis

In vitro shoots (1 genotype × 2 tissues × 2 culture mediums), aside with plant material from an adult tree (1 genotype × 2 tissues), were acid-hydrolyzed as described by Sluiter *et al*. (2012) and Saeman *et al*. (1963). Approximately 10-15 mg of the previously prepared AIR, was weighed into 10 mL Pyrex glass tubes and fitted with polypropylene caps. In a Hotte, 100 µL of 72% (w/w) H_2SO_4 was added, the tubes were capped and then placed in a water bath at 30 °C for 1 h. The tubes were mixed using a vortex mixer every 15 min. until complete the period of incubation. Then, 2.5 mL of deionized water was added to achieve a dilution of 4% of the samples under hydrolysis. The phase separation was eliminated by vortex mixing the tubes. The sealed samples were then placed in an autoclave at 121 °C for 20 min. and left inside until the temperature dropped to 70-60 °C to assure complete hydrolysis. At room temperature, 400 mg of $CaCO_3$ were transferred to each tube and immediately capped. The tubes under fizzing were gently mixed by inversion and left standing for 10 min., and then the pH (6.5-7) of random samples was measured using a strip. Tubes were centrifuged 22 ˚C/2000 rpm for 10 min., to obtain a particulate-free supernatant that was transferred to Eppendorf tubes until further analysis.

2.9 Acetyl bromide soluble lignin measurement (ABSL)

Acetyl bromide lignin was determined in duplicate for all the *A. unedo* samples (1 genotype × 2 tissues × 2 plant replicates), following the general procedures reported by Foster *et al*. (2010) and Fukushima and Hatfield (2004), with some modifications as described in da Costa *et al*. (2014). Approximately 10 mg of the previously prepared AIR was weighed into 10 mL Pyrex glass tubes fitted with polypropylene caps. For lignin solubilization, 500 µL of freshly prepared 21% (v/v) acetyl bromide solution in glacial acetic acid was added to the samples. The capped tubes were then placed in a water bath set at 50 °C for 2 h. By the end of this period, the tubes were mixed using a vortex mixer every 20 min. up to a total incubation period of 3 h. Sequentially, tubes were cooled on ice, and 2000 µL of 2 M NaOH were added to dilute the previous digestion. To assure the decomposition of polybromide ions, 350 µl of 0.5 M hydroxylamine hydrochloride were added to each tube (Monties, 1989). Further, the

tubes were mixed using a vortex mixer, and the final volume was adjusted to 10 mL with glacial acetic acid. An additional mixing was carried out, and the tubes were centrifuged at 22 ˚C/1500 rpm for 10 min. to obtain a particulate-free supernatant. Afterwards, 200 µL of each sample were transferred to UV transparent 96-well plates (greiner bio-one, UV-STAR MICROPLATE, 96-WELL, COC, F-BOTTOM), and the absorbance was measured using a plate reader (Perkin Elmer, Multimode Plate Reader 2300 EnSpire) coupled to the EnSpire Manager 4.1 software. A duplicated negative control containing no AIR was included to set the absorbance baseline at 280 nm.

The following equation was used to calculate the percentages of lignin in the cell wall biomass samples as dry weight:

$$ABLS = \frac{A_{280}}{SAC \times PL} \times \frac{V_R}{W_S} \times 100\%$$

where *ABSL* is the acetyl bromide soluble lignin percentage content (%); A_{280} is the absorption at 280 nm; (*SAC*) is the specific absorption coefficient of 23.077 g^{-1} L cm^{-1} Fukushima and Kerley (2011); *PL* is the 0.4889 cm^{-1} pathlength determined for the 96-well microplates with a volume of 200 µL per well used during the analysis; V_R is the reaction volume (mL) and W_s is the sample weight (mg).

2.10 Phenol-sulfuric acid method for total carbohydrates estimation

Using a 96-well microplate (greiner bio-one, UV-STAR MICROPLATE, 96-WELL, COC, F-BOTTOM), the total carbohydrates content was determined (in duplicate) as glucose equivalents by the phenol-sulfuric acid method as described by Dubois *et al*. (1956) and Masuko *et al*. (2005). Thus 100 µL of each sample previously acid-hydrolyzed (section 2.8) was added to the bottom of the test tube to avoid splashing, aside with 100 µL of 5.0% (w/v) phenol and 500 µL of 18 M H_2SO_4. The test tubes were softly agitated to homogenize the mixtures, and left incubating for 20 min. at room temperature. Afterwards, 250 µL of each reaction mixture was transferred in duplicate to a 96-well microplate, and the absorbance was measured at 490 nm using a plate reader (Perkin Elmer, Multimode Plate Reader 2300 EnSpire) coupled to the EnSpire Manager 4.1 software. A duplicate negative control, containing no AIR, was included to set the absorbance baseline at 490 nm. A standard curve was constructed based

in solutions of glucose of different concentrations, to calculate the total carbohydrate content as glucose equivalents for each sample cell wall extract.

The following equation was used to calculate the percentages of total carbohydrate content in the cell wall as glucose equivalents:

$$TC = \frac{SCgleq \times V_R}{W_S} \times 100\%$$

where *TC* is the total carbohydrate percentage in the cell wall as glucose equivalents (%); *SCgleq* is the sample concentration as glucose equivalents (mg/mL); V_R is the reaction volume (mL) and W_s is the sample weight (mg).

2.11 Light and fluorescence microscopy

Selected samples from an *A. unedo* tree (1 genotype × 2 tissues) and *in vitro* shoots (1 genotype × 2 tissues × 2 culture mediums) were fixed in a solution of 4 % PFA (paraformaldehyde), according to Ursache *et al*. (2018). Samples were placed in PFA for 48 h to ensure the complete conservation of tissues structure. By the end of this period, samples were washed twice (2 × 15 min.) in PBS 0.1 M. Specimens were dehydrated in an ascendant series of ethanol as following described: 30% (v/v) for 15 min.; 50% (v/v) for 15 min.; 70% (v/v) for 15 min.; 80% (v/v) for 15 min.; 90% (v/v) for 15 min.; 95% (v/v) for 15 min., and finally twice at 100% (v/v) for 30 min.

After dehydration, specimens were included in Spurr resin (Spurr, 1969), as following described: 10 ml of 100 % (v/v) ethanol : 5 ml of resin, for an excess of 48 h; 5 ml of 100 % (v/v) ethanol : 5 ml of resin, for 2 h; 5 ml of 100 % (v/v) ethanol : 10 ml of resin, for 2 h, and finally in 10 ml of pure resin overnight. The samples were placed in a rubber mold and kept at 60 ˚C for 24 h. The blocks were removed from the mold and cross-sectioned (1 µm thick) in a ultramicrotome (LKB Ultrotome III). Then, the cross sections were transferred to drops of deionized water over a glass microscope slide and kept overnight at 60 ˚C.

Sections were stained with a toluidine blue solution 1% (aqueous solution of toluidine blue, azur II 1% and sodium borate 1%; Hall, 1978) for general staining and with ruthenium red solution 0.01%, for pectic polysaccharides, as described by Ursache *et al*. (2018) and McFarlane *et al*. (2014). After 30 min. staining, the microscope slides were washed to remove the stain and observed using a Light microscope (Nikon Eclipse E400) and photographs were

collected with Nikon Digital Sight DS-U1 and processed with the software Act-2U. For fluorescence microscopy, cross-sections were stained with calcofluor white solution 0.1% as described by Ursache *et al*. (2018), and immediately observed using a microscope (Leica DM4000B), photographs were collected with a coupled camera (Leica DFC295).

2.12 Scanning electron microscopy (SEM)

For SEM analysis, selected samples from an adult *A. unedo* tree (1 genotype × 2 tissues), and *in vitro* shoots (1 genotype × 2 culture mediums × 2 tissues) were submitted to scanning electron microscopy. Samples were segmented in small pieces, placed on carbon stickers above metallic stubs, and observed without further preparations, under vaccum-freezed conditions, at 10.0 Kv, using a scanning electron microscope (flex SEM 1000, HITACHI).

2.13 Statistical analysis

The GraphPad Prism 6, version 6.01 was used to analyse the present data. Values are expressed as mean ± SD. Statistical analysis was performed by one-way and two-way analysis of variance (ANOVA) followed by a Tukey´s test. Differences were considered significant at $P<0.05$.

3. Results and Discussion

3.1 Ripening-derived quality, chemical and morphology parameters

3.1.1 Total soluble solids (˚Brix)

The ripening-derived alterations in fruits are accompanied by many morphologic and chemical changes such as flavor, smell, color and texture. Nowadays consumers have also in account food safety and nutritional value (Guerreiro *et al*., 2013; Airianah *et al*., 2016). The total soluble solids content in fruits, known as ˚Brix, is an easy and quick method to evaluate the maturation stage. However, despite this index mostly being used to assess the soluble sugars, also other molecules, like lipids or proteins should be present in the moisture.

As expected, the ˚Brix was different between the various developmental stages of strawberry tree fruits. The ˚Brix was 19.52˚ (ranging from 15.88˚ to 21.56˚) at the green ripening stage, 21.09˚ (ranging from 20.02˚ to 22.66˚) for the yellows, 21.92˚ (ranging from 19.18˚ to 23.62˚) at the orange stage, and 24.47˚ (ranging from 23.88˚ to 25.26˚) at the red ripening stage (Table 1). ANOVA revealed that the ripening stage is the main factor mostly contributing to the variation in the ˚Brix values ($\eta^2 = 0.50$). Box-and-whisker plots show that total soluble solids content increases along maturation and all the ripening stages of the fruit are significantly different, with exception for the yellow stage that revealed to be an intermediate stage between green and orange based on this chemical parameter (Fig. 9A).

The total soluble solids (TSS) in strawberry tree fruits have been assessed by several authors either as means of percentage or Brix degrees. Celikel *et al*. (2008) mentioned that TSS ranged from 15˚ to 30˚, while Sulusoglu *et al*. (2011) reported values for TSS percentages ranging between 16.50% and 31.68% whereas Vidrih *et al*. (2013) pointed 21.05˚ in fruits from Croatia. Also. In Portugal some authors had presented data about this parameter. Thus Cavaco (2007) reported 22.71˚ in red ripen fruits, similarly to what was found by Guerreiro *et al*. (2013) that measured 22 ˚Brix. Moreover, according to the work presented by Fonseca (2014) a range of 14.73˚ to 30.13˚ was reported for different locations and distinct maturation stages along all harvest season (September-December), relating the upcoming of lower temperatures and rainy weather with the tendency for the increase of the TSS. The data from our analyses are not considerably different from what was obtained by other authors with a range that can vary between 15.88˚ and 25.26˚. In the future, it would be interesting to compare different genotypes of *A. unedo* to detect differences and select those displaying ˚Brix values more interesting for the consumers. The fact that most of the material in the field is of seed origin, these data are difficult to obtain.

Table 1. Ripening-derived quality, chemical and morphology parameters. Values are expressed as mean ± standard deviation for the four ripening stages at three different trees.

	Green	Yellow	Orange	Red
		°Brix		
Tree A	21.12 ± 0.25	20.58 ± 0.15	23.62 ± 0.28	25.26 ± 0.30
Tree B	15.88 ± 0.04	20.02 ± 0.20	19.18 ± 0.16	23.88 ± 0.36
Tree C	21.56 ± 0.13	22.66 ± 0.37	22.96 ± 0.60	24.28 ± 0.04
Mean	19.52 ± 3.16	21.09 ± 1.39	21.92 ± 2.40	24.47 ± 0.71
		Acidity (%)		
Tree A	2.36 ± 0.05	0.98 ± 0.01	1.03 ± 0.04	1.02 ± 0.01
Tree B	2.55 ± 0.03	0.96 ± 0.00	1.03 ± 0.01	1.15 ± 0.02
Tree C	2.33 ± 0.01	1.11 ± 0.03	1.12 ± 0.02	0.95 ± 0.03
Mean	2.41 ± 0.12	1.02 ± 0.08	1.06 ± 0.05	1.04 ± 0.10
		Brix/acid ratio		
Tree A	8.96 ± 0.17	9.24 ± 0.06	22.86 ± 0.74	24.67 ± 0.30
Tree B	6.23 ± 0.08	20.89 ± 0.14	18.63 ± 0.36	20.78 ± 0.28
Tree C	4.98 ± 2.74	20.36 ± 0.79	20.54 ± 0.69	25.63 ± 0.81
Mean	6.72 ± 2.04	16.83 ± 6.58	20.68 ± 2.12	23.69 ± 2.58
		Fresh weight (g)		
Tree A	4.22 ± 0.96	6.20 ± 1.06	4.89 ± 0.44	5.83 ± 0.76
Tree B	4.31 ± 0.56	7.31 ± 0.92	6.37 ± 0.82	4.87 ± 1.42
Tree C	3.68 ± 0.38	5.05 ± 0.41	5.64 ± 1.16	5.34 ± 0.98
Mean	4.07 ± 0.34	6.19 ± 1.13	5.63 ± 0.74	5.35 ± 0.48
		Dry weight (g)		
Tree A	1.53 ± 0.31	2.01 ± 0.35	1.69 ± 0.14	2.11 ± 0.29
Tree B	1.30 ± 0.16	2.21 ± 0.34	1.89 ± 0.20	1.68 ± 0.53
Tree C	1.22 ± 0.16	1.67 ± 0.13	1.83 ± 0.33	1.73 ± 0.30
Mean	1.35 ± 0.16	1.96 ± 0.27	1.80 ± 0.10	1.84 ± 0.23
		Water content (%)		
Tree A	63.66 ± 1.21	67.49 ± 2.99	65.43 ± 1.17	63.84 ± 2.79
Tree B	69.81 ± 0.88	69.76 ± 1.84	70.29 ± 1.11	65.80 ± 2.38
Tree C	66.88 ± 0.96	66.94 ± 0.79	67.51 ± 1.43	67.42 ± 1.45
Mean	66.78 ± 3.07	68.06 ± 1.50	67.74 ± 2.44	65.69 ± 1.79
		Firmness (N)		
Tree A	74.04 ± 17.37	64.58 ± 8.96	12.00 ± 5.69	2.82 ± 1.23
Tree B	89.60 ± 9.18	43.14 ± 18.51	6.52 ± 2.08	0.82 ± 0.62
Tree C	110.90 ± 12.51	103.20 ± 11.11	35.64 ± 11.69	7.40 ± 2.77
Mean	91.51 ± 18.50	70.31 ± 30.44	18.05 ± 15.48	3.68 ± 3.37
		Polar diameter (mm)		
Tree A	17.60 ± 1.21	20.06 ± 1.37	18.42 ± 0.81	19.12 ± 0.85
Tree B	20.06 ± 1.09	21.54 ± 0.82	21.12 ± 0.88	17.68 ± 1.64
Tree C	16.78 ± 1.32	19.12 ± 0.43	20.12 ± 1.72	19.44 ± 1.67
Mean	18.15 ± 1.71	20.24 ± 1.22	19.89 ± 1.37	18.75 ± 0.94
		Equatorial diameter (mm)		
Tree A	20.32 ± 1.79	23.40 ± 1.47	21.46 ± 0.55	22.86 ± 1.75
Tree B	20.36 ± 1.37	24.56 ± 1.22	23.96 ± 1.32	21.06 ± 2.74
Tree C	19.64 ± 0.69	21.88 ± 1.11	22.84 ± 1.27	21.66 ± 1.12
Mean	20.11 ± 0.40	23.28 ± 1.34	22.75 ± 1.25	21.86 ± 0.92

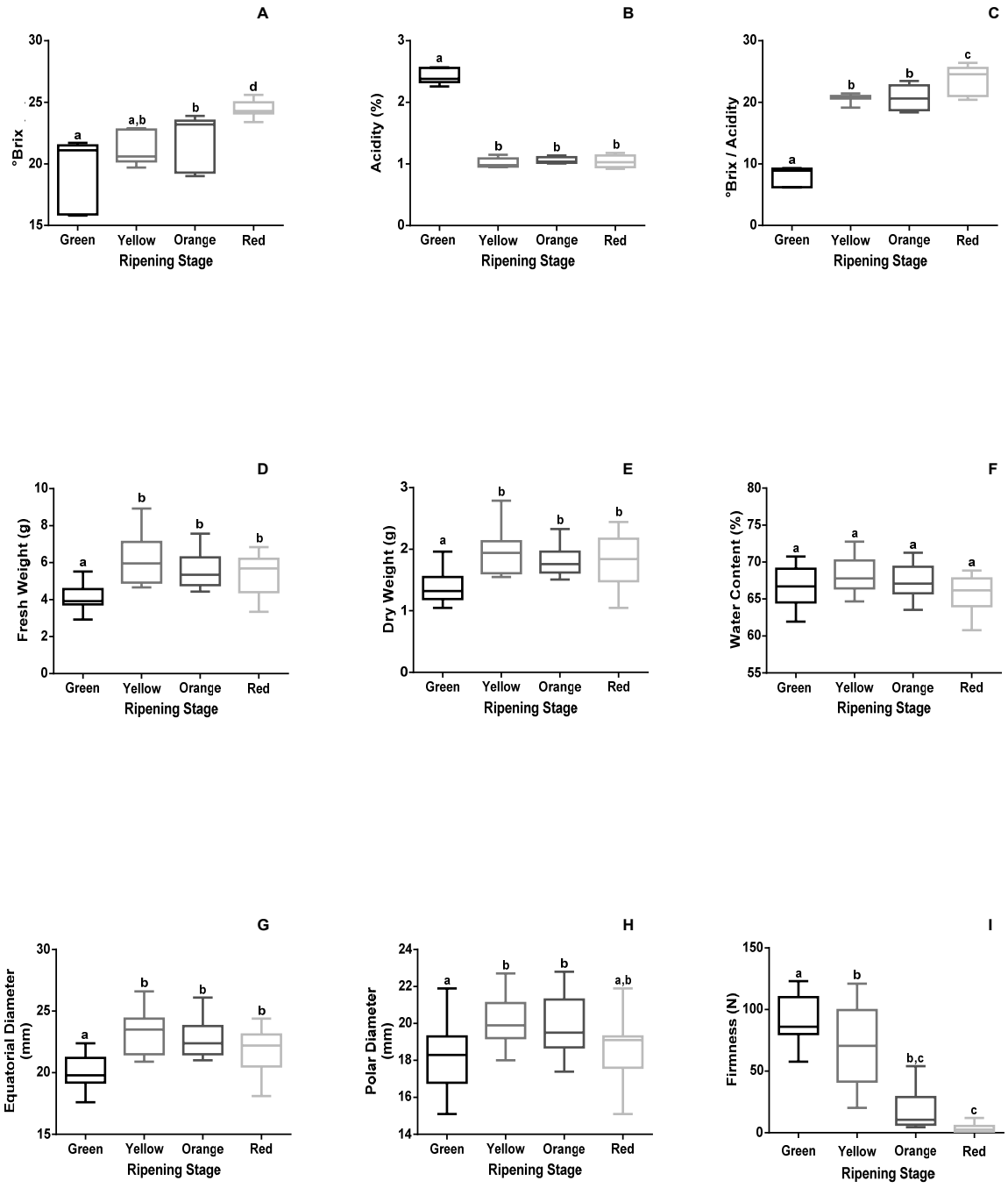

Figure 9. Distribution of values of the ripening-derived quality, chemical and morphology parameters. N = 60 (3 × 4 × 5), five fruits of each ripening stage among the three selected trees. Means were statistically compared using one-way ANOVA followed by a Tukey's test (different superscript letters indicate significant differences at $P<0.05$).

3.1.2 Acidity

The content of ascorbic acid through the four ripening stages, showed a reduction from green fruits (ranging from 2.33% to 2.55%) to the red ones (ranging from 0.95% to 1.15%) (Table 1). According to the Tukey test significant differences were found only between green fruits and the following ripening stages (P<0.001), while the yellow, orange and red fruits present similar percentage of ascorbic acid and show little variation across these ripening stages (Fig. 9B). Maturation revealed to be the main source of variation, $\eta^2 = 0.98$. Likewise, Alarcão-e-Silva *et al*. (2001) also announced a strong decrease in this vitamin, comparing unripen fruits with fully ripen fruits. Since Vitamin C is an organic acid, metabolic mechanisms may explain the conversion of this organic acid in polysaccharides, and the decline over maturation in contrast to the increase of TSS (Castrejón *et al*., 2008; Sun *et al*., 2013; Chea *et al*., 2019). Moreover, other explanations have been reported to explain the acidity variation in *A. unedo* fruits, pointing sunlight to cause a decrease on the acidity, while rain could cause its increase (Fonseca, 2014).

3.1.3 ˚Brix /acid ratio

Flavor of fruits is highly determined by the proportion of TSS and organic acids which, makes the ˚Brix/acid ratio an essential tool to decide the best time point to harvest (Jayasena and Cameron, 2008). In green immature fruits this ratio was 6.72 (ranging from 4.9 to 8.9), while in the yellow fruits 16.8 (ranging from 9.2 to 20.9), 20.7 (ranging from 18.6 to 22.9) in the orange fruits, and 23.7 (ranging from 20.8 to 25.6) in the red fruits (Table 1). ANOVA showed that maturation is the main factor ($\eta^2 = 0.93$) affecting the ˚Brix/acid ratio.

The ˚Brix/acid ratio showed an increase along fruit maturation. The yellow and orange fruits are at an intermediate stage in the maturation process, since it was not found significant differences between them regarding this quality parameter. On the contrary, the green fruits and red fruits showed to be distinct ripening stages (P<0.001; Fig. 9C). Moreover, similarly to what was found with the ˚Brix evolution (Fig. 9A) and contrary to what happens with acidity (Fig. 9B), the ˚Brix/Acid showed to suffer an increase across maturation (Fig. 9C), that was expected considering the evolution of TSS and acidity previously described.

Finally, considering these results, the ˚Brix showed to be a tool for monitoring ripening of strawberry tree fruits, as well the ˚Brix/acid ratio. However, the chemical parameter of

acidity showed to be less suitable for monitoring the maturation, since was not possible to distinguish the last three ripening stages (yellow, orange and red).

3.1.4 Fresh and dry weight – water content

The fresh weight of green fruits was 4.07 g (ranging from 3.68 g to 4.22 g), 6.19 g (ranging from 5.05 g to 7.31 g) at the yellow ripening stage, 5.63 g (ranging from 4.89 g to 6.37 g) in orange fruits, and 5.35 g (ranging from 4.87 g to 5.83 g) in red fruits (Table 1). ANOVA showed statistically significant different results (P<0.001) only between green fruits and the following ripening stages, with an effect size of η^2 = 0.38 for the maturation factor. Box-and-whisker plots show that fresh weight increases from green fruits to yellow fruits, and then a progressive decreasing is observed until the fruit is fully ripen (Fig. 9D). These results are in accordance with those presented by Anastácio (2014) that described the same evolution for fresh weight along maturation in *A. unedo* fruits. Moreover, Guerreiro *et al*. (2013) justifies the weight loss in *A. unedo* fruits as a phenomenon of dehydration occurring during ripening. Concerning the dry weight measured, after lyophilization of the fruits, it was 1.35 g in the green fruits and 1.84 g in the red ones. ANOVA showed that maturation is the main factor contributing to the variation on fruit dry weight (η^2 = 0.36). Box-and-whisker plots showed that dry weight follows the same trend described by fresh weight, and statistically significant different results were only found between green fruits and the other maturation stages (P<0.001; Fig. 9E).

Regarding the water content, calculated based in the fresh and dry weights, it was 66.78% in green fruits whereas in the red ones it was 65.69% (Table 1). ANOVA showed that maturation is the main factor with an effect size (η^2) of 0.37. However, despite of box-and-whisker plots suggest a similar trend to those observed for dry and fresh weight (Fig. 9D and 9E), no significant differences were found (P>0.05; Fig. 9F). The water content has been previously assayed in *A. unedo* fruits by other authors, and the results here presented are in global agreement with them. According to Özcan and Haciseferoğullari (2007) the water content in red fruits was around 53.72%, while Barros *et al*. (2010) reported a higher value of 59.70% also in fully ripen fruits. On the other hand, Ruíz-Rodriguez *et al*. (2011) analyzed fruits from different locations and found a wide range of values, reporting that the water content in ripen fruits could vary between 46.82% and 71.89%. Moreover, this parameter was found to be constant along maturation. It is plausible that changes could be related with different edafo-climatic conditions and harvest periods, such as water availability, sunlight exposure or wind which promotes fruit dehydration (Ruíz-Rodriguez *et al*., 2011). Nevertheless, the unusual

lower water content of strawberry tree berries is only compared with another Ericaceae species such the cranberries (*Vaccinium oxycoccus* L.), while in other common fruits, such as apples and plums the water content values range from 75% to 95% (Souci *et al*., 2008).

3.1.5 Polar and equatorial diameter

Regarding the polar diameter of the green fruits it was measured 18.15 mm in green fruits, 20.24 mm in the yellows, 19.89 mm in the orange fruits and 18.75 mm in the red ones (Table 1). Concerning the equatorial diameter of the green fruits it was 20.11 mm (ranging from 19.64 mm to 20.36 mm) whereas the red fruits it was 21.86 mm (ranging from 21.06 mm to 22.86 mm) (Table 1). Box-and-whisker plots of the ANOVAs for polar (Fig. 9G; P=0.008; η^2 = 0.37) and equatorial (Fig. 9H; P<0.001; η^2 = 0.23) diameters, resemble the evolution of fresh and dry weight during maturation (Fig. 9E and 9D). Despite these observations, the water content is considered to cause just partially these variations, since water remains apparently constant along maturation.

Hence, it is possible to suggest that size and weight variation in *A. unedo* fruits may be explained by an increasing in biomass synthesis during maturation. Moreover, in all the ripening stages here assayed, it is coherent that the equatorial diameter is always superior to the polar diameter.

3.1.6 Firmness

Firmness analysis showed an enormous reduction from green fruits 91.51 N (ranging from 74.04 N to 110.90 N), to the red ones 3.68 N (ranging from 0.82 N to 7.40 N) (Table 1). ANOVA showed statistically different results (P<0.001) for all the ripening stages, with exception to the orange fruits which are not significantly different from yellow fruits and red fruits, henceforward being considered an intermediate stage concerning their firmness. Maturation revealed to be the principal factor affecting firmness (η^2 = 0.80).

The principal causes of fruit softening have been highly correlated with the hydrolysis of pectins promoted by several enzymes like pectate lyases (PL), endo-polygalacturonases (PG), pectin methylesterases (PME) and galactanases (β-Gase), in fruits like strawberries and tomatoes (Zhou *et al*., 2016; Wang *et al*., 2018). Not just the content of pectins present in the cell wall are considered in fruit softening, but also the hydrolysis of pectins in the middle lamella interfere with the cell-to-cell adhesion capacity, and consequently with fruit firmness

(Wang *et al*., 2018). Airianah *et al*. (2016) working with several fruits, including strawberry tree fruits, showed that ripening phenomenon is in part a result of an oxidative process mediated by reactive oxygen species (ROS), contrary to what is defended by most of the cell wall models. Ripening fruits, similarly, to other senescent tissues like leaves in the autumn, showed to have up-regulated lipoxygenases driving fatty acids oxidation. The OH radicals produced, cause important alterations in pectic polymers, which are then broken in smaller sugars responsible for increasing fruits sweetness during maturation (Airianah *et al*., 2016). According to Vicente *et al*. (2007), a substantial increase in small soluble polymers of xylose, during ripening of many *Vaccinium* species, was related to strong alterations in hemicelluloses present in the cell wall. In the same way, Chea *et al*. (2019) confirmed the importance of the degradation of hemicelluloses during ripening of *Vaccinium corymbosum* fruits, aside with an also notorious increase in soluble monosaccharides like rhamnose and galactose, both constituent monosaccharides in pectins. In respect to cellulose, less relations have been found between this polymer and the mechanisms underlying ripening (Sun *et al*., 2013). Thus, since cell wall polysaccharides are degraded by enzymatic attack and/or oxidative processes, monosaccharides and oligosaccharides that were part of bigger polysaccharides in the cell wall are now solubilized and contributing for the increasing sweet flavor as ripening goes on and the fruit softens (Vicente *et al*., 2007; Sun *et al*., 2013; Airianah *et al*., 2016; Zhou *et al*., 2016; Wang *et al*., 2018; Chea *et al*., 2019). In the same way, as the box-and-whisker plots show an inverse evolution of firmness (Fig. 9I) and ˚Brix (Fig. 9A) as fruits mature, firmness is here presented as a parameter which may be used as a predictor of the evolution of other quality parameters like ˚Brix (Chea *et al*., 2019).

3.1.7 Phenolic profile of *A. unedo* fruits

Phenolic compounds are a widespread group of chemicals largely present in plants. Tree species, like *A. unedo*, display a great diversity of these compounds that play important roles in plant development and in the interaction of plants with biotic and abiotic factors (Pawlowska *et al*., 2006; Harnly *et al*., 2007).

The examination of phenolic compounds along different ripening stages was assessed by a comparison of their spectra and retention times (Fig. 10 and 11). Regarding the collected spectra and chromatograms for the phenolic profile of the fruits from the tree A at 280 nm (Fig. 10 and 11), it is predicted that the compounds (*a*, RT = 8.5), (*b*, RT = 11.9), (*c*, RT =13.3), (*d*,

RT = 14.5) and (*f*, RT = 16.7), have less or none variation across the four ripening stages. On the other hand, the presence of the phenolic compound (*e*, RT = 15.784) is apparently restricted to the last two ripening stages, in orange and red fruits (Fig. 11). According to Guimarães *et al*. (2013), the flavan-3-ols like catechins and proanthocyanidins, and galloyl derivatives were assessed in this region at 280 nm, thus some correlations are expected to be made in the future analysis. These authors had tentatively identified, in the region comprised between the compounds (*a*) and (*f*), the following phenolics: galloylquinic acid (RT = 9.9, λ_{max} = 274 nm), galloylhexoside acid (RT = 11.3, λ_{max} = 278 nm), a proanthocyanidin dimer ((epi)gallocatechin + (epi)catechin), and galloyl shikimic acid (RT = 12.9, λ_{max} = 276 nm). These tentative identifications made by these authors agree with previous studies made by Pawlowska *et al*. (2006) and Mendes *et al*. (2011).

The region between RT = 17.0 and RT = 30.0, resembling a mountain, revealed to be very difficult to analyze, in result of the huge number of compounds and possibly due to their overlapped elution (Fig. 11). Concerning the last compounds indicated by (*g*, RT = 30.0), (*h*, RT = 30.9), (*i*, RT = 31.3), (*k*, RT = 32.8), (*l*, RT = 33.4), (*m*, RT = 34.7), (*n*, RT = 35.4), (*o*, RT = 36.8), (*p*, RT = 36.1) and (*q*, RT = 37.5), all of them did not show any variation across the four ripening stages, with exception for (*j*, RT = 31.9) which apparently it is more noticeable in the last three ripening stages, yellow, orange and red fruits (Fig. 11).

Regarding the chromatograms from the fruits of the Tree A at 340 nm (Fig. 11), the presence of the phenolic compounds (*a*), (*b*), (*c*), (*d*), (*e*) and (*f*), was not detected there, what might suggest that this phenolic compounds should be further investigated only at 280 nm , while the compounds (*g*), (*h*), (*i*), (*j*), (*k*), (*l*), (*m*), (*n*), (*o*), (*p*) and (*q*) showed to be more outstanding at 340 nm (Fig. 11), thus it might be useful further investigations of this compounds at 340 nm. Nonetheless, these results are proof that both wavelengths, 280 and 340 nm, should be considered to a complete assessment of the phenolic profile of *A. unedo* fruits. Further chromatograms of the phenolic profile of fruits from tree B (Fig. 12) and tree C (Fig. 13) were also collected.

Concerning *A. unedo* fruits, several assays have been carried out to determine their phenolic profile (Salem *et al*. 2018). Strawberry tree fruits revealed high contents of quercetin derivatives (quercetin rhamnoside, quercetin galloylhexoside derivative, quercetin 3-*O*-rutinoside), myricetin derivatives like myricetin rhamnoside, and several galloyl derivatives (galloylquinic acid, galloyl shikimic acid, digalloylquinic acid, and digalloylquinic shikimic acid) (Guimarães *et al*., 2013; Salem *et al*., 2018). However, Pawlowska *et al*. (2006) were unable to report the presence of myricetin derivatives in *A. unedo* fruits. Among all the phenolic

compounds, gallic acid was found as the major phenolic acid, as well as gentisic and protocatechuic acids. In turn, *p*-hydroxybenzoic, vanillic and *m*-anisic acids were indicated as minor phenolic acids present in fruits (Ayaz *et al*., 2000). Anthocyanins are other important phenolic compounds identified in *A. unedo* fruits, responsible for fruits, flowers and vegetable colors like blue, red or orange (Pawlowska *et al*., 2006), and important bioactivities as chemoprotective, antioxidant, antidiabetic or antibiotic (Ayaz *et al*., 2000). Besides, anthocyanins have been employed in food industry as natural colorants, avoiding the side effects of synthetic dyes, like allergies or hyperactivity in children (Lopez *et al*., 2018). *A. unedo* revealed to be a potential natural source for these flavonoids, given its richness in delphinidin 3-*O*-glucoside, cyanidin 3-*O*-pentoside, and cyanidin 3-*O*-glucoside the most abundant anthocyanin in this species (Guimarães *et al*., 2013). According to Alarcão-e-Silva *et al*. (2001), the peculiar bitter and astringent taste of the ripen fruit is due its phenolics richness, especially tannins. These polyphenols have been proved to be efficient as blood pressure reducers and adjusting immunosuppressors, whereas they could be in the origin of liver necrosis (Garcia-Salas *et al*., 2010). Decreasing in total phenolic content were observed during ripening, especially tannins, however these alterations are quite despicable when comparisons are made with other wild berries (Alarcão-e-Silva *et al*., 2001).

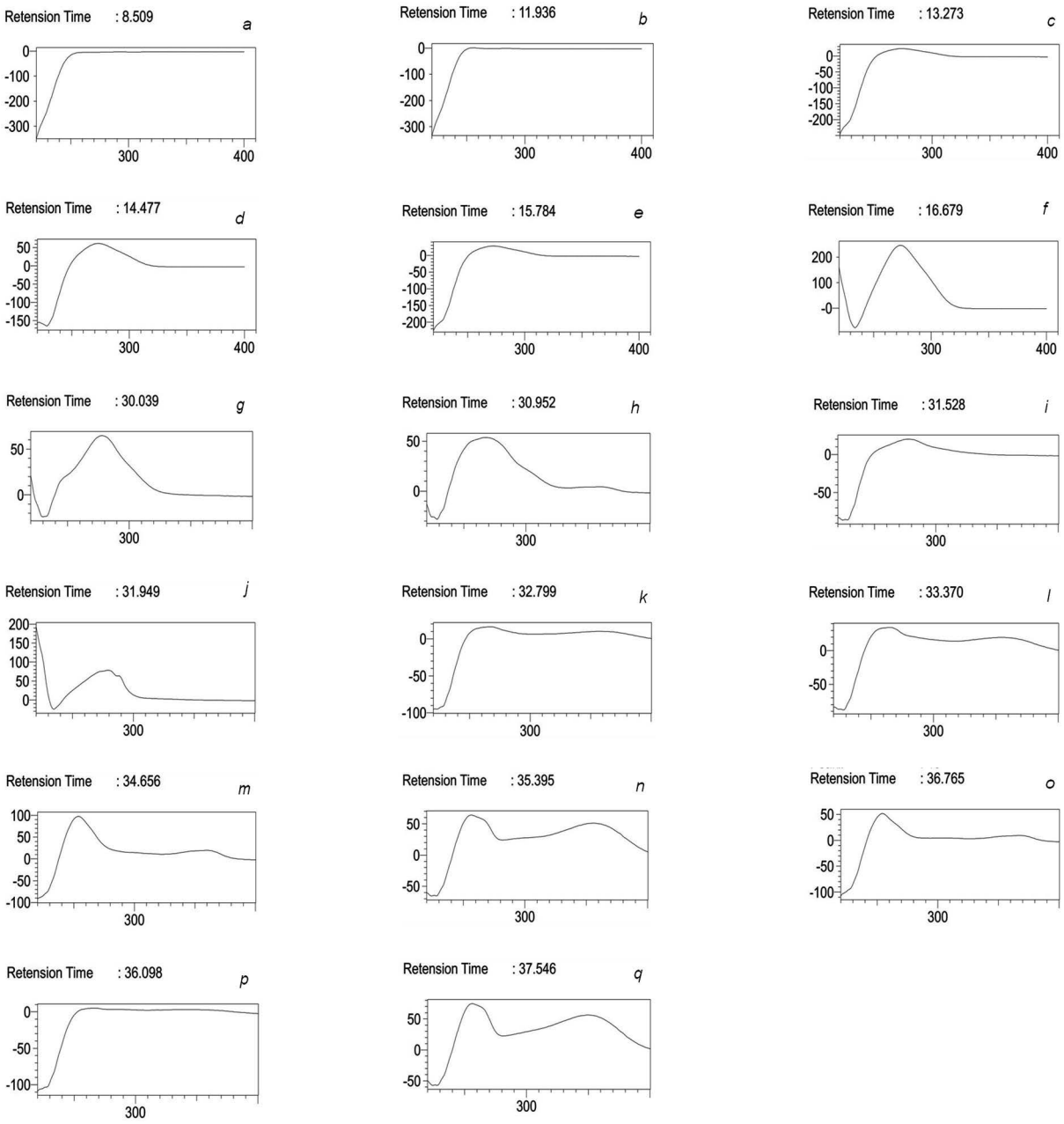

Figure 10. UV spectra acquired at 280nm for the phenolic profile of the fruits from the tree A.

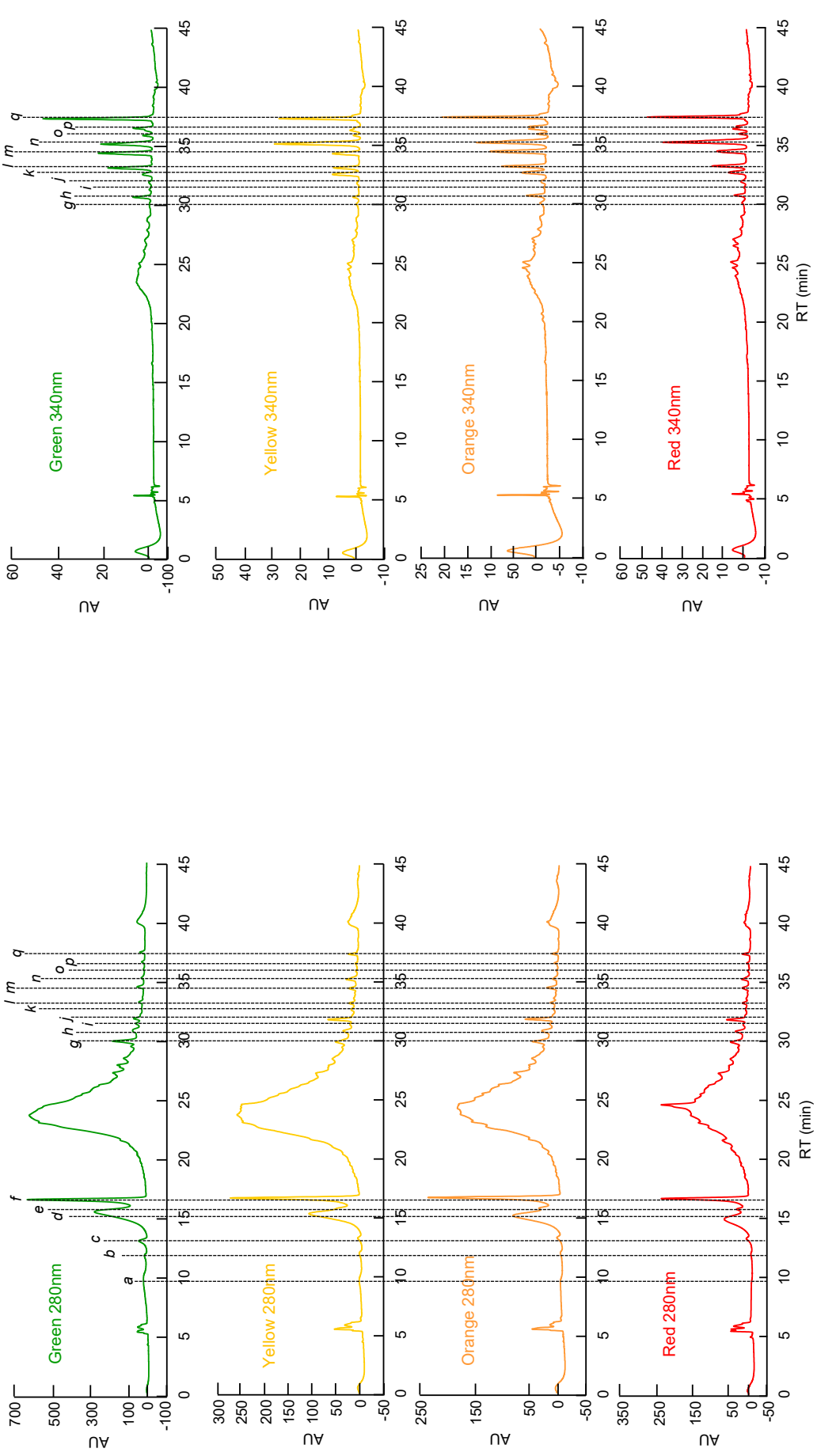

Figure 11. Phenolic profile of *A. unedo* fruits from tree A, across four ripening stages. The spectra were collected at 280 nm and 340 nm, by RP-HPLC-PDA.

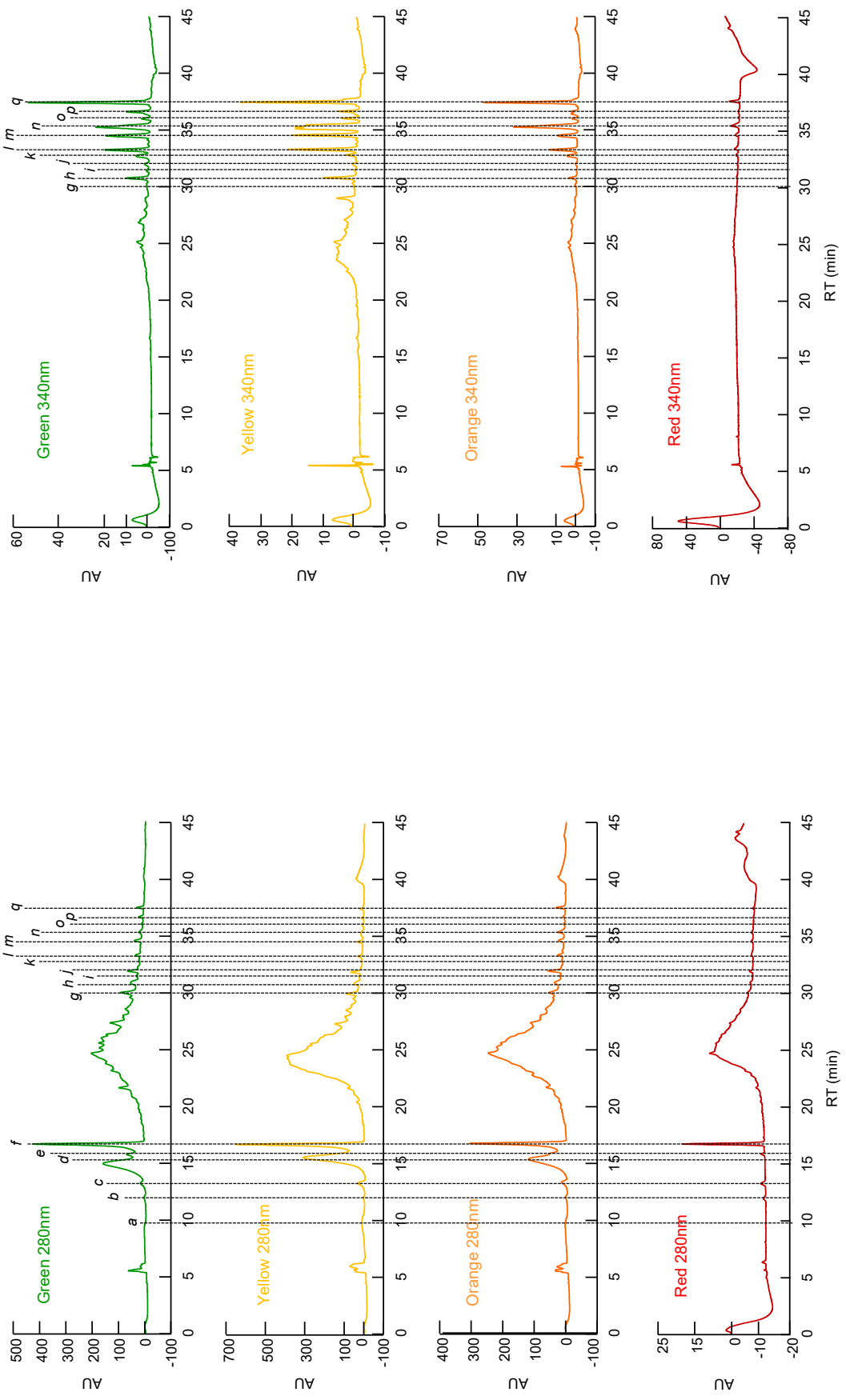

Figure 12. Phenolic profile of *A. unedo* fruits from tree B, across four ripening stages. The spectra were collected at 280 nm and 340 nm, by RP-HPLC-PDA.

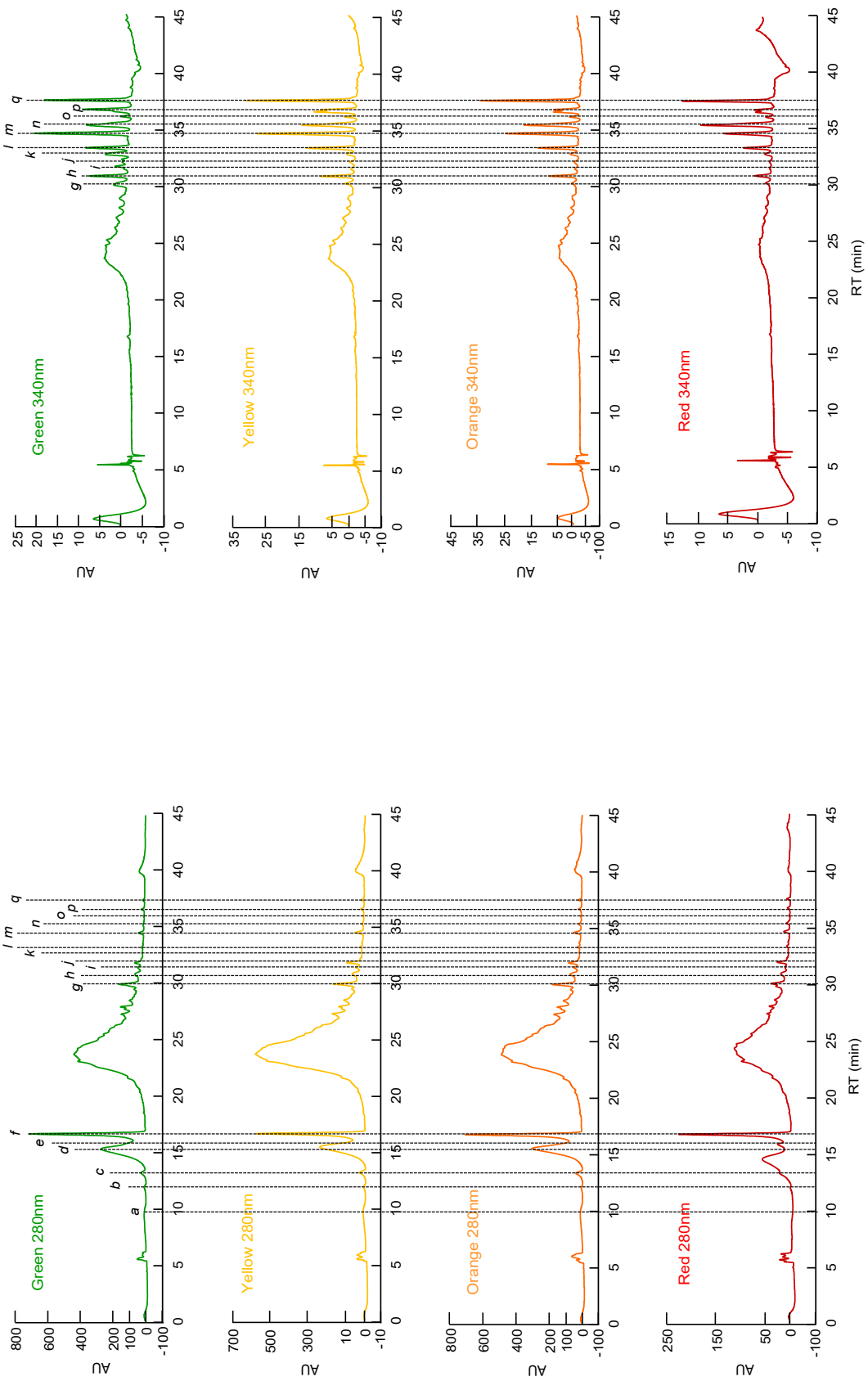

Figure 13. Phenolic profile of *A. unedo* fruits from tree C, across four ripening stages. The spectra were collected at 280 nm and 340 nm, by RP-HPLC-PDA.

3.2 Biomass characterization by FTIR-ATR spectroscopy

Fourier transform infrared spectroscopy (FTIR) is an effective tool, as it is possible to examine cell wall biomass in a non-destructive and non-invasive way. Moreover, the cost procedure is low, and the technique allows to assess the bulk chemistry based on the vibrations of chemical bonds present in molecules (Szymanska-Chargot *et al*., 2013). In addition, Attenuated Total Reflection (ATR) associated with infrared spectroscopy (IR) enables cell wall biomass samples to be analyzed in solid state without extensive preparation. Resulting spectra enclose a range of bands hiding chemical features of samples, however the analysis of this large data sets generated implies certain exploratory techniques. Principal component analysis was chosen to reduce the large set of variables into new smaller variables called principal components (PC), thus being possible to expose what really differentiate samples in respect to their composition (da Costa, 2016).

3.2.1 Characterization of the cell wall of fruits by FTIR-ATR spectroscopy

To reduce interference from components not belonging to the cell wall, it is recommended the examination of isolated cell wall preparations, like alcohol-insoluble residues (AIR), instead of the intact biomass (da Costa *et al*., 2015).

A general PCA model was created to reveal the main clusters between FTIR-ATR spectra of the four ripening stages (Fig. 14A). In order to refine the model and better explain the main chemometric trends between the ripening stages, outlying samples were removed. As a very general rule, the proper treatment of outliers depends on the analysis purpose, if we are looking for large-scale tendencies, they often better be removed. Two main clusters were observed in this model, the first, containing only the red fruits, while the second contained the green, yellow and orange fruits, which remained overlapped (Fig. 14A). Segregation occurred along PC2 that captured just 7.6% of variance, even so PC2 loadings are here shown to assess compositional differences, since the PCA model predicts the occurrence of a single major shift on cell wall structure and composition during fruits maturation. Based on the interpretation of the PC2 loadings, four spectral bands were detected as the main discriminant regions between the two formed clusters (Fig. 14B and 14C). The attribution of spectral areas to their corresponding components was made according to the literature (Table 2).

All the spectral features were related to polysaccharides. The negative loading represented by 929 cm^{-1} (*a*) is associated to β-linkages between sugar units in both cellulose

and hemicellulose, likewise other negative loadings, 1019 cm^{-1} (*b*) and 1099 cm^{-1} (*c*), were related to pectic polysaccharides. Concerning the positive loading 1700 cm^{-1} (*d*), it was the only assignment achieved for red fruits, also related to polysaccharides. According to Park *et al*. (2013) this band suggests the presence of functional groups like ketones, aldehydes, esters or carboxyl groups in polysaccharides.

As previously reported by Moore *et al*. (2014), despite FTIR spectroscopy coupled with PCA could be used as a powerful technique to evaluate the evolution of ripening in fruits, more sophisticated approaches are demanded to uncover the subtle remodeling in the cell walls across fruits maturation. It is from this perspective, that the FTIR-PCA approach has most value, as its predictive properties allows for better planning and analysis strategy

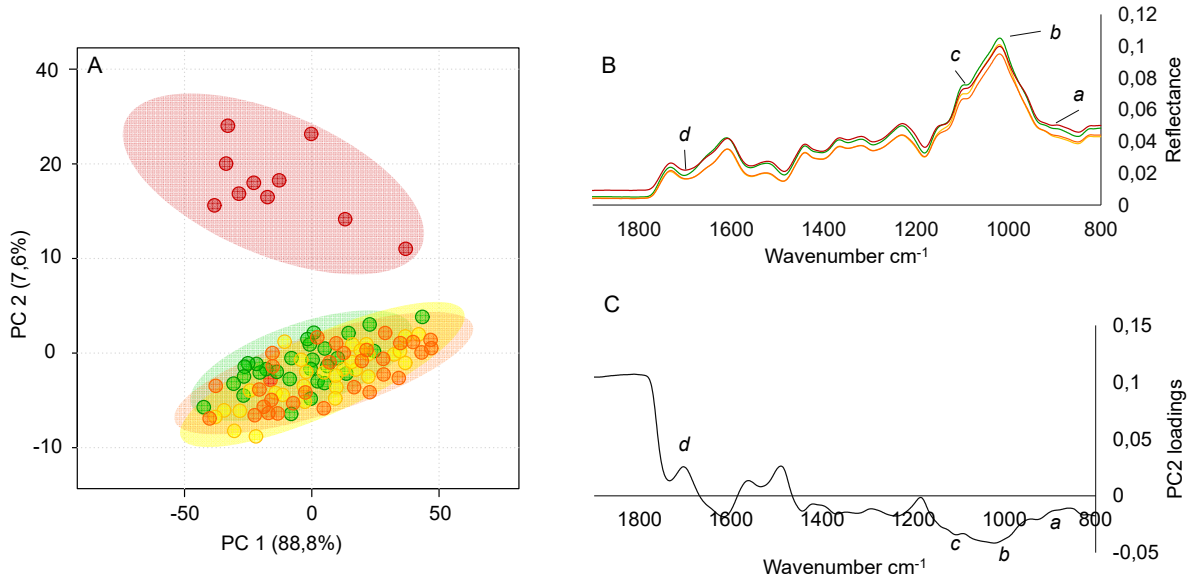

Figure 14. Principal component analysis of fruits FTIR-ATR spectra of selected samples from AIR biomass of four ripening stages: green, yellow, orange and red. (A) plot of principal component one (PC1) and principal component two (PC2) scores for selected samples. (B) Mean FTIR spectra of the four ripening stages in the range 1900–800 cm^{-1}. (C) PC1 loading plot for all the four ripening stages. Spectral bands: 929 cm^{-1} (*a*); 1019 cm^{-1} (*b*); 1099 cm^{-1} (*c*); 1700 cm^{-1} (*d*).

Table 2. Assignment of relevant FTIR-ATR reflectance bands characteristic of the cell wall of *A. unedo* fruits.

Band	Wavenumber (cm^{-1})	Group	Assignment	References
a	929	Polysaccharides	Associated with cellulose and hemicellulose	930 cm^{-1} (Kačuráková *et al*., 2000; Sills and Gossett, 2012; Xu *et al*., 2013)
b	1019	Polysaccharides	Pectic polysaccharides	1014 cm^{-1} (Coimbra *et al*., 1999) 1017 cm^{-1} (Kačuráková *et al*., 2000; da Costa *et al*., 2014) 1018 cm^{-1} (McCann *et al*., 2001)
c	1099	Polysaccharides	C-O stretching, C-C stretching ring pectin	1097cm^{-1} (Szymanska-Chargot *et al*., 2015) 1100 cm^{-1} (Chylinska *et al*., 2016)
d	1700	Polysaccharides	C=O and C=C stretching vibrations in polysaccharides	1700 cm^{-1} (Park *et al*., 2013)

3.2.2 Characterization of the intact biomass of fruits by FTIR-ATR spectroscopy

Subsequently to the cell wall analysis based on AIR samples, the FTIR-PCA approach was used to provide an in-depth analysis using fruits intact (INT) biomass, thus disclosing other chemical features related to the maturation of strawberry tree fruits. In order to refine the model and better explain the main chemometric trends between the ripening stages, outlying samples were removed.

The first PCA includes all collected spectra across the four ripening stages and thirteen spectral bands were detected as the main discriminant, in the fingerprint region of the spectra (Fig. 15A and 15B). The attribution of spectral areas to their corresponding intact biomass components was made according to the literature (Table 3). No clustering was observed concerning green and yellow fruits, but spectral segregation was obtained for orange and red fruits. Subsequently, for an in-depth assessment of compositional differences, other PCA models were constructed after spectral data had been split into separate subsets comprising each ripening stage.

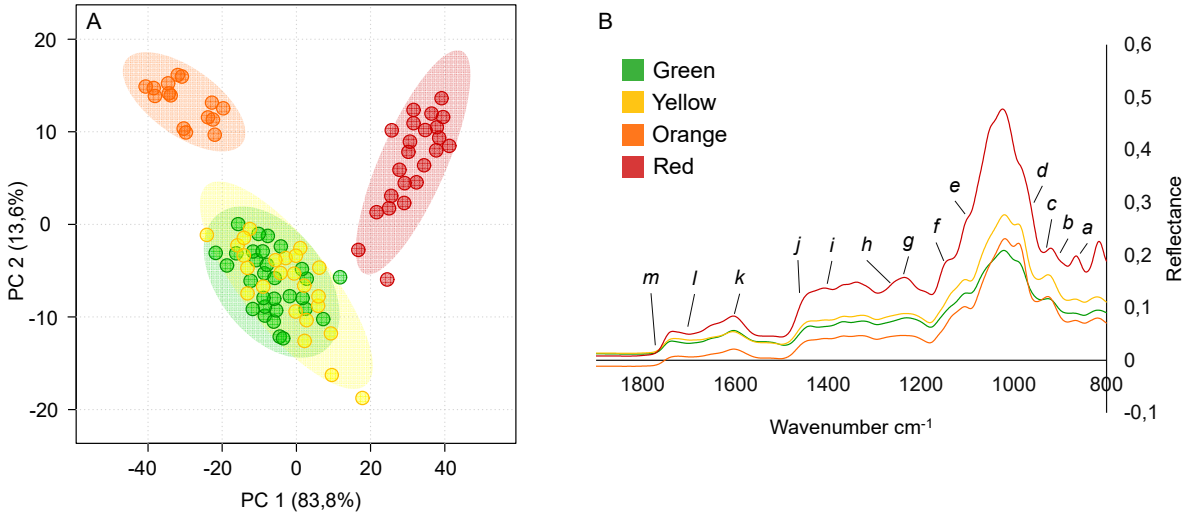

Figure 15. Principal component analysis of fruits FTIR-ATR spectra of selected samples from INT biomass of four ripening stages: green, yellow, orange and red. (A) plot of principal component one (PC1) and principal component two (PC2) scores for selected samples. (B) Mean FTIR spectra of the four ripening stages in the range 1900–800 cm^{-1}. Spectral bands: 860 cm^{-1} (*a*); 894 cm^{-1} (*b*); 931 cm^{-1} (*c*); 960 cm^{-1} (*d*); 1093 cm^{-1} (*e*); 1153 cm^{-1} (*f*); 1230 cm^{-1} (*g*); 1261 cm^{-1} (*h*); 1400 cm^{-1} (*i*); 1457 cm^{-1} (*j*); 1602 cm^{-1} (*k*); 1720 cm^{-1} (*l*); 1760 cm^{-1} (*m*).

Table 3. Assignment of relevant FTIR-ATR reflectance bands characteristic of the intact biomass of *A. unedo* fruits.

Band	Wavenumber (cm^{-1})	Group	Assignment	References
a	860	Polysaccharides	Associated with the aldopyranoses and the furanoid compounds	859 cm^{-1} (Kačuráková *et al*., 2000)
b	894	Polysaccharides	Antisymmetric out-of-phase ring stretching in cellulose	894 cm^{-1} (Szymanska-Chargot *et al*., 2015)
c	931	Polysaccharides	Associated with both cellulose and hemicellulose	930 cm^{-1} (Kačuráková *et al*., 2000; Sills and Gossett, 2012; Xu *et al*., 2013) 934 cm^{-1} (Szymanska-Chargot *et al*., 2015)
d	960	Polysaccharides	C=O bending vibration in pectins	960 cm^{-1} (Szymanska-Chargot *et al*., 2013) 963 cm^{-1} (Wilson *et al*., 2000; Schulz and Baranska, 2007)
e	1093	Polysaccharides	C-O and C-C stretching in ring pectin	1090 cm^{-1} (Kačuráková *et al*., 2000) 1093 cm^{-1} (Szymanska-Chargot *et al*., 2013)
f	1153	Polysaccharides	Associated with xyloglucan	1151 cm^{-1} (Deepa *et al*., 2015) 1153 cm^{-1} (Kačuráková *et al*., 2000; Chylinska *et al*., 2016)
g	1230	Polysaccharides	OH bending vibration in pyranose ring of pectins	1230 cm^{-1} (Szymanska-Chargot *et al*., 2015)
h	1261	Polysaccharides	Associated with the C=O groups in pectins	1260 cm^{-1} (Moore *et al*., 2014)

i	1400	Polysaccharides	Symmetric vibration of COOH in pectins	1400 cm^{-1} (Moore *et al*., 2014; Chylinska *et al*., 2016)
j	1457	Lipids	CH_2 bending scissoring associated to cutin and waxes	1457 cm^{-1} (Heredia-Guerrero *et al*., 2014)
k	1602	Polysaccharides	COO^- antisymmetric stretching in pectins	1600 cm^{-1} (Szymanska-Chargot *et al*., 2015)
l	1720	Polysaccharides Proteins	Associated with C=O, COOH and NH groups in proteins and pectins	1720 cm^{-1} (Moore *et al*., 2014)
m	1760	Polysaccharides	COOH stretching vibrations in pectins	1760 cm^{-1} (Chylinska *et al*., 2016; Golubtsova, 2017)

Concerning PCA model for yellow and green fruits, despite PC1 captured 78.5% of variance clustering was observed along PC2 which explained just 10.9% of variance (Fig. 16A). A *t*-test was performed to assess the compositional differences between these groups, and all the assignments were found to be related with polysaccharides, 860 cm^{-1} (*a*), 931 cm^{-1} (*c*), 960 cm^{-1} (*d*) and 1602 cm^{-1}(*k*) (Table 3). According to box-and-whisker plots the assigned compounds were found in higher content in yellow fruits, despite only one exception found for the band 1602 cm^{-1} (*k*) (Fig. 16B). This spectral band suggests that pectic polysaccharides bearing esterified groups such as carboxylate (COO^-), are more abundant in green fruits comparing with yellow fruits. This observation is supported by the results of Steele *et al*. (1997), that had noticed a strong decline in pectin esterification during ripening of tomatoes, between the unripen green tomatoes and the red-ripe stage. Regarding the other assignments, the spectral area 860 cm^{-1} (*a*) is a hallmark for sugars as it suggests the presence of building blocks for polysaccharides, such as aldopyranoses and furanoid rings (Kačuráková *et al*., 2000). In turn, 931 cm^{-1} (*c*) can be associated both with cellulose and hemicelluloses, and the overlapping assignments here predicted may be explained based on the similarities of their molecular structures (Szymanska-Chargot *et al*., 2013). Other assays carried out by Szymanska-Chargot *et al*. (2015) suggest that, this band could either indicate the presence of xyloglucan or glucomannan polymers, both hemicellulosic polysaccharides. In turn, the spectral band 960 cm^{-1} (*d*) predicts carbonyl (C=O) bending vibrations specific for Rhamnogalacturonan I (RGI) molecules, part of pectin backbones (Szymanska-Chargot *et al*., 2013).

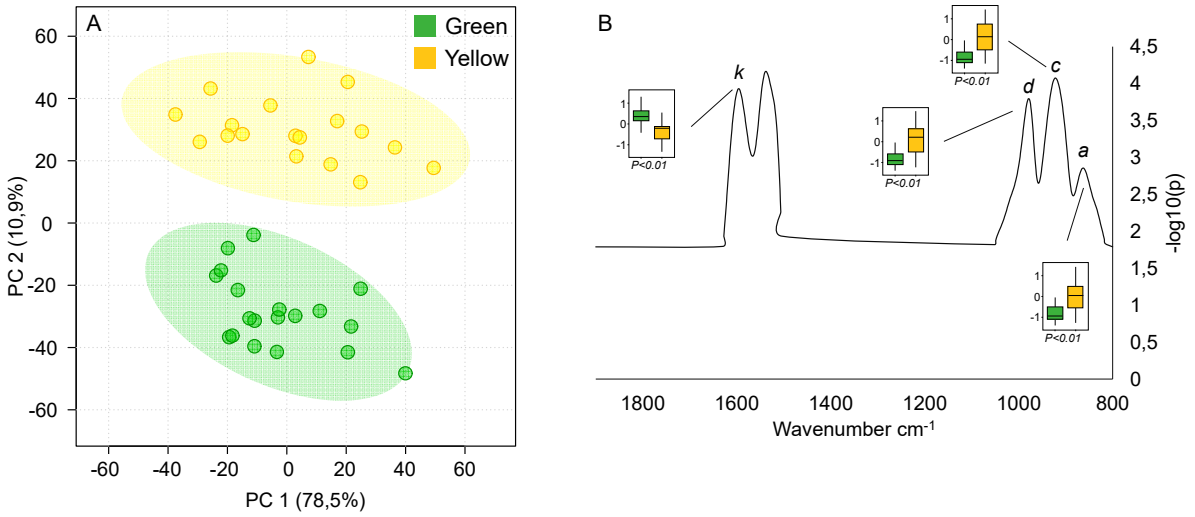

Figure 16. Principal component analysis of fruits FTIR-ATR spectra of selected samples from INT biomass of the green and yellow ripening stages. (A) plot of principal component one (PC1) and principal component two (PC2) scores for selected samples. (B) *t*-test with box-and-

whisker plots indicating the amounts of the compounds in each ripening stage (P<0.01 for all the assigned compounds). Spectral bands: 860 cm^{-1} (*a*); 931 cm^{-1} (*c*); 960 cm^{-1} (*d*); 1602 cm^{-1} (*k*).

The PCA model presented for yellow and orange fruits shows that segregation occurred mainly along PC1 that captured 96.9% of variance, while PC2 explained 2.1% of variance (Fig. 17A). Nonetheless, PC1 loadings were not informative about compositional differences between both groups, so a *t*-test was performed to evaluate the compositional differences. According to box-and-whisker plots, all compounds are present in higher concentrations in the yellow fruits (Fig. 17. B) and compositional differences were found to be related with the following spectral bands: 860 cm^{-1} (*a*), 894 cm^{-1} (*b*), 960 cm^{-1} (*d*), 1093 cm^{-1}(*e*), 1400 cm^{-1} (*i*), 1720 cm^{-1} (*l*) and 1760 cm^{-1}(*m*) (Table 3) . The interpretation of spectral features in the range of 1200 cm^{-1} to 1600 cm^{-1}, were somewhat unsuccessful (Fig. 17B).

However, the interpretation of this *t*-test suggests that, as ripening proceeds, more pectic polysaccharides are synthesized and thus incorporated in cell wall structure of yellow fruits, what could explain the high amounts of pectins in these fruits (Chylinska *et al*., 2016). On the other hand, low amounts in orange fruits suggests that the compounds here assigned were degraded and removed from the cell wall. Hence, it is plausible to suggest that these same compounds were subsequently solubilized in the fruit, between the yellow and orange stages, explaining the increase tendency of ˚Brix during maturation, which is followed by the decrease of fruit firmness, as previously discussed (Section 3.1.6). These observations could be correlated with the assignments made for 960 cm^{-1} (*d*), 1093 cm^{-1} (*e*), 1400 cm^{-1} (*i*), 1720 cm^{-1} (*l*) and 1760 cm^{-1} (*m*), all of them suggesting the presence of pectins. Moreover, according to Moore *et al*. (2014) the band 1720 cm^{-1} (*l*) may also suggest the presence of structural proteins in the cell wall.

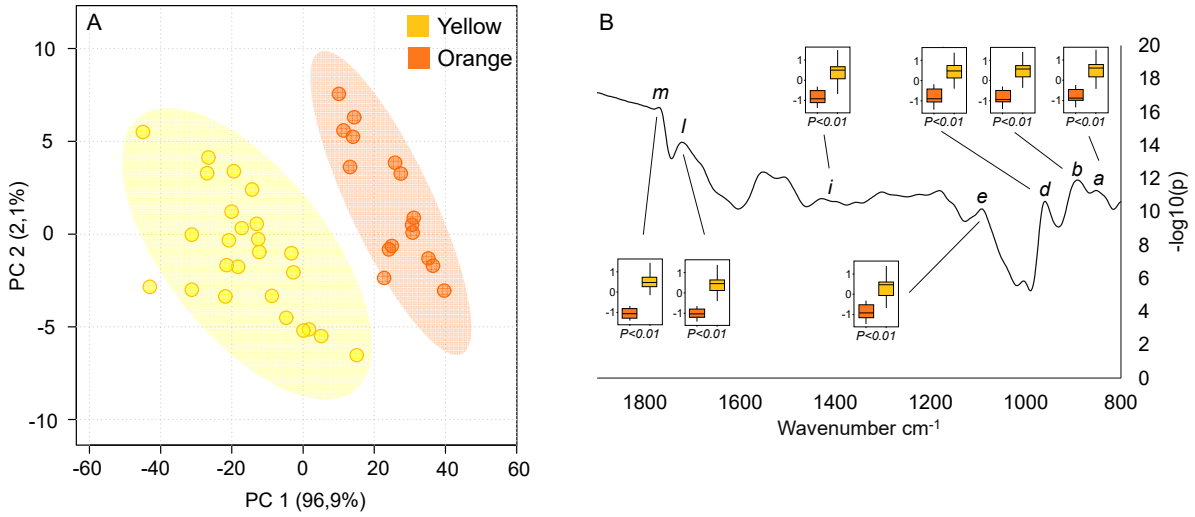

Figure 17. Principal component analysis of fruits FTIR-ATR spectra of selected samples from INT biomass of the yellow and orange ripening stages. (A) plot of principal component one (PC1) and principal component two (PC2) scores for selected samples. (B) *t*-test with box-and-whisker plots indicating the amounts of the compounds in each ripening stage ($P<0.01$ for all the assigned compounds). Spectral bands: 860 cm^{-1} (*a*); 894 cm^{-1} (*b*); 960 cm^{-1} (*d*); 1093 cm^{-1} (*e*); 1400 cm^{-1} (*i*); 1720 cm^{-1} (*l*); 1760 cm^{-1} (*m*).

Regarding the PCA model for orange and red fruits, just 8.4% of variance was captured by PC2, whereas 89.9% of variance was related with PC1 (Fig. 18A). A *t*-test was chosen to assess compositional differences, and according to box-and-whisker plots all the compounds revealed to be present in the red fruits in higher amounts when compared to orange fruits (Fig. 18B). These results suggest that during maturation most of the structural compounds in the cell wall were removed from there, by enzymatic and/or oxidative mechanisms, and are thus solubilized in the fruit, once again explaining the decreasing in fruits firmness. Many pectic-associated bands were found, such as 960 cm^{-1} (*d*), 1093 cm^{-1} (*e*), 1230 cm^{-1} (g), 1261 cm^{-1} (*h*), 1602 cm^{-1} (*k*) and 1760 cm^{-1} (*l*) (Table 3), suggesting the role played by these acidic polymers along maturation in the fruits of *A. unedo*. The spectral band 1153 cm^{-1} (*f*) was assigned for xyloglucan and is indicative of the linkage between the galactose units, what may be related with important alterations in the hemicellulosic fraction during maturation (Chylinska *et al.*, 2016). Concerning the spectral band at 1457 cm^{-1} (*j*) assigned to CH_2 bending vibrations of cutin and waxes, it suggests that just nearly by the end of maturation these compounds are deposited above the fruit cuticle in considerable amounts (Heredia-Guerrero *et al.*, 2014).

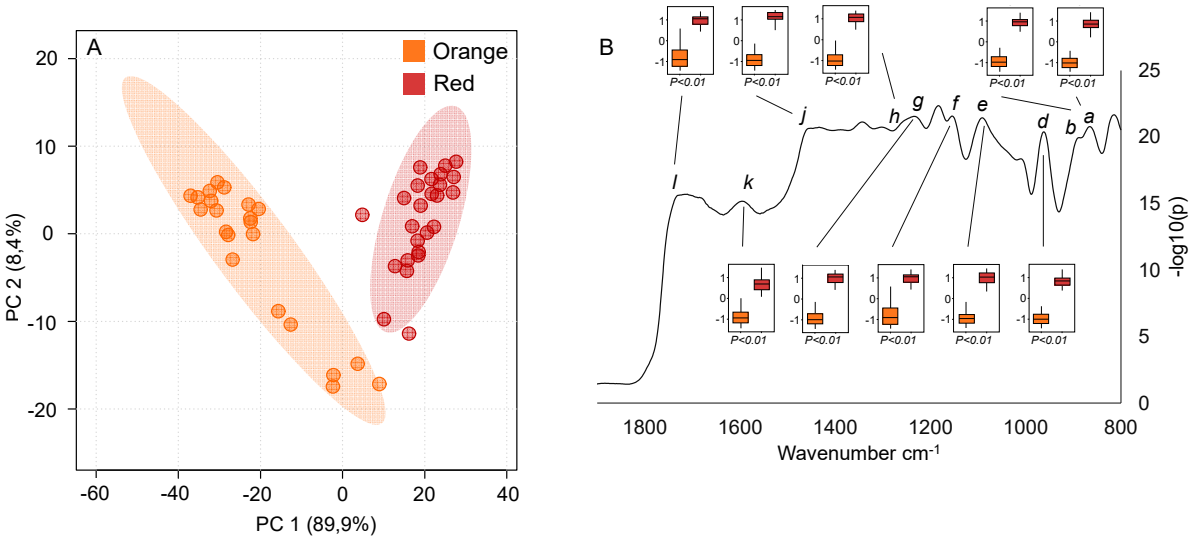

Figure 18. Principal component analysis of fruits FTIR-ATR spectra of selected samples from INT biomass of the orange and red ripening stages. (A) plot of principal component one (PC1) and principal component two (PC2) scores for selected samples. (B) *t*-test with box-and-whisker plots indicating the amounts of the compounds in each ripening stage ($P<0.01$ for all the assigned compounds). Spectral bands: 860 cm^{-1} (*a*); 894 cm^{-1} (*b*); 960 cm^{-1} (*d*); 1093 cm^{-1} (*e*); 1153 cm^{-1} (*f*); 1230 cm^{-1} (*g*); 1261 cm^{-1} (*h*); 1457 cm^{-1} (*j*); 1602 cm^{-1}(*k*); 1720 cm^{-1} (*l*).

A PCA model was elaborated to evaluate red and green fruits chemical differences. Two clusters were observed along PC1 which captured 87.7% of variance, while PC2 captured just 7.9% of variance (Fig. 19A). However, PC1 loadings were not comprehensive and a *t*-test was performed. According to box-and-whisker plots all the assigned compounds 860 cm^{-1} (*a*), 894 cm^{-1} (*b*), 960 cm^{-1} (*d*), 1093 cm^{-1} (*e*), 1153 cm^{-1} (*f*), 1261 cm^{-1} (*h*), 1400 cm^{-1} (*i*), 1457 cm^{-1} (*j*), 1602 cm^{-1}(*k*) and 1720 cm^{-1} (*l*) (Table 3), were found in higher amounts in the red fruits (Fig. 19B), which could be result of their removal from the cell wall since the early ripening stages (Vicente *et al*., 2007; Sun *et al*., 2013; Airianah *et al*., 2016; Zhou *et al*., 2016; Wang *et al*., 2018; Chea *et al*., 2019). A visual inspection predicts that compositional differences between green and red fruits are related to a broad range of assignments (Table 3), resembling the ones made in the PCA model of orange and red fruits (Fig. 18). What really distinguishes this PCA model from the previous PCA for orange and red fruits, is the assignment here made for 1400 cm^{-1} (*i*) that predicts symmetric vibrations in COOH groups incorporated in pectic polysaccharides, and the lack of the spectral band 1230 cm^{-1} (*g*) that is indicative of vibrations in the pyranose ring in pectins.

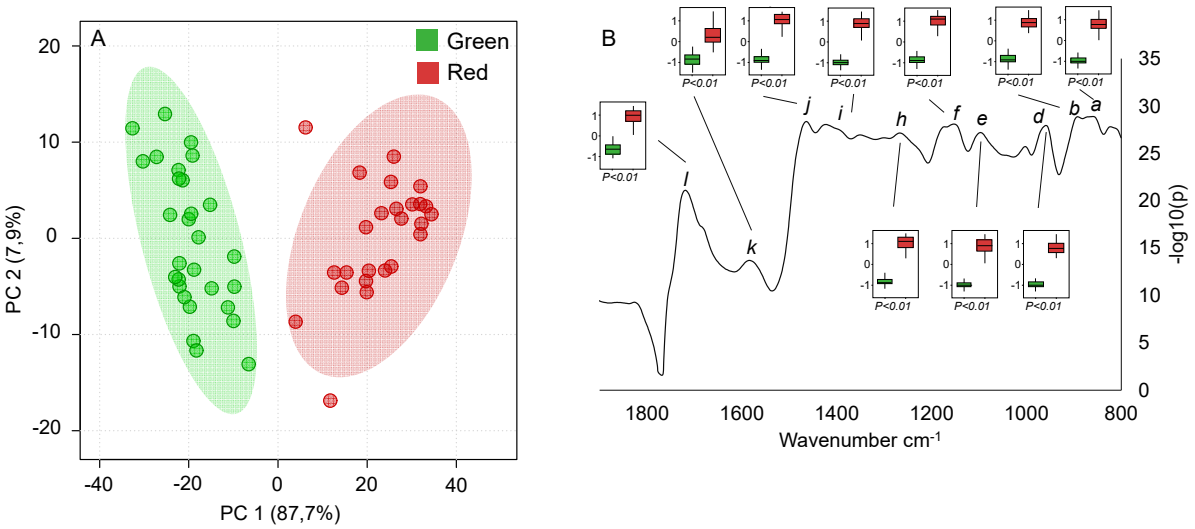

Figure 19. Principal component analysis of fruits FTIR-ATR spectra of selected samples from INT biomass of the green and red ripening stages. (A) plot of principal component one (PC1) and principal component two (PC2) scores for selected samples. (B) *t*-test with box-and-whisker plots indicating the amounts of the compounds in each ripening stage ($P<0.01$ for all the assigned compounds). Spectral bands: 860 cm^{-1} (*a*); 894 cm^{-1} (*b*); 960 cm^{-1} (*d*); 1093 cm^{-1} (*e*); 1153 cm^{-1} (*f*); 1261 cm^{-1} (*h*); 1400 cm^{-1} (*i*); 1457 cm^{-1} (*j*); 1602 cm^{-1}(*k*); 1720 cm^{-1} (*l*).

From these data, it is plausible to conclude that most structural and non-structural chemical differences occur during the final stages of maturation. This it has to do with the fact that the last PCAs (Fig. 18 and 19) are somewhat a complementary proof of the results obtained for the characterization of the cell wall of the fruits (Section 3.2.1; Fig. 14), that had predicted the distinction just between two major ripening groups, the immature (green, yellow, orange fruits) and the mature (red fruits).

3.2.3 Characterization of the cell wall of *in vitro* shoots by FTIR-ATR spectroscopy

Five PCA models were created to assess the main chemical differences in the cell wall of *in vitro* vitrified and non-vitrified shoots. In order to refine the model and better explain the main chemometric trends between different tissues, outlying samples were removed.

The first PCA includes selected spectra of all datasets and sixteen spectral bands were detected as the main discriminant, in the fingerprint region of the spectra (1900 cm^{-1}-800 cm^{-1}; Fig. 20A and 20B). The attribution of spectral areas to their corresponding components was made according to the literature (Table 4). Segregation was achieved for non-vitrified stems and vitrified stems, while non-vitrified leaves and vitrified leaves are slightly overlapped (Fig. 20A and 20B). Subsequently, to an in-depth assessment of chemical-compositional differences, other PCA models were constructed after spectral data had been split into separate subsets comprising each *in vitro* tissue.

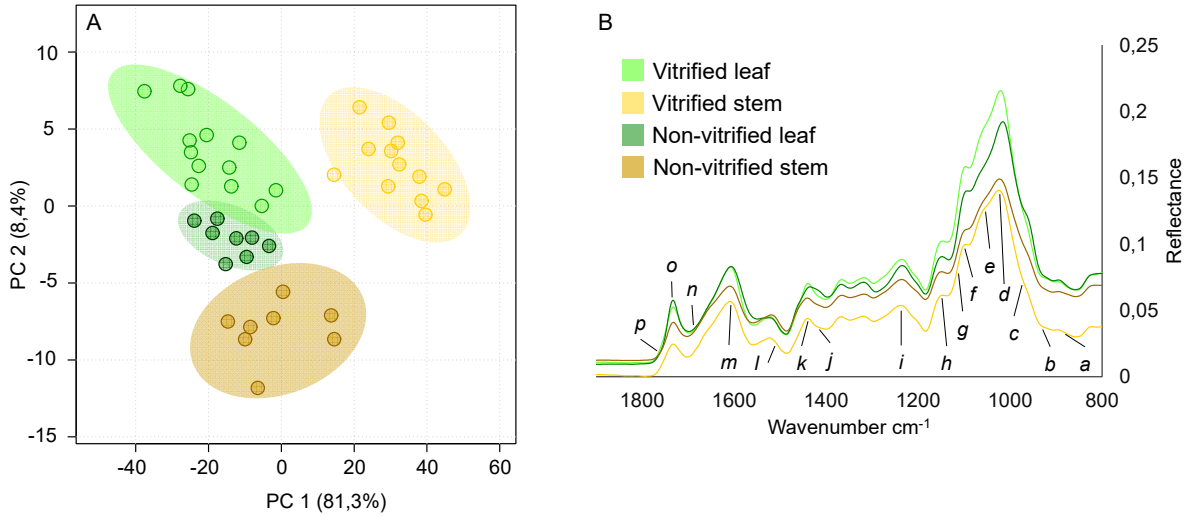

Figure 20. Principal component analysis of the FTIR-ATR spectra of selected samples from AIR biomass of four different tissues: vitrified leaf, vitrified stem, non-vitrified leaf and non-vitrified stem. (A) Plot of principal component one (PC1) and principal component two (PC2) scores for selected samples. (B) Mean FTIR spectra of the four different tissues in the range 1900–800 cm^{-1}. Spectral bands: 860 cm^{-1} (*a*); 931 cm^{-1} (*b*); 962 cm^{-1} (*c*); 1004 cm^{-1} (*d*); 1060 cm^{-1} (*e*); 1093 cm^{-1} (*f*); 1120 cm^{-1} (*g*); 1153 cm^{-1} (*h*); 1280 cm^{-1} (*i*); 1419 cm^{-1} (*j*); 1463 cm^{-1} (*k*); 1589 cm^{-1} (*l*); 1600 cm^{-1} (*m*); 1700 cm^{-1} (*n*); 1728 cm^{-1}(*o*); 1760 cm^{-1} (*p*).

Table 4. Assignment of relevant FTIR-ATR reflectance bands characteristic of the cell wall of *in vitro* shoots of *A. unedo*.

Band	Wavenumber (cm^{-1})	Group	Assignment	References
a	860	Polysaccharides	Associated with the aldopyranoses and the furanoid compounds	859 cm^{-1} (Kačuráková *et al*., 2000)
b	931	Polysaccharides	Associated with cellulose and hemicellulose	930 cm^{-1} (Kačuráková *et al*., 2000; Sills and Gossett, 2012; Xu *et al*., 2013)
c	962	Polysaccharides	C=O bending vibration in pectins	960 cm^{-1} (Szymanska-Chargot *et al*., 2013) 963 cm^{-1} (Schulz and Baranska, 2007; Wilson *et al*., 2000)
d	1004	Polysaccharides	C-O and ring stretching vibrations in cellulose	1003 cm^{-1} (Abidi *et al*., 2014) 1000 cm^{-1} (Szymanska-Chargot *et al*., 2013)
e	1060	Polysaccharides	C-O stretching and O-C-H in-plane bending vibrations in cellulose	1060 cm^{-1} (Wilson *et al*., 2000; Schulz and Baranska, 2007; Adapa *et al*., 2009) 1061 cm^{-1} (da Costa *et al*., 2014)
f	1093	Polysaccharides	C-O and C-C stretching in pectins	1090 cm^{-1} (Kačuráková *et al*., 2000) 1093 cm^{-1} (Szymanska-Chargot *et al*., 2013)
g	1120	Polysaccharides	C-O and C-C stretching in cellulose	1120 cm^{-1} (Kačuráková *et al*., 2000; Szymanska-Chargot *et al*., 2013)
h	1153	Polysaccharides	Associated with xyloglucan	1151 cm^{-1} (Deepa *et al*., 2015)

				1153 cm^{-1} (Kačuráková *et al*., 2000; Chylinska *et al*., 2016)
i	1280	Polysaccharides	C-H bending in cellulose	1280 cm^{-1} (Sills and Gossett, 2012; Xu *et al*., 2013)
j	1419	Polysaccharides	COO^- stretching vibration in pectins	1419 cm^{-1} (Schulz and Baranska, 2007)
k	1463	Lignin	Asymmetric bending vibration in CH_3 and CH_2 groups	1460 cm^{-1} (Souza *et al*., 2013) 1465 cm^{-1} (Sills and Gossett, 2012; Lupoi *et al*., 2015)
l	1589	Lignin	Skeletal stretching vibrations	1589 cm^{-1} (Lupoi *et al*., 2015)
m	1600	Lignin	C=C in plane symmetrical stretching vibration of aromatic ring in lignin	1602 cm^{-1} (Mandal and Chakrabarty, 2011)
n	1700	Polysaccharides Lignin	C=O and C=C stretching vibrations in polysaccharides and lignin	1700 cm^{-1} (Park *et al*., 2013) 1704 cm^{-1} (Lupoi *et al*., 2015)
o	1728	Polysaccharides Lignin	C=O stretching vibration in pectins; Hemicelluloses and lignin	1730 cm^{-1} (Mandal and Chakrabarty, 2011)
p	1760	Polysaccharides	COOH stretching vibrations in pectins	1760 cm^{-1} (Chylinska *et al*., 2016; Golubtsova, 2017)

Regarding the comparison between the cell walls of non-vitrified leaves and non-vitrified stems, PC1 explains 78.3% of variance and PC2 captures only 12.2% (Fig. 21A). A *t*-test was chosen to assess chemical differences, and all the assigned compounds (Table 4) were found in higher amounts in the cell walls of leaves comparing with stems (Fig. 21B). The pronounced spectral bands 1093 cm^{-1} (*f*) and 1419 cm^{-1} (*j*) were assigned to pectic polysaccharides, as well 962 cm^{-1} (*c*). In turn, 1004 cm^{-1} (*d*) suggests the presence of cellulose in higher amounts in leaves. Concerning the spectral band 1153 cm^{-1} (*h*), it is considered specific to the glyosidic linkage between galactose units in xyloglucan, a common hemicellulose (Chylinska *et al*., 2016). In respect to 1589 cm^{-1} (*l*), and contrary to what was expected, this spectral band was assigned to specific vibrations in the backbone of lignin, indicating that this molecule is present in higher amounts in leaves (Fig. 21B; Lupoi *et al*., 2015). Concerning 1728 cm^{-1} (*o*) it may suggest the presence of ester linkages in *p*-coumaric and ferulic acids present in lignin, and also predict higher amounts of lignin in leaves, once again unexpectedly (Fig. 21B). Nonetheless, at the wavenumber of 1728 cm^{-1} other compounds may have their absorptions bands overlapped, like C=O stretching vibration of the acetyl and uronic ester groups in pectic polysaccharides, or even so hemicelluloses. (Mandal and Chakrabarty, 2011). On the other hand, according with Sain, and Panthapulakkal (2006) this spectral area is highly specific for lignin polymers that are associated to hemicellulose fibers, so it is possible to suggest that both compounds are being detected here these results (Fig 21).

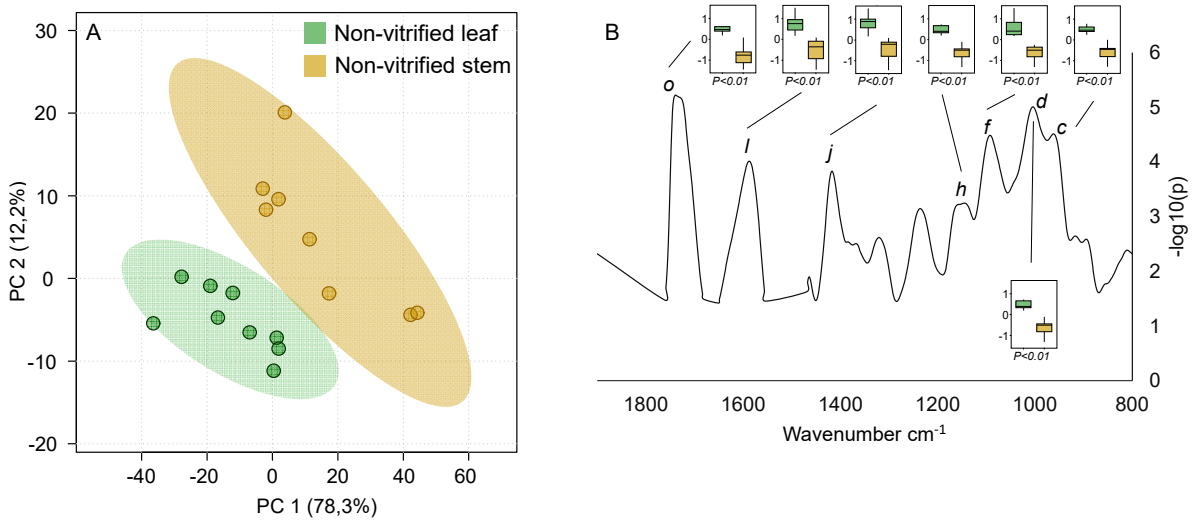

Figure 21. Principal component analysis of the FTIR-ATR spectra of selected samples from AIR biomass of the non-vitrified leaves and non-vitrified stems. (A) Plot of principal component one (PC1) and principal component two (PC2) scores for selected samples. (B) *t*-test with box-and-whisker plots indicating the amounts of the compounds in each tissue ($P<0.01$

for all the assigned compounds). Spectral bands: 962 cm^{-1} (*c*); 1004 cm^{-1} (*d*); 1093 cm^{-1} (*f*); 1153 cm^{-1} (*h*); 1419 cm^{-1} (*j*); 1589 cm^{-1} (*l*); 1728 cm^{-1}(*o*).

Regarding the PCA model for vitrified leaves and vitrified stems, clustering occurred along PC1 that captured 92.5% of variance (Fig. 22A), even so a *t*-test was considered more advantageous to the assessment of chemical differences. The box-and-whisker plots show that all the compounds were found in higher amounts in vitrified leaves comparing with vitrified stems (Fig. 22B). Two spectral bands were assigned to pectin, the well-defined 1760 cm^{-1}(*p*) related to stretching vibrations in carboxylate groups (Chylinska *et al*., 2016; Golubtsova, 2017), and the smooth spectral are assigned by 1093 cm^{-1} (*f*). In turn, cellulose was identified by the bands at 931 cm^{-1} (*b*) and 1120 cm^{-1} (*g*). Once again, the spectral bands 1463 cm^{-1}, 1600 cm^{-1} and 1700 cm^{-1} suggest the presence of lignin in higher amounts in leaves than in stems (Fig. 22B), despite contrary to what would be expected. On the other hand, Park *et al*. (2013) found that the spectral band 1700 cm^{-1} could also indicate other functional groups like ketones, esters, aldehydes and carboxyls from uronic acids that may suggest pectic polysaccharides, and/or aromatic structures such as lignin.

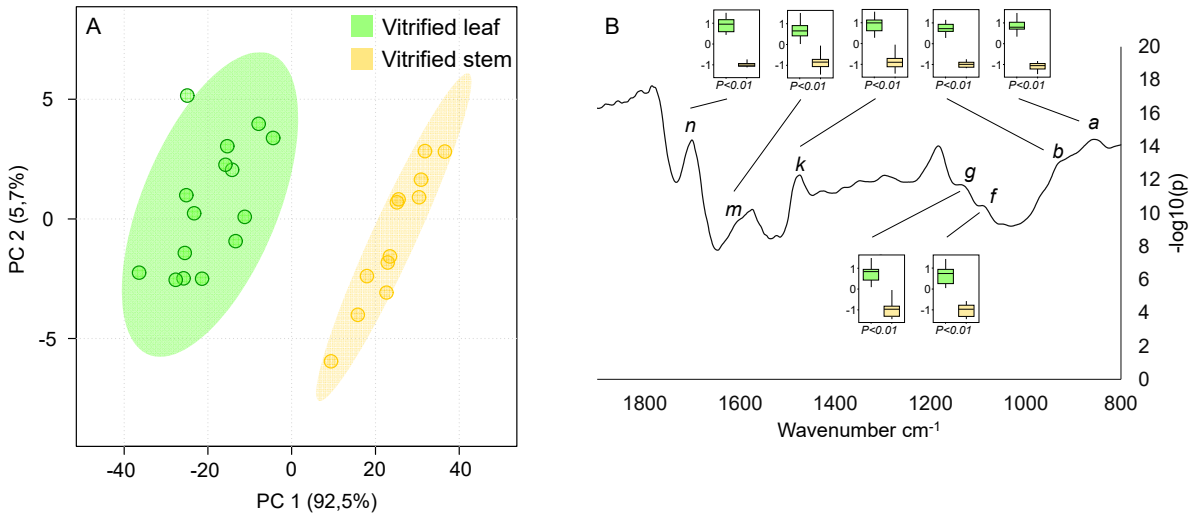

Figure 22. Principal component analysis of the FTIR-ATR spectra of selected samples from AIR biomass of the vitrified leaves and vitrified stems. (A) Plot of principal component one (PC1) and principal component two (PC2) scores for selected samples. (B) *t*-test with box-and-whisker plots indicating the amounts of the compounds in each tissue ($P<0.01$ for all the assigned compounds). Spectral bands: 860 cm^{-1} (*a*); 931 cm^{-1} (*b*); 1093 cm^{-1} (*f*); 1120 cm^{-1} (*g*); 1463 cm^{-1} (*k*); 1600 cm^{-1} (*m*); 1700 cm^{-1} (*n*).

Concerning the PCA model to assess the chemical differences between non-vitrified leaves and vitrified leaves, it was found that clustering occurred along PC2 that captured 8.4% of variance, despite 81.3% of variance is explained by PC1 (Fig. 23A). A *t*-test was performed to determine the main compounds responsible for the distinction between both groups (Fig. 23B). The distinct spectral areas 1060 cm^{-1} (*e*) and 1120 cm^{-1} (*g*) were both assigned to cellulose, as well the less noticeable spectral band 1280 cm^{-1} (*i*), while the noticeable shoulder at 1153 cm^{-1} (*h*) was attributed to xyloglucan. The band around 1760 cm^{-1} (*p*) was the only that could be related to pectins. These results suggest that the chemical differences regarding the cell wall of non-vitrified and vitrified leaves are much more related to cellulose, than matrix polysaccharides like pectin or hemicelluloses, and since none attribution was made to lignin, implies that this compound does not cause any segregation between both type of leaves.

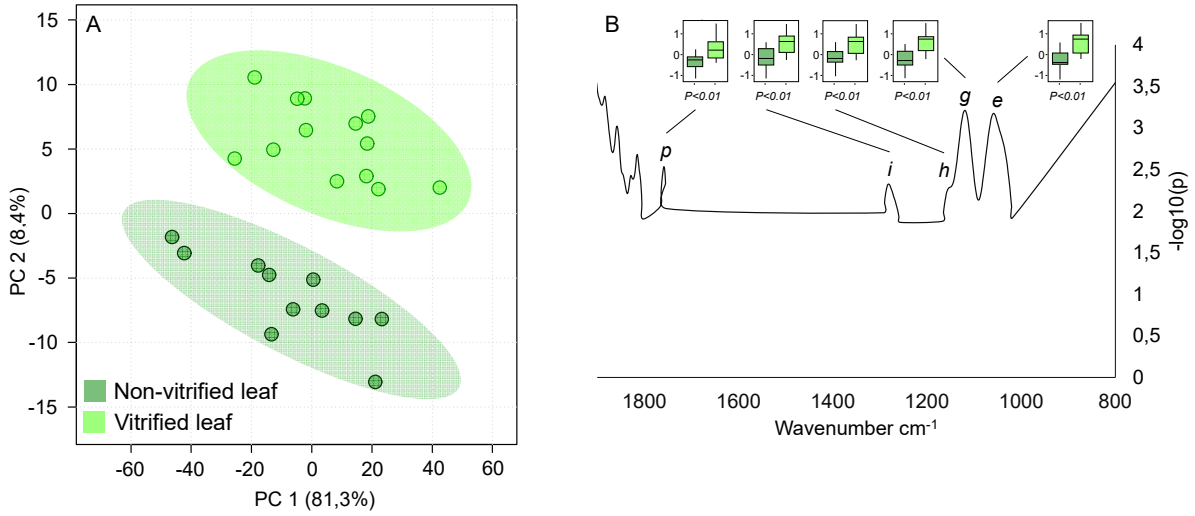

Figure 23. Principal component analysis of the FTIR-ATR spectra of selected samples from AIR biomass of the non-vitrified leaves and vitrified leaves. (A) Plot of principal component one (PC1) and principal component two (PC2) scores for selected samples. (B) *t*-test with box-and-whisker plots indicating the amounts of the compounds in each tissue ($P<0.01$ for all the assigned compounds). Spectral bands: 1060 cm^{-1} (*e*); 1120 cm^{-1} (*g*); 1153 cm^{-1} (*h*); 1280 cm^{-1} (*i*); 1760 cm^{-1} (*p*).

In respect to the PCA model constructed to distinguish non-vitrified from vitrified stems, segregation occurred mainly along PC1 that explains 92.5% of variance contrary to PC2 that captured just 5.7% (Fig. 24A). A *t*-test was performed to assess chemical differences (Fig. 24B). The spectral band at 931 cm^{-1} (*b*) was assigned both with cellulose and hemicelluloses as

previously discussed, and the shoulder around 1120 cm^{-1} (*g*) assigned to cellulose, as well as the smooth band at 1280 cm^{-1} (*i*). In turn, the spectral bands 1419 cm^{-1} (*j*) and 1760 cm^{-1} (*p*) are both suggesting the presence of higher amounts of esterified pectic polysaccharides in non-vitrified stems comparing to vitrified stems. As expected, regarding the spectral bands 1463 cm^{-1}(*k*) and 1589 cm^{-1} (*l*), these assignments are indicative that in non-vitrified stems, lignin is synthesized an incorporated in the cell wall in higher amounts. Finally, the spectral area defined by 1700 cm^{-1} (*n*) could either suggest the presence of lignin, or polysaccharides like hemicelluloses, as previous discussed (Fig. 22; Park *et al*., 2013).

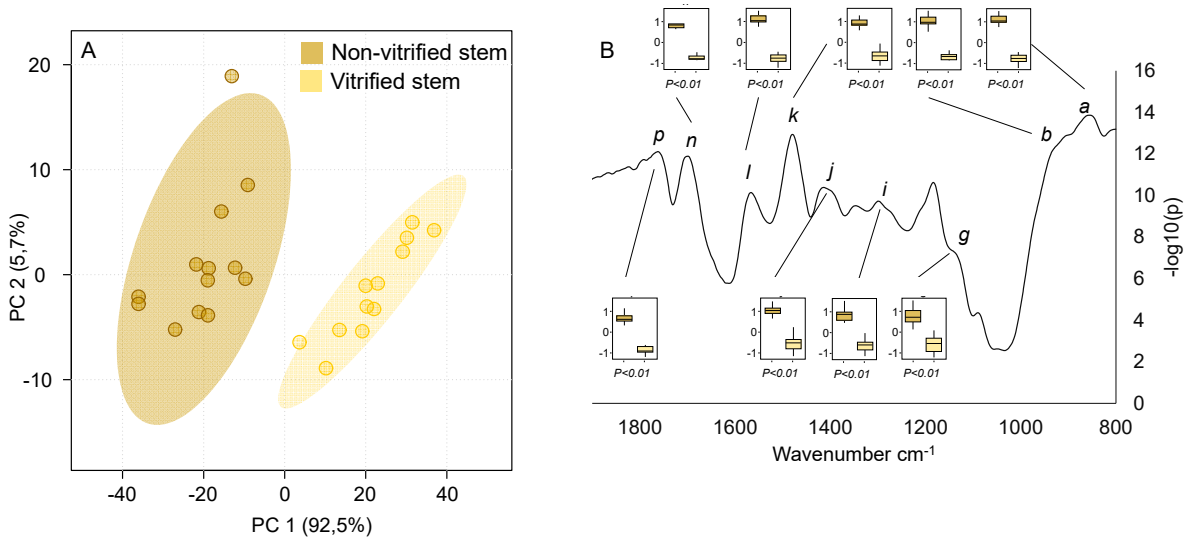

Figure 24. Principal component analysis of the FTIR-ATR spectra of selected samples from AIR biomass of the non-vitrified stems and vitrified stems. (A) Plot of principal component one (PC1) and principal component two (PC2) scores for selected samples. (B) *t*-test with box-and-whisker plots indicating the amounts of the compounds in each tissue ($P<0.01$ for all the assigned compounds). Spectral bands: 860 cm^{-1} (*a*); 931 cm^{-1} (*b*); 1120 cm^{-1} (*g*); 1280 cm^{-1} (*i*); 1419 cm^{-1} (*j*); 1463 cm^{-1}(*k*); 1589 cm^{-1} (*l*); 1700 cm^{-1} (*n*); 1760 cm^{-1} (*p*).

3.3 Acetyl bromide soluble lignin measurement

Given the complexity of the lignin macromolecule, an analytical method for the absolute determination of lignin in plant biomass does not exist (Fukushima and Hatfield, 2004). However, one method, the acetyl bromide soluble lignin (ABSL) procedure, which relies on lignin solubilization followed by the determination of absorbance at 280 nm, has been privileged (da Costa *et al*., 2015). Reasons for this have to do with it being precise, relatively straightforward, and because it may be used with little sample amounts (Fukushima and Dehority, 2000).

Lignin content is expressed as acetyl bromide soluble lignin percentage (ABSL%) of cell wall biomass dry weight (Table 5). Unfortunately, the ABSL ANOVA did not confirm statistical differences (P>0.05 for both leaves and stems; Fig. 25), even though the respective effect sizes were determined: $\eta^2_{\text{plant organ}} = 0.06$; $\eta^2_{\textit{in vitro}\text{ condition}} = 0.09$; $\eta^2_{\text{plant organ x }\textit{in vitro}\text{ condition}} = 0.67$. Nonetheless, the ABSL analysis was very informative when comparing the mean values within the same plant organ. Hence, the mean lignin content in leaves was found to be higher in the tree, followed by *in vitro* non-vitrified leaves, and lastly lower mean values were registered for vitrified leaves. The same pattern of lignin content was observed for stems (Table 5). However, surprising and unexpected, when comparing the mean values for each plant organ, it was found that leaves showed higher lignin content than stems (Fig. 25; Table 5).

These results are strongly supported by FTIR spectroscopy that has predicted these same results for the cell wall biomass (Fig. 21 and 22; section 3.2.3.). For the best of our knowledge, lignin determinations in *A. unedo* are here reported for the first time, but ABSL lignin was already reported for stems of *Arbutus menziesii* Pursh, native of North America (Agarwal *et al*., 2019). These authors found that ABSL was around 17.7% in *A. menziesii* stems, which is exactly the same value here presented for the ABSL of stems from the tree (Table 5.). According to these authors, the lignin content in the American madrone is lower when compared with dicot species like *Populus deltoides* Marshall 25.7 %, *Salix babylonica* L. 24.4% and *Carya ovata* (Mill.) K. Koch 23.2%. Nonetheless *A. menziesii* ABSL lignin content revealed to be slightly superior in comparison to either *Betula papyrifera* Marshall 15.4% or *Populus tremuloides* Michx. 15.1%. Regardless of what has been observed in other species, the higher amounts of lignin found in leaf samples when compared with stems, was an expected result that needs further analysis.

The ABSL method has some drawbacks since, it may overestimate lignin content due to oxidative degradation of cell wall matrix polysaccharides (hemicelluloses and pectin) during

the incubation with the acid solution. Therefore, it cannot be excluded that the higher values obtained during the analysis of leaf samples may in fact be due to degraded xyloglucan, xylan and pectin, which are typically more abundant in foliar biomass, and have strong absorbance at 280 nm (Moreira Vilar, 2014; Fagerstedt, 2015). To confirm this hypothesis, more studies are needed, namely the determination of matrix polysaccharides and the abundance of phenolic acids, such as hydroxycinnamates. For the first ones, the samples for this analysis are already prepared following the TFA procedure (trifluoroacetic acid hydrolysis), however, due to time constraints, it was not possible to analyze these samples by HPLC-RI (High-Performance Liquid Chromatography coupled to Refractive Index detector). Another approach may consist of determining lignin percentages by complementary methods, such as the Klason, or the acid detergent lignin determination procedures (Fukushima and Hatfield, 2004).

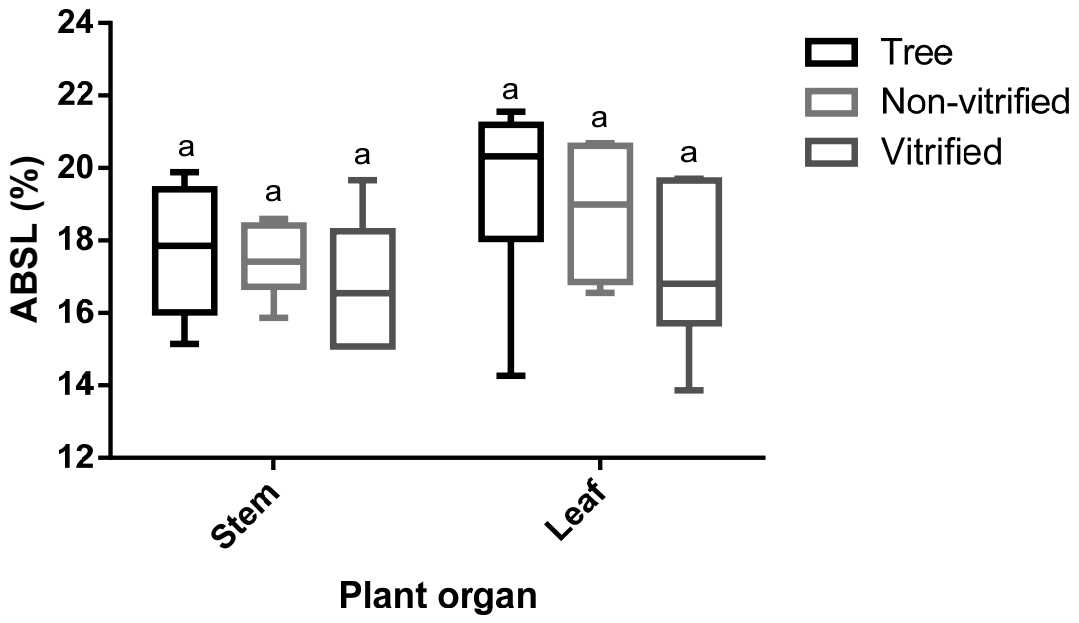

Figure 25. Distribution of acetyl bromide soluble lignin (ABSL) measurements as percentage of CWM from leaf and stem from tree tissues, *in vitro* non-vitrified tissues and *in vitro* vitrified tissues. Means were statistically compared using two-way ANOVA followed by a Tukey's test (different superscript letters indicate significant differences at $P<0.05$).

Table 5. Acetyl bromide lignin (ABSL) per percentage of cell wall material dry weight (% CWM). Values are mean ± standard deviation. N = 36 (6 × 3 × 2), six plant replicates were selected between the three types of tissues and between the two organs.

Plant organ	Leaf	Stem
Tree	19.42 ± 2.64	17.72 ± 1.64
Non-vitrified	18.79 ± 1.97	17.44 ± 0.99
Vitrified	17.19 ± 2.21	16.78 ± 1.75
Mean	18.47 ± 1.15	17.31 ± 0.48

3.4 Total carbohydrates estimation in the cell wall

The phenol-sulfuric acid method is an easy and rapid way of estimating virtually all classes of carbohydrates. However, the measured absorbance may vary since saccharide conversion into furfural is not completely achieved, thus the results must be expressed arbitrarily as equivalents of glucose (da Costa, 2016).

Total carbohydrates are expressed per percentage of cell wall material dry weight (Table 6). According to the performed ANOVA for the total carbohydrates estimation, significant statistical differences (P<0.05) were confirmed between leaf and stem samples, proving to be the main source of variation (η^2=8.09). In turn, no statistical significance (P>0.05) was found either, when comparing different tissues sources (tree, non-vitrified, vitrified) within the same plant organ, or in respect to the interaction of both factors (P>0.05). According to the results, the yield of carbohydrates in stems is much higher in stems when comparing within leaf samples (Fig. 26; Table 6). Despite no significant differences had been found, a slight increase in total carbohydrates content occurs from *in vitro* vitrified leaves to the tree leaves (Fig. 26; Table 6). Likewise, no statistical significance was found within stem samples, however the increasing pattern is here more evident from *in vitro* vitrified stems to the tree stems (Fig. 26; Table 6).

In an attempt to the preliminary nature of these results, for the estimation of sugars in different types of vegetative biomass of *A. unedo*., it is important to correlate these data with in-depth results acquired by HPLC-RI. The samples prepared following the TFA hydrolysis procedure were already prepared, but due to technical difficulties they could not be analyzed in time for this work deadline.

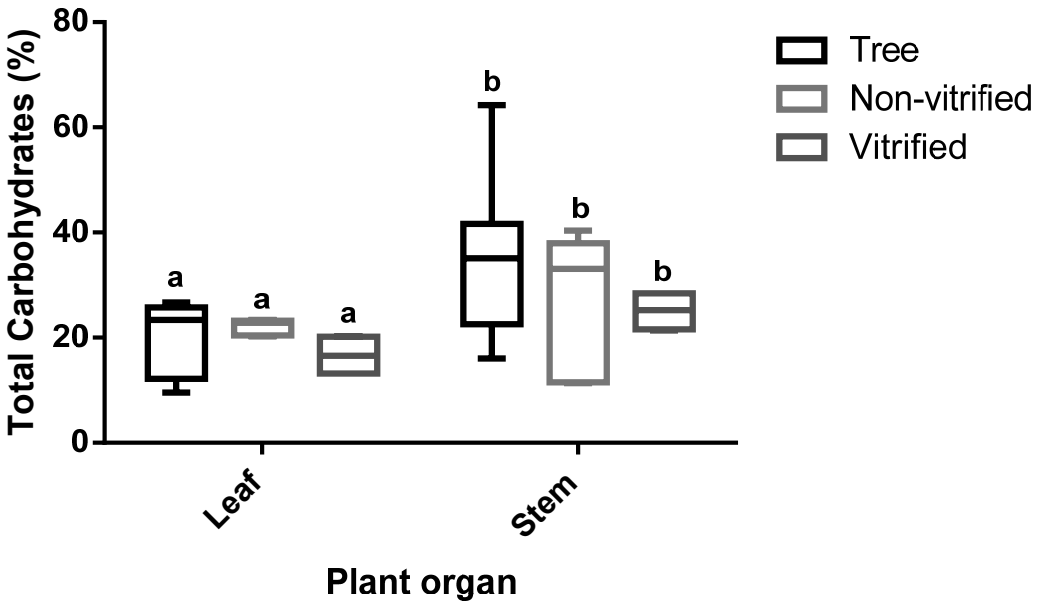

Figure 26. Distribution of the total carbohydrates measurements as percentage of CWM from leaf and stem from tree tissues, *in vitro* non-vitrified tissues and *in vitro* vitrified tissues. Means were statistically compared using two-way ANOVA followed by a Tukey's test (different superscript letters indicate significant differences at $P<0.05$).

Table 6. Total carbohydrates per percentage of cell wall material dry weight (% CWM). Values are mean ± standard deviation. N = 36 (6 × 3 × 2), six plant replicates were selected between the three types of tissues and between the two organs.

Plant organ	Leaf	Stem
Tree	20.34 ± 7.06	35.14 ± 13.72
Non-vitrified	22.16 ± 1.41	27.76 ± 12.93
Vitrified	16.65 ± 3.98	25.08 ± 3.86
Mean	19.72 ± 2.81	29.33 ± 5.21

3.5 Anatomical studies

3.5.1 Microscopy analysis of stems from an *A. unedo* tree

The cross sections of strawberry tree stem growing in the greenhouse, stained with toluidine blue (Fig. 27A) and calcofluor white (Fig. 27B) revealed secondary vascular differentiation of xylem, being possible to discern the earlywood and latewood growth rings.

According to Schweingruber *et al*. (2011), the xylem of *A. unedo* is classified as semi-ring-porous, the vessels are typically arranged in radial multiples and parenchyma is absent, which is supported by these observations (Fig. 27A, 27B and 27C). Within the Ericaceae family, the anatomy of the xylem is quite homogenous, however there some exceptions in contrast to the observations made in the genus *Arbutus*, such as *Erica scoparia* L. in which the xylem is diffuse-purous with solitary vessels, and the genus *Vaccinium* which has scalariform-perforated vessels (Schweingruber *et al*., 2011). In order to the ruthenium red staining, it was possible to distinguish phloem, xylem, and the vascular cambium in a line where cells appear to be disrupted (Fig. 27C). The cell walls of phloemic fibers revealed to have more affinity for this dye when compared with the cell walls in xylem that were barely stained, indicating that phloem cell walls are pectin enriched (Fig. 27C). The reason for these differences it has to do with the fact that xylem is mostly constituted by secondary cell walls, which have low amounts, or no pectin at all (Knox, 2008; Srivastava *et al*., 2017).

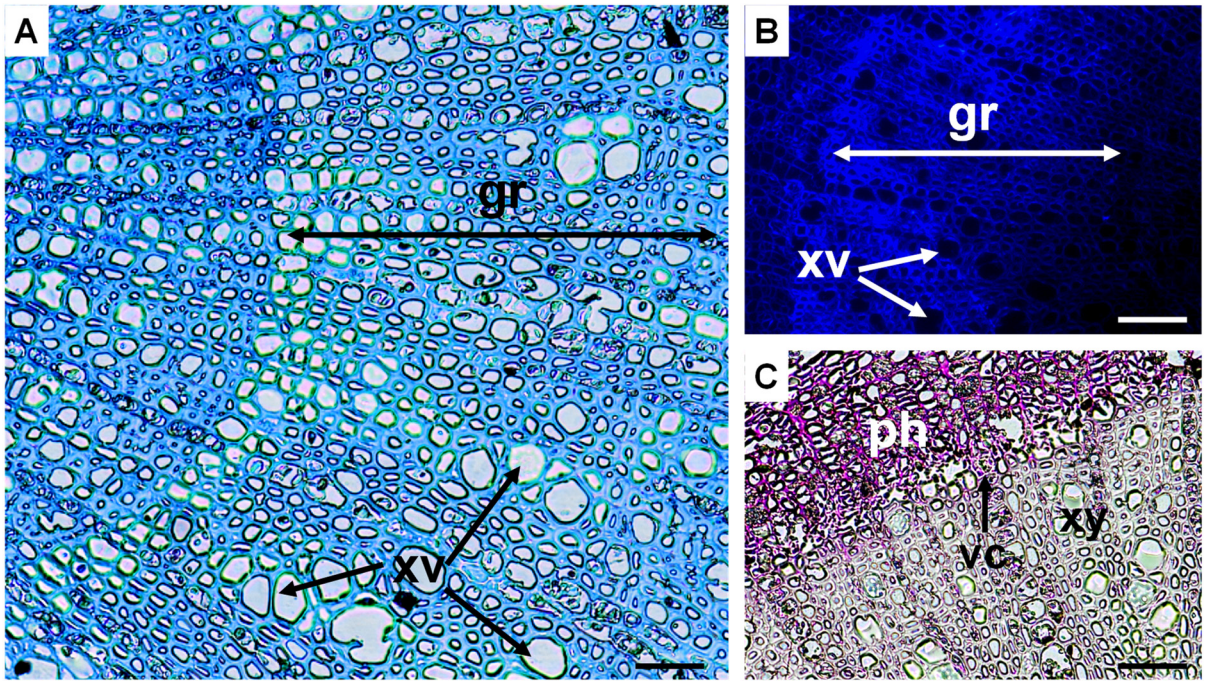

Figure 27. Light (A and C) and fluorescence (B) microscopy of the stem from an *A. unedo* tree growing in a greenhouse. (A) Cross section stained with toluidine blue. (B) Cross section treated with calcofluor white. (C) Cross section stained with ruthenium red. ph - phloem, gr - growth rings, vc - vascular cambium, xv - xylem vessels, xy - xylem. Bars = 50 µm.

The stem of the same plant was also analyzed by scanning electron microscopy (SEM), revealing other anatomical features (Fig. 28). Thus, glandular and non-glandular trichomes could be observed (Fig. 28A). According to Dias (2014), both types of trichomes are frequently

found in the surface of young stems, however as lignification occurs the structures will degenerate and will be less abundant in mature stems. A well-differentiated and organized epidermis is observed, where some stomata were present (Fig. 28A) The cross section of the stem revealed a typical dicot organization with well-differentiated tissues, such as the central pith, the development of secondary xylem, and a thickened periderm (Fig. 28B). The semi-porous xylem and the arrangement of vessels in radial multiples, as reported by Schweingruber *et al*. (2011), were anatomical features also observed in these SEM micrographs (Fig. 28B).

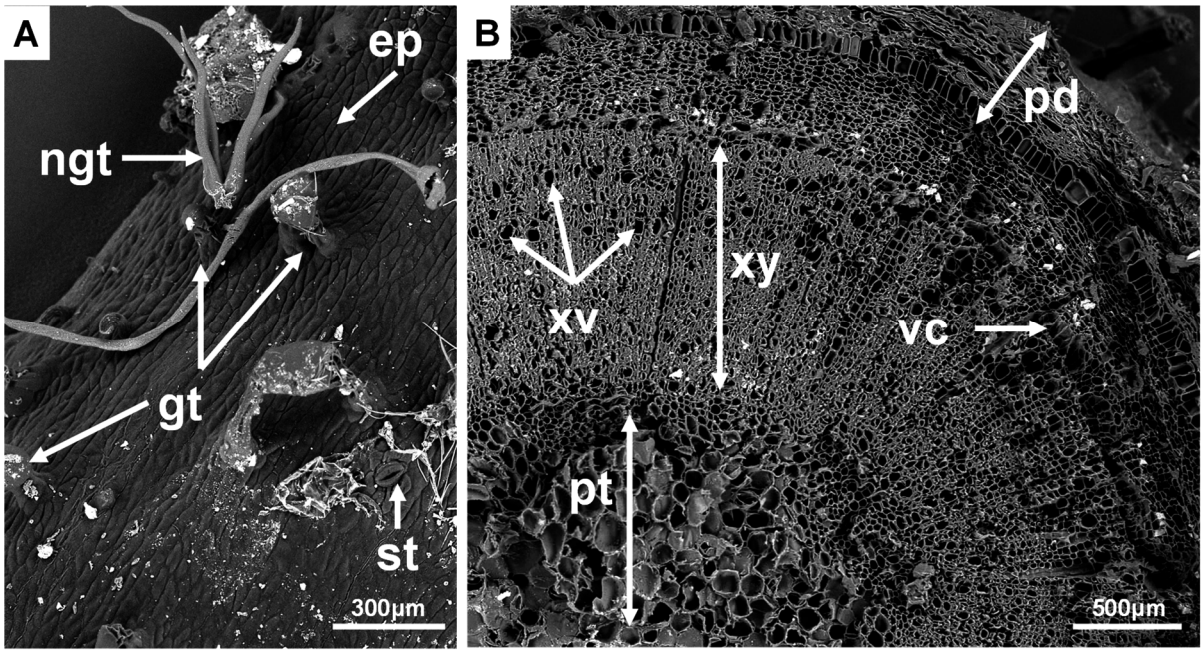

Figure 28. SEM analysis of the stem from an *A. unedo* tree growing in a greenhouse. (A) Stem surface. (B) Cross section. ep - epidermis, gt - glandular trichomes, ngt - non-glandular trichomes, pd - periderm, pt - pith, st - stoma, vc - vascular cambium, xv - xylem vessels, xy - xylem.

3.5.2 Microscopy analysis of non-vitrified stems from *in vitro* shoots of *A. unedo*

When cross sections of *in vitro* non-vitrified shoots were observed (Fig. 29A, 29B and 29C), it was found that the same type of organization than observed in an adult tree occurs. Calcofluor white and the cross section stained with toluidine blue revealed a broad area of xylem (Fig. 29A and 29B). An intense staining with ruthenium red in the outer layers of the stem might suggest that the periderm is rich in pectic polysaccharides, in contrast to the inner part like the xylem vessels where staining revealed to be less efficient (Fig. 29C). Regarding

the periderm, which includes the phellem (suber), phellogen and phelloderm layers, it was not possible to distinguish these tissues that are quite smashed in a compacted layer (Fig. 29B and 29C). However, it is important to highlight the fact that according to Schweingruber *et al.* (2011) the Ericaceae periderm is quite homogeneous within the family, but the phellem layer could comprise from one to several layers of rectangular cells.

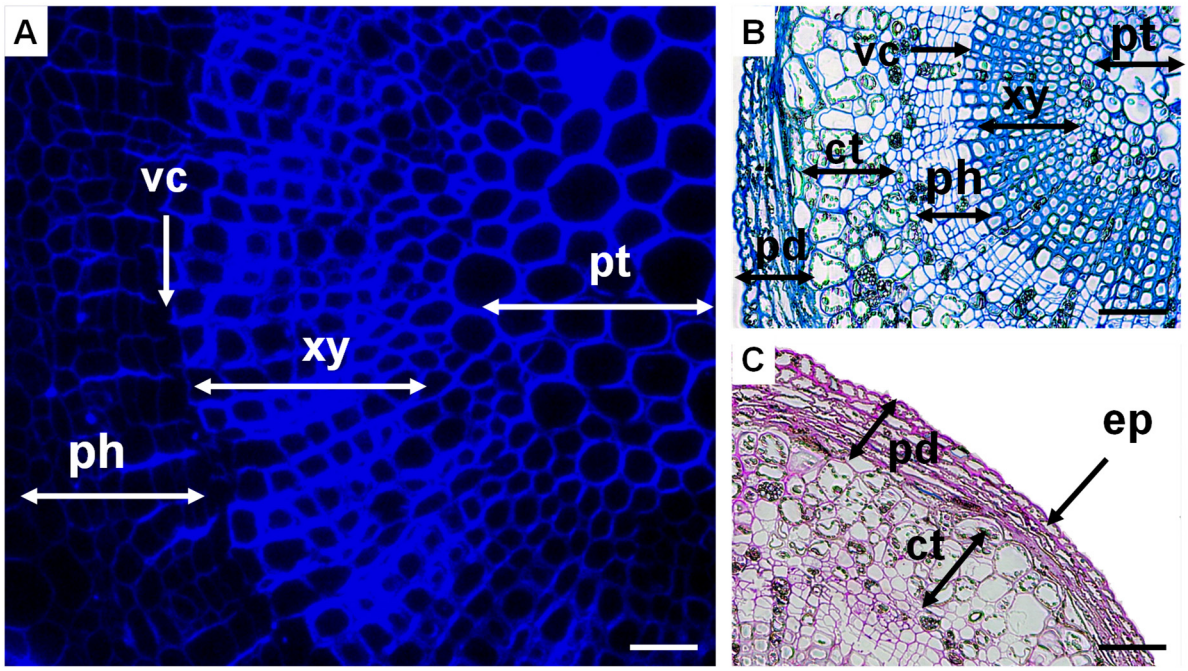

Figure 29. Light (B and C) and fluorescence (A) microscopy of *A. unedo* non-vitrified stems from *in vitro* shoots cultured in solid medium. (A) Cross section treated with calcofluor white. (B) Cross section stained with toluidine blue. (C) Cross section stained with ruthenium red. ct - cortex, ep - epidermis, pd - is the periderm layer, ph - phloem, pt - is the pith, vc - vascular cambium, xy - xylem. Bars = 50 µm.

SEM analysis of the cross section of the stem showed the typical organization of this plant organ, in which some secondary growth already occurred. Moreover, sclerenchyma cells were found in the pith (Fig. 30A; Zeiger *et al.*, 2015). Several glandular and non-glandular trichomes could be observed at the surface of the stem (Fig. 30B and 30C), as previously reported by Dias (2014).

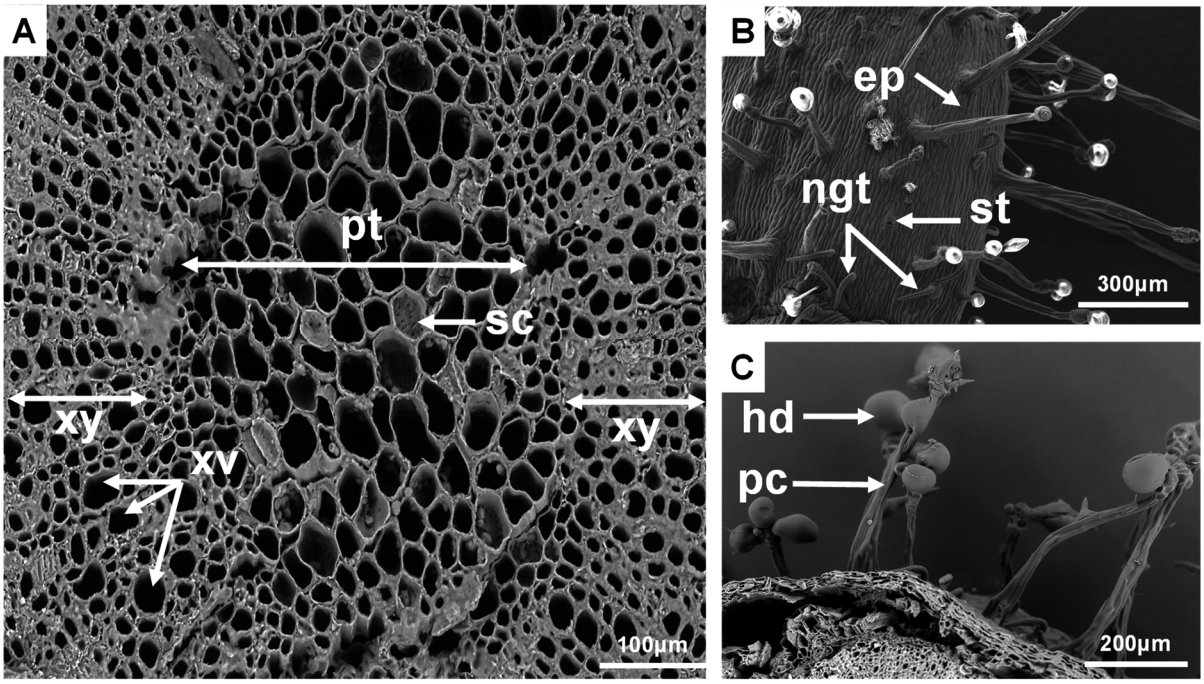

Figure 30. SEM analysis of *A. unedo* non-vitrified stems from *in vitro* shoots cultured in solid medium. (A) Cross section, (B) Stem surface, (C) Cross section showing the periphery of the stem. ep - epidermis, hd - secretory head of the trichome, ngt - non-glandular trichomes, pc - peduncle of the trichome, pt - pith, sc - sclerenchyma cells, st - stoma, (xv) xylem vessels, xy - xylem.

3.5.3 Microscopy analysis of vitrified stems from *in vitro* shoots of *A. unedo*

Cross sections of the stem showed a poorly developed periderm with two evident layers below the epidermis (Fig. 31A, 31B and 31C). The phellem (suber) was identified as a single layer of rectangular cells localized immediately bellow the epidermis. Henceforward, it is possible to suggest that the phellogen is localized below the phellem layer (Fig. 31A, 31B and 31C; Schweingruber *et al*., 2011). The cortex appears to be hypertrophic and the cells are somewhat spaced (Fig. 31A, 31B and 31C), an anomalous feature previously reported for *in vitro* vitrified stems of jojoba, *Simmondsia chinensis* (Link) Schn. (Apóstolo and Llorente, 2000). Regarding the vascular bundles, secondary vascular tissues are observed to be less differentiated in vitrified stems, suggesting an incipient development of the vascular cambium and reduced lignification of the xylem that reflects the lack of differentiated vessels (Fig. 31A, 31B and 31C). All these anomalies are correlated to what was previously observed in vitrified stems of *Solanum melanogena* L. (Picoli *et al*., 2001) and *Castanea sativa* Mill. (Ziv and Chen, 2008). Additionally, regarding the calcofluor staining unexpected isolated sclerenchyma cells

were identified between the cortex region and the vascular bundle (Fig. 31B), despite Ziv (1991) argued that vitrified stems lack sclerenchymatous tissue. Moreover, it was observed a filiform-shaped non-glandular trichome in the epidermis (Fig. 31B), as previously described by Dias (2014).

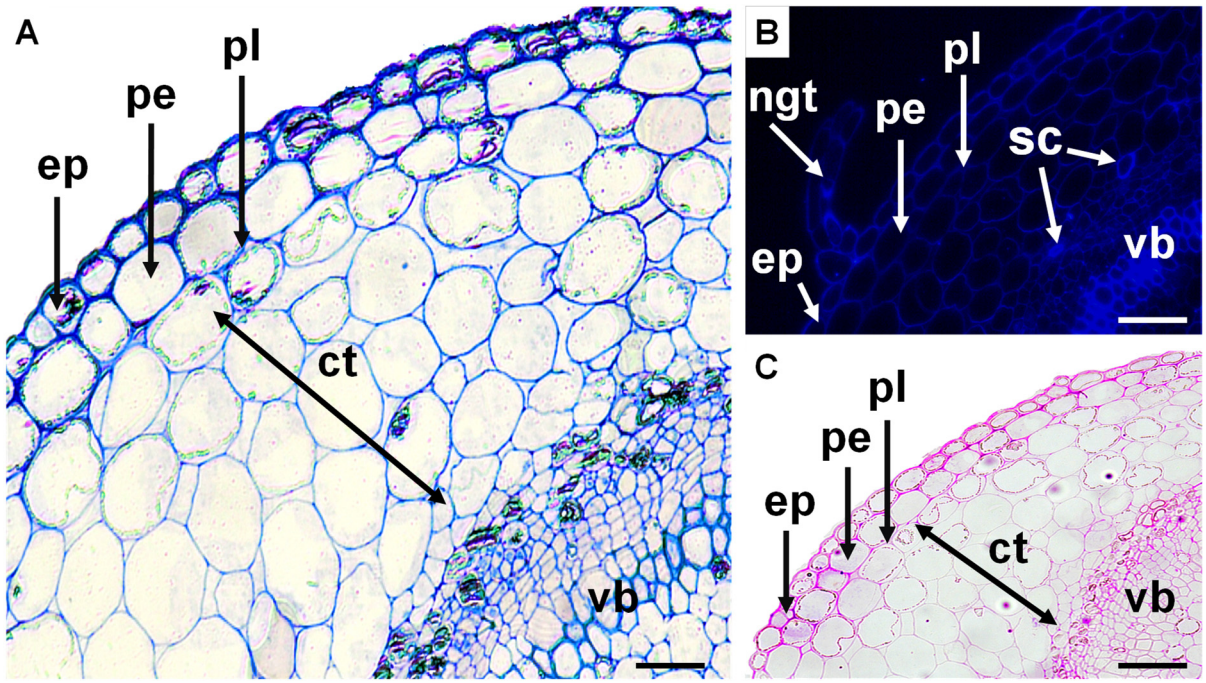

Figure 31. Light (A and C) and fluorescence (B) microscopy of *A. unedo* vitrified stems from *in vitro* shoots cultured in liquid medium. (A) Cross section stained with toluidine blue. (B) Cross section treated with calcofluor white. (C) Transversal section stained with ruthenium red. ep - epidermis, ct - cortex, ngt - non-glandular trichome, pe - phellem, pl - phellogen, sc - sclerenchyma cells, vb - vascular bundle. Bars = 50 µm.

SEM observations of vitrified stems showed that, the hyperhydricity-related features were not so evident in this organ, as it happens in leaves (Ziv, 1991). Unfortunately, cross sectioned vitrified stems left many anatomic features to unveil, since the tissues were smashed by cutting, showing how delicate is the structure of vitrified stems (Fig. 32A). According to Apóstolo and Llorente (2000), the reduced synthesis of lignin and the incipient development of secondary vascular tissues might be the explanation for such fragility. Regarding the glandular trichomes (Fig. 32B), they seem to present underdeveloped heads when compared with the trichomes of non-vitrified stems (Fig. 30C), which might be due to reduced synthesis and accumulation of secretory substances in vitrified stems. Moreover, the peduncle seems to be somewhat twisted, what could indicate any morphology abnormality. Concerning the non-glandular trichomes, these observations are correlated with the reported by Dias (2014) that

described them as filiform, with a slightly granulose surface and appearing prostrated in the stem surface, as here shown (Fig. 32B).

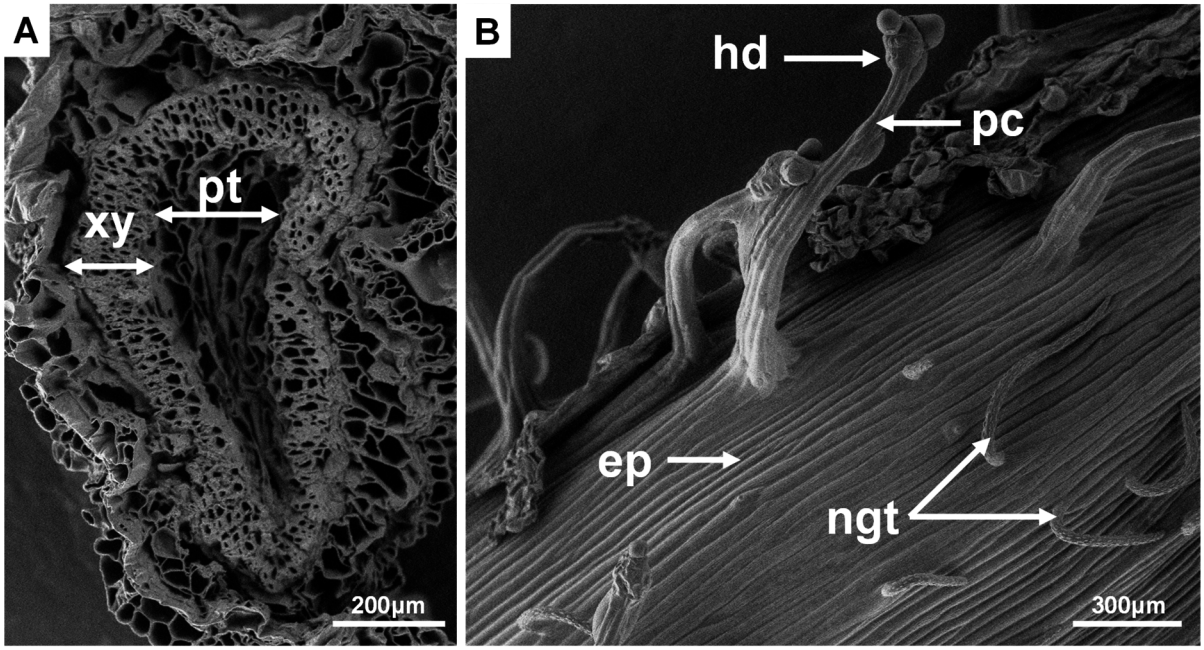

Figure 32. SEM analysis of *A. unedo* vitrified stems from *in vitro* shoots cultured in liquid medium. (A) Cross section. (B) Stem surface. ep - epidermis, hd - secretory head of the trichome, ngt - non-glandular trichomes, pc - peduncle of the trichome, pt - pith, xy - xylem.

3.5.4 Microscopy analysis of leaves from an *A. unedo* tree

Cross sections of leaf samples from a tree growing in a greenhouse, observed at the midrib region, revealed that leaves have a well-differentiated epidermis with thickened cell walls, which are covered by a dense cuticle (Fig 33A). The cortex, made up of several layers of parenchyma cells, possess also some scattered sclerenchyma cells (Fig. 33A, 33B and 33C). At the center of the midrib a well-developed xylem was present (Fig. 33A, 33B and 33C). When fluorescence microscopy was used following a treatment of the tissues with calcofluor white, xylem vessels and sclerenchyma thickened cell walls showed to be highly fluorescent (Fig. 33B). Regarding ruthenium red staining, it was possible to notice a higher intensity staining at the epidermis and at the cortex region, suggesting that acidic polysaccharides like pectin are present in higher amounts in these cell walls **(**Fig. 33C**)**. On the contrary, xylem vessels and sclerenchyma cells showed to be slightly stained, indicating that thickened secondary cell walls

lack polysaccharides like pectin in large amounts (Fig. 33C; Knox, 2008; Srivastava *et al*., 2017).

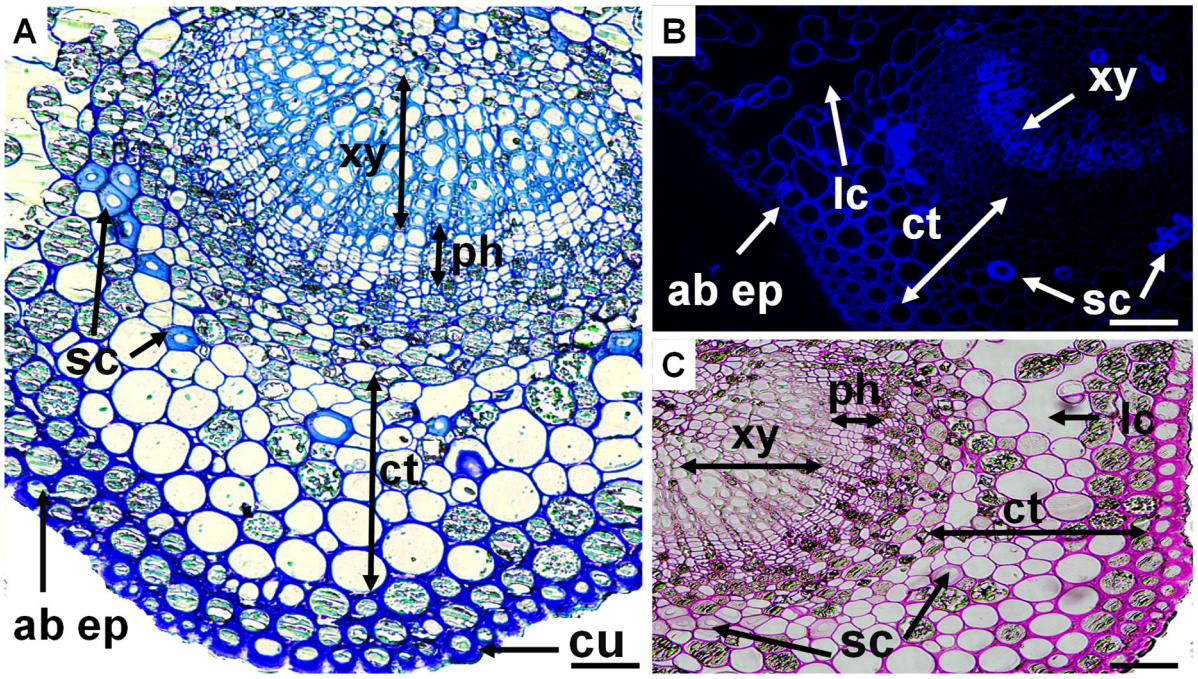

Figure 33. Light (A and C) and fluorescence (B) microscopy of leaves from an *A. unedo* tree growing in a greenhouse. (A) Cross section stained with toluidine blue. (B) Cross section treated with calcofluor white. (C) Cross section stained with ruthenium red. ab ep - abaxial surface epidermis, ct - cortex area, cu - cuticle, lc - lacunae, ph - phloem, sc - sclerenchyma cells, xy - xylem. Bars = 50 µm.

SEM observations of these leaves confirmed the presence of a well-organized and developed epidermis with thickened cell walls and covered by a thick cuticle in the abaxial surface (Fig. 34A). Thickened cell walls at the epidermis and dense cuticles broad covered by waxes, are reported as xeromorphic characteristics that *A. unedo* developed to resist severe periods of drought in the Mediterranean macchia (Rotondi *et al*., 2003). According to these authors, many of these morphologic features, have also been observed in other species typical of the Mediterranean region such as *Myrtus communis*, *Olea europaea* and several *Quercus* species. A relationship between these features, and a protection against intense UV-B radiation during summer season, has been suggested (Yadav *et al*., 2004). SEM analysis also showed that the adaxial epidermis has a very wrinkled pattern, probably related to the various environmental stresses to which the species is subjected on its habitat (Fig. 34B). The abaxial surface was covered by many stomata complexes that appear to lack subsidiary cells (Fig. 34C and 34D). According to Rotondi *et al*. (2003) the abaxial surface of *A. unedo* leaves has 177 stomata per

mm^2, each one measuring 2.08 µm in diameter. Other Mediterranean species like *Pistacia lentiscus* have 254 stomata per mm^2, each one measuring 3.64 µm in diameter, while each stoma in *Myrtus communis* measures just 1.67 µm, however the reduced diameter appear to be balanced by the large density of 342 stomata per mm^2.

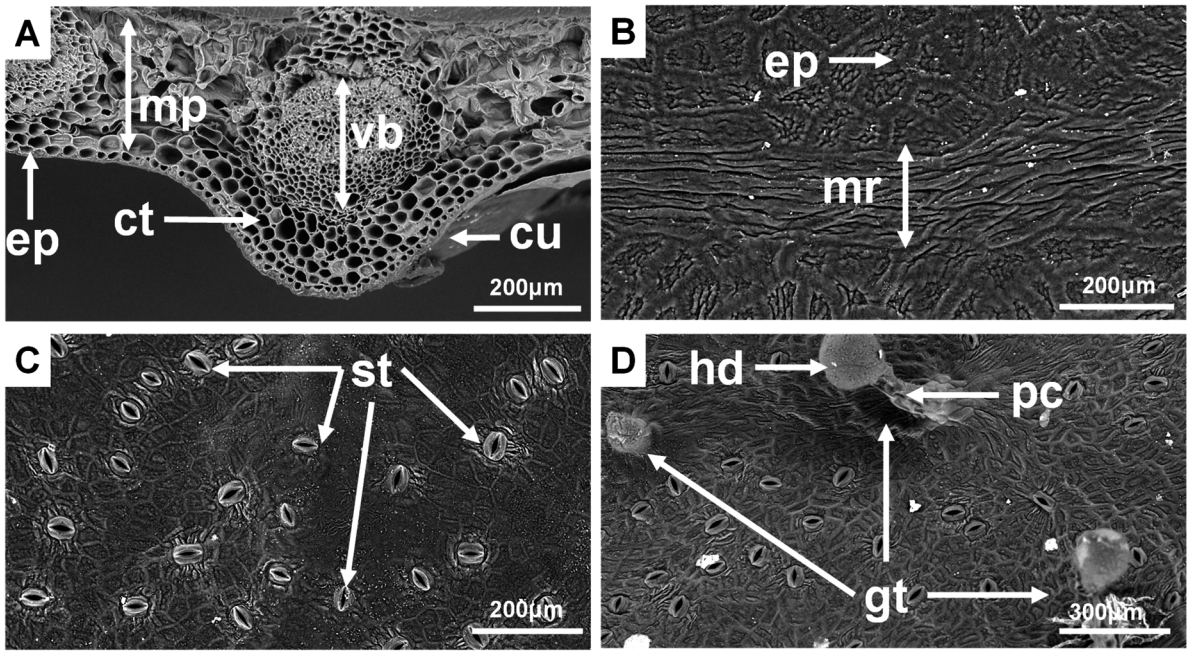

Figure 34. SEM analysis of leaves from an *A. unedo* tree growing in a greenhouse. (A) Cross section at the midrib area. (B) Leaf adaxial surface. (C and D) Leaf abaxial surface. ct - cortex, cu - cuticle, ep - epidermis, gt - glandular trichomes, hd - secretory head of the trichome, mp - mesophyll, mr - midrib, pc - peduncle of the glandular trichome, st - stomata, vb - vascular bundle.

3.5.5 Microscopy analysis of non-vitrified leaves from *in vitro* shoots of *A. unedo*

Microscopy observations of non-vitrified leaves, showed a palisade parenchyma at the adaxial surface, consisting of one or two layers of elongated parenchyma cells (Fig. 35A and 35B). Cross sections of the leaf blade stained with ruthenium red showed stomata complexes in the abaxial leaf surface and a well-differentiated spongy parenchyma with large lacunae (Fig. 35C).

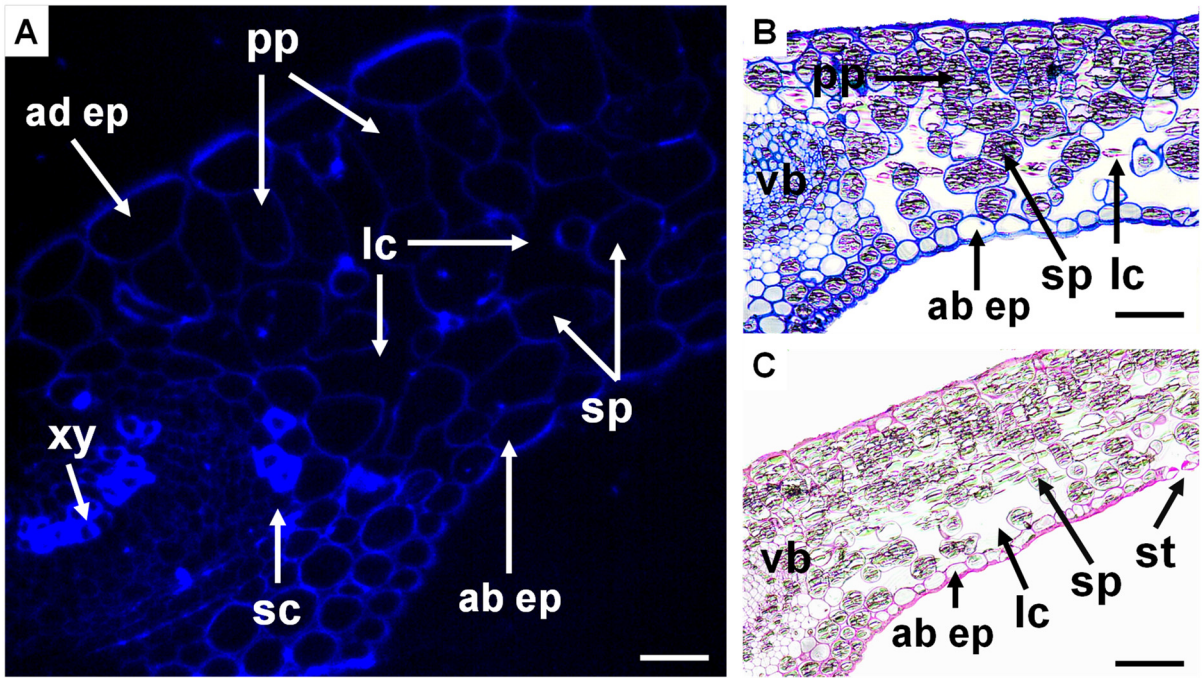

Figure 35. Light (B and C) and fluorescence (A) microscopy of *A. unedo* non-vitrified leaves from *in vitro* shoots cultured in solid medium. (A) Cross section treated with calcofluor white. (B) Cross section stained with toluidine blue. (C) Cross section stained with ruthenium red. ab ep - abaxial surface epidermis, ad ep - adaxial surface epidermis, lc - lacunae, ph - phloem, pp - palisade parenchyma, sc - sclerenchyma cells, sp - spongy parenchyma, st - stomata, vb - vascular bundle, xy - xylem. Bars = 50 µm.

SEM observations of non-vitrified leaves were also carried out and the pattern of epidermal cell distribution in the adaxial surface (Fig. 36A) was completely different from the leaves of the tree (Fig. 34B). Different patterns in the organization of the epidermis reflect the surrounding conditions *in vitro* (Zoubayed *et al*., 2001; Apóstolo *et al*., 2005). According to these authors, high relative humidity and the accumulation of ethylene and CO_2 inside the flasks and tubes, are the principal causes of abnormal stomatal functioning, reduced amounts of epicuticular wax, poor cuticle development and thinner cell walls. Subsequently, plantlets are not able to cope with water stress suffered upon transfer to soil during the acclimatization phase (Apóstolo *et al*., 2005). Anatomical observations made by these authors in leaves of *in vitro* growing shoots of *Cynara scolymus* L., showed that differentiation and growth of roots leads to structural changes in leaves favorable for the survival of plants transferred to soil, including a well-differentiated cuticle, thickened cell walls, functional stomata, better mesophyll organization, developed vascular bundles, and the presence of sclerenchyma cells. Likewise, the same observations were made by Louro *et al*. (1999), during *in vitro* root development of

Eucalyptus urophylla S. T. Blake. Cross sections (Fig. 36B) confirmed what was previously observed by light and fluorescence microscopy (Fig. 35). Notwithstanding, both glandular and non-glandular trichomes were found to be confined around the midrib region, being absent in the rest of the adaxial leaf surface (Fig. 36B), like previously reported by Dias (2014). Regarding the glandular trichomes it is important to highlight the proliferation of epidermal cells raising to a multicellular peduncle (Fig. 36B), as also previously showed by Dias (2014). On the other hand, the epidermis of the abaxial surface are filled with stomata (Fig. 36C), while these structures are absent in the adaxial surface (Fig. 36A), which is also supported by the observations of Yadav *et al*. (2004).

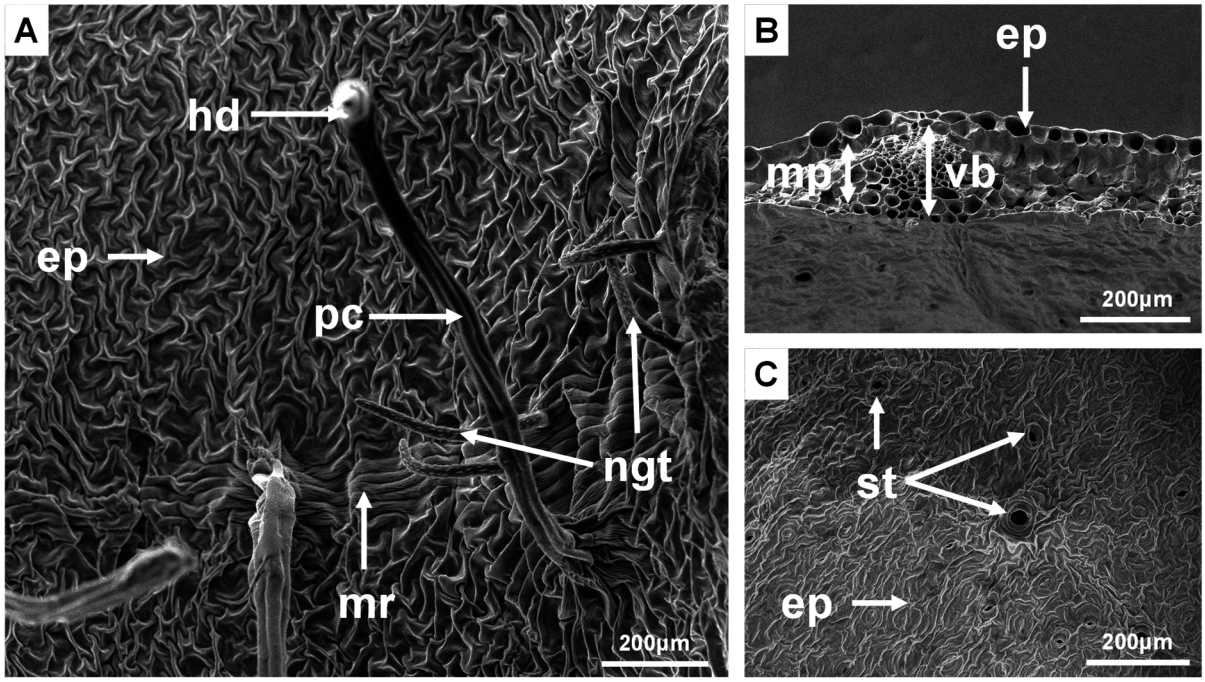

Figure 36. SEM analysis of *A. unedo* non-vitrified leaves from *in vitro* shoots cultured in solid medium. (A) Leaf adaxial surface. (B) Cross section at the midrib area. (C) Leaf abaxial surface. ep - epidermis, hd - secretory head of the trichome, mp - mesophyll, mr - midrib, ngt - non-glandular trichomes, pc - peduncle of the trichome, st - stomata, vb - vascular bundle.

3.5.6 Microscopy analysis of vitrified leaves from *in vitro* shoots of *A. unedo*

According to Ziv (1991), hyperhydricity-related abnormalities are much more evident regarding *in vitro* vitrified leaves, than *in vitro* vitrified stems. The midrib, and partially the mesophyll, were here privileged to analyze the atypical anatomy of vitrified leaves by light and fluorescence microscopy. Vitrified leaves stained only slightly with ruthenium red and toluidine

blue (Fig. 37A and 37C), as well when treated for fluorescence observations with calcofluor white (Fig. 37B), because of the thinner cell walls of the different tissues in these leaves. Both the adaxial and abaxial epidermis, showed to be unorganized and less differentiated than in leaves of the tree (Fig. 33), and *in vitro* non-vitrified leaves (Fig. 35). This histological analysis also showed that a clear differentiation between palisade and spongy parenchyma did not occur, and there are a large number of lacunae both in the adaxial and abaxial surfaces (Fig. 37A, 37B and 37C). This lack of differentiation was also found in vitrified leaves of the *Handroanthus impetiginosus* (Mart. ex DC) Mattos (Jausoro *et al*., 2010) and *Eucalyptus urophylla* (Louro *et al*., 1999). According to Jausoro *et al*. (2010), the lacunar spaces observed in vitrified leaves are formed by lysogenesis. Moreover, the relatively higher amounts of water in vitrified leaves is localized in these lacunae, contributing for the vitreous aspect and affecting gases exchanges, thus provoking hypoxia conditions that are nowadays assumed as a major cause of vitrification (Gribble *et al*., 2003; de Klerk *et al*., 2017). The midrib showed to be very underdeveloped, what could be related with the incipient development of the vascular cambium and subsequent disorganization of the vascular bundle (Fig. 37A, 37B and 37C).

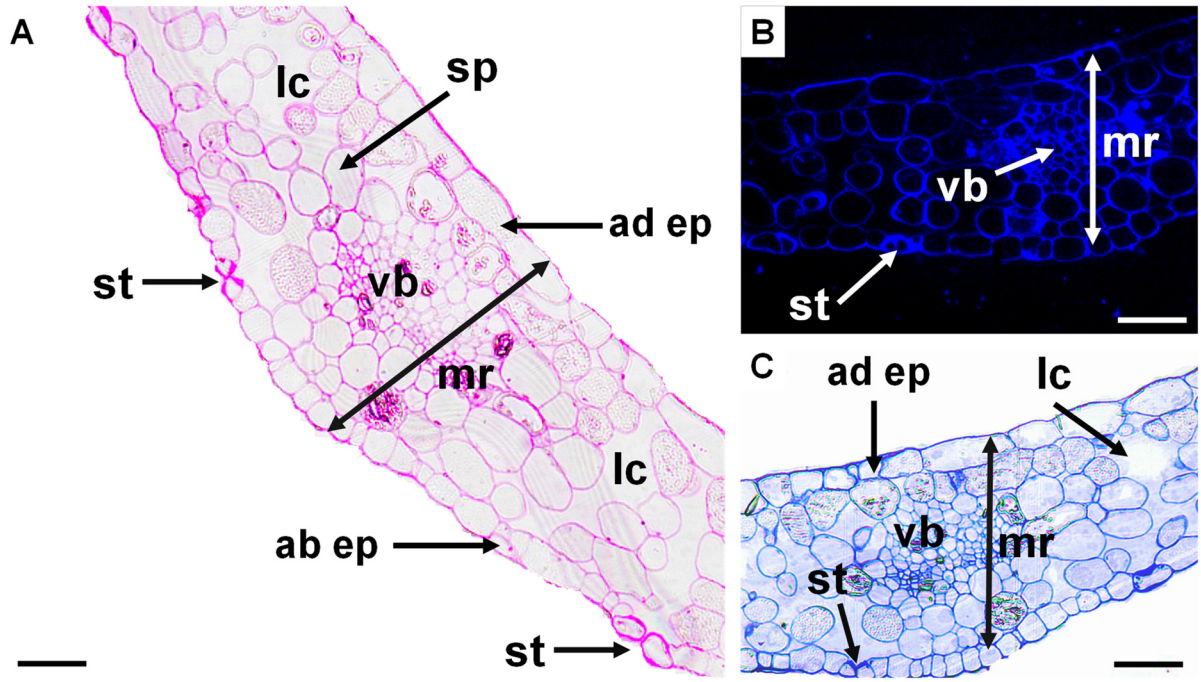

Figure 37. Light (A and C) and fluorescence (B) microscopy of *A. unedo* vitrified leaves from *in vitro* shoots cultured in liquid medium. (A) Cross section stained with ruthenium red. (B) Cross section treated with calcofluor white. (C) Cross section stained with toluidine blue. ab ep - abaxial surface epidermis, ad ep - adaxial surface epidermis, lc - lacunae, mr - midrib region, sp - spongy parenchyma, st - stomata, vb - vascular bundle. Bars = 50 µm.

SEM analysis of vitrified leaves revealed that the abaxial leaf surface displayed many stomata (Fig. 38A). However, these stomata appear to have an abnormal shape, globose, wrinkled, and much larger when compared with stomata of leaves from the greenhouse tree **(**Fig. 34C and 34D). According to Jausoro *et al*. (2010), the density of stomata of *in vitro* vitrified leaves of *H. impetiginosus* was around 20 per mm^2, comparing with normal leaves where stomata density was 14.35 per mm^2. Concerning the width of the stomata, these authors also noticed that vitrified leaves had larger stomata (17.43 μm) when compared with normal leaves (15.33 μm). In addition, other *in vitro* vitrified leaves have been showed abnormalities in guard cells morphology, as previously reported by Fontes *et al*. (1999) in *Capsicum annuum* L., and by Apóstolo and Llorente (2000) in *Simmondsia chinensis* (Link) C. K.. The hypothesis for this abnormal wrinkled shape in the stomata it has been suggested to do with loosening of elasticity due to modifications in the orientation and disposition of the cellulose microfibrils (Ziv and Chen, 2008). Moreover, according to Fontes *et al*. (1999), the enlarged size and globose-shaped stomata in vitrified leaves might be due to a greater water absorption from the liquid medium culture, that leads to turgidity of these cells. Since evapotranspiration is compromised by inefficient stomata and the saturated environment in water vapor, thus guard cells alter their conformation. SEM analysis of vitrified leaves in cross section did not gave much information since the leaves were difficult to cut due to its thin thickness (Fig. 38B). Concerning the adaxial and abaxial epidermis (Fig. 38A and 38C), they showed to be less differentiated when compared with SEM analysis of *in vitro* non-vitrified leaves (Fig. 36A and 36C) and leaves from the tree growing in a greenhouse (Fig. 34B, 34C and 34D). Regarding the glandular and non-glandular trichomes, they showed to be less present in vitrified leaves of *A. unedo* (Fig. 38C), despite Jausoro *et al*. (2010) described the inverse pattern in vitrified leaves of *H. impetiginosus*.

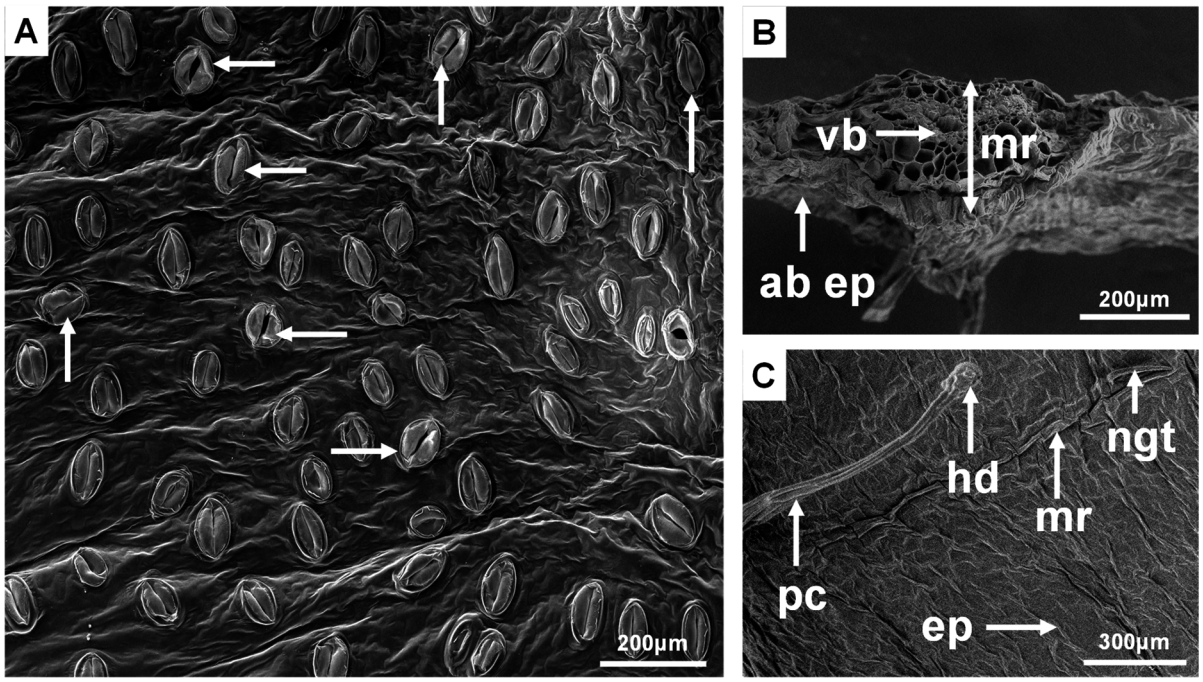

Figure 38. SEM analysis of *A. unedo* vitrified leaves from *in vitro* shoots cultured in liquid medium. (A) Leaf abaxial surface, arrows are indicating stomata. (B) Cross section at the midrib area (C) Leaf adaxial surface. ab ep - abaxial epidermis, ep - epidermis, hd - glandular head of the trichome, mr - midrib, ngt - non-glandular thricome, pc - peduncle of the glandular trichome, vb - vascular bundle.

4. Conclusions and Future Perspectives

The evergreen shrub *A. unedo*, widely distributed in Portugal and in the rest of the Mediterranean, has been revealing a potential endogenous resource and a relevant species from the pomological and ornamental point of view, nonetheless it still to be considered a Neglected and Underutilized Crop (NUC) species. The present thesis aimed to contribute to an in-depth knowledge of this species, giving rise to its values, thus being possible its economic and environmental valorization.

The assess of ripening-derived composition and chemical parameters, allied to the FTIR spectroscopy technique, revealed that most of the events occurring during fruit maturation are related with the structural and non-structural fraction of polysaccharides. To a full understanding of the cell wall remodeling in fruits of *A. unedo*, further studies are needed. For this purpose, it is suggested to analyze a larger number of samples, and apply transcriptomic studies focusing on the genes responsible for the construction of the cell wall, providing a complete comprehension of the model of maturation in *A. unedo*. In the near future, to fulfill the entire carbohydrate profile of the fruits, the samples already prepared by the TFA hydrolysis, will be submitted to HPLC-RI. In turn, the preliminary phenolic profile across the different ripening stages should be further investigated by HPLC coupled to sophisticated techniques like mass spectrometry, since phenolics are known to be involved in some ripening-derived features like the color of the fruits.

In respect to the assessment of the *A. unedo* anatomy of leaves and stems, either from *in vitro* non-vitrified and vitrified shoots, or from a strawberry-tree growing in a greenhouse, marked morphology differences were observed using different microscopy techniques, especially in vitrified tissues. However, further histochemical studies are needed, using a broader range of specific dyes for each cell wall polymer, and the application of molecular probes like monoclonal antibodies (mAbs) and carbohydrate binding molecules (CBMs). Notwithstanding, to a full understanding of the cell wall alterations between vitrified and normal tissues, the carbohydrates present in the cell wall of these tissues should be also investigated by HPLC-RI. In attempt to the surprising results of higher amounts of lignin in leaves than in stems, obtained by ABSL quantification and FTIR-ATR spectroscopy, other methods should be considered, such as the Klason procedure, in order to confirm these observations.

Finally, despite the efforts to unveil various dilemmas related to fruits maturation and the outcomes of tissue culture in liquid medium that leads to vitrification, additional work needs to be done to a full comprehension of these problems, thus contributing to the valorization of *A. unedo* as an endogenous resource.

5. References

Abidi, N., Cabrales, l. & Haigler, C. H. (2014). Changes in the cell wall and cellulose content of developing cotton fibers investigated by FTIR spectroscopy. Carbohydrate Polymers, 100, 9-16.

Adapa, P. K., Karunakaran, C., Tabil, l. G. & Schoenau, G. J. (2009). Potential applications of infrared and Raman spectromicroscopy for agricultural biomass. Agricultural Engineering International: CIGR Journal, Vol. XI.

Agarwal, U. P., Ralph, S. A., Padmakshan, D., Liu, S., & Foster, C. E. (2019). Estimation of syringyl units in wood lignins by FT-Raman spectroscopy. Journal of Agricultural and Food Chemistry, 67, 4367-4374.

Airianah, O. B., Vreeburg, R. A., & Fry, S. C. (2016). Pectic polysaccharides are attacked by hydroxyl radicals in ripening fruit: evidence from a fluorescent fingerprinting method. Annals of Botany, 117, 441-455.

Alarcão-e-Silva, M. L. C. M. M., Leitão, A. E. B., Azinheira, H. G., & Leitão, M. C. A. (2001). The *Arbutus* berry: studies on its color and chemical characteristics at two mature stages. Journal of Food Composition and Analysis, 14, 27-35.

Albuquerque, B. R., Prieto, M. A., Vazquez, J. A., Barreiro, M. F., Barros, L., & Ferreira, I. C. (2018). Recovery of bioactive compounds from *Arbutus unedo* L. fruits: Comparative optimization study of maceration/microwave/ultrasound extraction techniques. Food Research International, 109, 455-471.

Anastácio, J. R. (2014). Contributo para o estudo do medronheiro (*Arbutus unedo* L.): caracterização morfológica de clones e fisiologia pós-colheita do fruto. Master Dissertation, ISA, Lisboa.

Apóstolo, N. M., Brutti, C. B., & Llorente, B. E. (2005). Leaf anatomy of *Cynara scolymus* L. in successive micropropagation stages. In Vitro Cellular & Developmental Biology-Plant, 41, 307-313.

Apóstolo, N. M., & Llorente, B. E. (2000). Anatomy of normal and hyperhydric leaves and shoots of in vitro grown *Simmondsia chinesis* (Link) Schn. In Vitro Cellular & Developmental Biology-Plant, 36, 243-249.

Ayaz, F. A., Kucukislamoglu, M., & Reunanen, M. (2000). Sugar, non-volatile and phenolic acids composition of strawberry tree (*Arbutus unedo* L. var. *ellipsoidea*) fruits. Journal of Food Composition and Analysis, 13, 171-177.

Barnett, J. R., & Bonham, V. A. (2004). Cellulose microfibril angle in the cell wall of wood fibres. Biological Reviews, 79, 461-472.

Barros, L., Carvalho, A. M., Morais, J. S., & Ferreira, I. C. (2010). Strawberry-tree, blackthorn and rose fruits: Detailed characterization in nutrients and phytochemicals with antioxidant properties. Food Chemistry, 120, 247-254.

Blanco, E., Casado, M. A., Costa, M., Escribano, R., García, M., Génova, M., & Regato, P. (2005). Los bosques ibéricos. Una interpretación geobotánica. Planeta, 4th edn. Barcelona.

Bonawitz, N. D., & Chapple, C. (2010). The genetics of lignin biosynthesis: connecting genotype to phenotype. Annual Review of Genetics, 44, 337-363.

Botelho, G., Gomes, F., Ferreira, F. M., & Caldeira, I. (2015). Influence of maturation degree of Arbutus (*Arbutus unedo* L.) fruits in spirit composition and quality. International Journal of Biological Food, Veterinary and Agricultural Engineering, 9, 478-483.

Canhoto, J. M. (2010). Biotecnologia vegetal - da clonagem de plantas à transformação genética. Coimbra University Press, Coimbra.

Castrejón, A. D. R., Eichholz, I., Rohn, S., Kroh, L. W., & Huyskens-Keil, S. (2008). Phenolic profile and antioxidant activity of highbush blueberry (*Vaccinium corymbosum* L.) during fruit maturation and ripening. Food Chemistry, 109, 564-572.

Castroviejo, S., Aedo, C., Cirujano, S., Laínz, M., Montserrat, P., Morales, R., Muñoz Garmendia, F., Navarro, C., Paiva, J., and Soriano, C. (1993). Flora Iberica, Vol. 3 Real Jardín Botánico, CSIC, Madrid.

Cavaco, T. (2007) Caracterização química e bioquímica dos frutos de *Arbutus unedo* L. e de *Rubus fruticosus* Agg. - Contribuição para a sua valorização. Master Dissertation, Algarve University, Faro.

Celikel, G., Demirsoy, L., & Demirsoy, H. (2008). The strawberry tree (*Arbutus unedo* L.) selection in Turkey. Scientia Horticulturae, 118, 115-119.

Chawla, H. S. (2009). Introduction to plant biotechnology. Third edition. Enfield: Science Publishers.

Chea, S., Yu, D. J., Park, J., Oh, H. D., Chung, S. W., & Lee, H. J. (2019). Fruit softening correlates with enzymatic and compositional changes in fruit cell wall during ripening in 'Bluecrop'highbush blueberries. Scientia Horticulturae, 245, 163-170.

Chong, J., Soufan, O., Li, C., Caraus, I., Li, S., Bourque, G., & Xia, J. (2018). MetaboAnalyst 4.0: towards more transparent and integrative metabolomics analysis. Nucleic Acids Research, 46, 486-494.

Chylinska, M., Szymanska-Chargot, M. & Zdunek A. (2016). FT-IR and FT-Raman characterization of non-cellulosic polysaccharides fractions isolated from plant cell wall. Carbohydrate Polymers, 154, 48-54.

Coimbra, M. A., Barros, A., Rutledge, D. N. & Delgadillo, I. (1999). FTIR spectroscopy as a tool for the analysis of olive pulp cell-wall polysaccharide extracts. Carbohydrate Research, 317, 145-154.

da Costa, R. M. F., Lee, S. J., Allison, G. G., Hazen, S. P., Winters, A. & Bosch, M. (2014). Genotype, development and tissue-derived variation of cell-wall properties in the lignocellulosic energy crop *Miscanthus*. Annals of Botany, 114, 1265-1277.

da Costa, R. M. F., Allison, G. G. & Bosch, M. (2015) Cell wall biomass preparation and Fourier-transformed mid-infrared (FTIR) spectroscopy to study cell wall composition. Bio-protocol, 5, e1494, doi: 10.21769/BioProtoc.1494.

da Costa, R. M. F. (2016). Constructing a Comprehensive Picture of *Miscanthus* Cell Wall to Advance its Deconstruction. PhD Thesis, Aberystwyth University, Aberystwyth.

de Klerk, G. J., Van Den Dries, N., & Krens, F. A. (2015). Hyperhydricity: underlying mechanisms. In VI International Symposium on Production and Establishment of Micropropagated Plants, 1155, 269-276.

de Souza, A. P., Leite, D. C., Pattathil, S., Hahn, M. G., & Buckeridge, M. S. (2013). Composition and structure of sugarcane cell wall polysaccharides: implications for second-generation bioethanol production. BioEnergy Research, 6, 564-579.

Deepa, B., Abraham, E., Cordeiro, N., Mozetic, M., Mathew, A. P., Oksman, K., Faria, M., Thomas, S. & Pothan, L. A. (2015). Utilization of various lignocellulosic biomass for the production of nanocellulose: a comparative study. Cellulose, 22, 1075-1090.

Dias, V. L. A. (2014). Estruturas secretoras em Medronheiro (*Arbutus unedo* L.): caracterização morfológica, estrutural e histoquímica e avaliação da atividade proteásica da secreção. Master Dissertation, University of Coimbra, Coimbra.

Dubois, M., Gilles, K. A., Hamilton, J. K., Rebers, P. T., & Smith, F. (1956). Colorimetric method for determination of sugars and related substances. Analytical Chemistry, 28, 350-356.

Fagerstedt, K., Saranpää, P., Tapanila, T., Immanen, J., Serra, J., & Nieminen, K. (2015). Determining the composition of lignins in different tissues of silver birch. Plants, 4, 183-195.

Fonseca, D. (2014) Valuation of strawberry tree fruits (*Arbutus unedo* L.): From chemical characterization to the development of new food products. Master Dissertation, Aveiro University, Aveiro.

Fortalezas, S., Tavares, L., Pimpão, R., Tyagi, M., Pontes, V., Alves, P., & Santos, C. (2010). Antioxidant properties and neuroprotective capacity of strawberry tree fruit (*Arbutus unedo*). Nutrients, 2, 214-229.

Foster, C. E., Martin, T. M., & Pauly, M. (2010). Comprehensive compositional analysis of plant cell walls (lignocellulosic biomass) part I: lignin. JoVE, e1745. doi:10.3791/1745.

Fontes, M. A., Otoni, W. C., Carolino, S. M. B., Brommonschenkel, S. H., Fontes, E. P. B., Fári, M., & Louro, R. P. (1999). Hyperhydricity in pepper plants regenerated in vitro: involvement of BiP (binding protein) and ultrastructural aspects. Plant Cell Reports, 19, 81-87.

Fry, S. C. (2010). Cell wall polysaccharide composition and covalent crosslinking. Annual Plant Reviews Online, 1-42. doi:10.1002/9781444391015.

Fukushima, R. S., & Dehority, B. A. (2000). Feasibility of using lignin isolated from forages by solubilization in acetyl bromide as a standard for lignin analyses. Journal of Animal Science, 78, 3135-3143.

Fukushima, R. S., & Hatfield, R. D. (2004). Comparison of the acetyl bromide spectrophotometric method with other analytical lignin methods for determining lignin concentration in forage samples. Journal of Agricultural and Food Chemistry, 52, 3713-3720.

Fukushima, R. S., & Kerley, M. S. (2011). Use of lignin extracted from different plant sources as standards in the spectrophotometric acetyl bromide lignin method. Journal of Agricultural and Food Chemistry, 59, 3505-3509.

Garcia-Salas, P., Morales-Soto, A., Segura-Carretero, A., & Fernández-Gutiérrez, A. (2010). Phenolic-compound-extraction systems for fruit and vegetable samples. Molecules, 15, 8813-8826.

George, E. F., Hall, M. A., & De Klerk, G. J. (2008). The components of plant tissue culture media I: macro-and micro-nutrients. In Plant propagation by tissue culture. Springer, Dordrecht. 65-113.

Godinho-Ferreira, P., Azevedo, A., & Rego, F. (2005). Carta da tipologia florestal de Portugal Continental. Silva Lusitana, 13, 1-34.

Gomes, M. F. F. N. (2011). Strategies for the improvement of *Arbutus unedo* L. (strawberry tree): in vitro propagation, mycorrhization and diversity analysis. PhD Thesis, University of Coimbra, Coimbra.

Gomes, F., & Canhoto, J. M. (2009). Micropropagation of strawberry tree (*Arbutus unedo* L.) from adult plants. In Vitro Cellular & Developmental Biology-Plant, 45, 72-82.

Gomes, F., Simões, M., Lopes, M. L., & Canhoto, J. M. (2010). Effect of plant growth regulators and genotype on the micropropagation of adult trees of *Arbutus unedo* L. (strawberry tree). New Biotechnology, 27, 882-892.

Golubtsova, J. (2017). Study of Fruit Raw Material by Fourier Transform Infrared Spectroscopy. Journal of Pharmaceutical Journal and Research, 9, 1081-1090.

González, G. A. L. (2007). Guía de los árboles y arbustos de la Península Ibérica y Baleares: (especies silvestres y las cultivadas más comunes). 3rd edn. Mundi-Prensa Libros.

Gorzsás, A., Stenlund, H., Persson, P., Trygg, J., & Sundberg, B. (2011). Cell-specific chemotyping and multivariate imaging by combined FT-IR microspectroscopy and

orthogonal projections to latent structures (OPLS) analysis reveals the chemical landscape of secondary xylem. Plant Journal, 66, 903-914.

Gribble, K. D., Sarafis, V., & Conroy, J. P. (2003). Vitrified plants: towards an understanding of their nature. Phytomorphology, 53, 1-10.

Guerreiro, A. C., Gago, C. M., Miguel, M. G., & Antunes, M. D. (2013). The effect of temperature and film covers on the storage ability of *Arbutus unedo* L. fresh fruit. Scientia Horticulturae, 159, 96-102.

Guerriero, G., Fugelstad, J., & Bulone, V. (2010). What do we really know about cellulose biosynthesis in higher plants?. Journal of Integrative Plant Biology, 52, 161-175.

Guimarães, R., Barros, L., Dueñas, M., Carvalho, A. M., Queiroz, M. J. R., Santos-Buelga, C., & Ferreira, I. C. (2013). Characterization of phenolic compounds in wild fruits from Northeastern Portugal. Food Chemistry, 141, 3721-3730.

Harnly, J. M., Bhagwat, S., & Lin, L. Z. (2007). Profiling methods for the determination of phenolic compounds in foods and dietary supplements. Analytical and Bioanalytical Chemistry, 389, 47-61.

Harholt, J., Suttangkakul, A., & Scheller, H. V. (2010). Biosynthesis of pectin. Plant Physiology, 153, 384-395.

Harris, P. J., & Stone, B. A. (2009). Chemistry and molecular organization of plant cell walls. Biomass recalcitrance: deconstructing the plant cell wall for bioenergy, 61-93.

Heredia-Guerrero, J. A., Benítez, J. J., Domínguez, E., Bayer, I. S., Cingolani, R., Athanassiou, A., & Heredia, A. (2014). Infrared and Raman spectroscopic features of plant cuticles: a review. Frontiers in Plant Science, 5, 305, doi: 10.3389/fpls.2014.00305.

Heywood, V. H. (1993). Flowering plants of the world. Oxford University Press, Oxford

Hileman, L. C., Vasey, M. C., & Parker, V. T. (2001). Phylogeny and biogeography of the Arbutoideae (Ericaceae): implications for the Madrean-Tethyan hypothesis. Systematic Botany, 26, 131-144.

Jausoro, V., Llorente, B. E., & Apóstolo, N. M. (2010). Structural differences between hyperhydric and normal in vitro shoots of *Handroanthus impetiginosus* (Mart. ex DC) Mattos (Bignoniaceae). Plant Cell, Tissue and Organ Culture, 101, 183-191.

Jayasena, V., & Cameron, I. (2008). ° Brix/acid ratio as a predictor of consumer acceptability of Crimson Seedless table grapes. Journal of Food Quality, 31, 736-750.

Joshi, C. P., Thammannagowda, S., Fujino, T., Gou, J. Q., Avci, U., Haigler, C. H., & Harris, D. (2011). Perturbation of wood cellulose synthesis causes pleiotropic effects in transgenic aspen. Molecular Plant, 4, 331-345.

Kačuráková, M., Capek, P., Sasinková, V., Wellner, N., & Ebringerová, A. (2000). FT-IR study of plant cell wall model compounds: pectic polysaccharides and hemicelluloses. Carbohydrate Polymers, 43, 195-203.

Kevers, C., Coumans, M., Coumans-Gillès, M. F., & Caspar, T. H. (1984). Physiological and biochemical events leading to vitrification of plants cultured *in vitro*. Physiologia Plantarum, 61, 69-74.

Knox, J. P. (2008). Revealing the structural and functional diversity of plant cell walls. Current Opinion in Plant Biology, 11, 308-313.

Khoddami, A. (2013) Techniques for analysis of plant phenolic compounds. Molecules, 18, 1420-3049.

Konstantinidis, P., Tsiourlis, G., & Xofis, P. (2006). Effect of fire season, aspect and pre-fire plant size on the growth of *Arbutus unedo* L. (strawberry tree) resprouts. Forest Ecology and Management, 225, 359-367.

Kumar, M., & Turner, S. (2015). Plant cellulose synthesis: CESA proteins crossing kingdoms. Phytochemistry, 112, 91-99.

Labbé, N., Rials, T. G., Kelley, S. S., Cheng, Z. M., Kim, J. Y., & Li, Y. (2005). FT-IR imaging and pyrolysis-molecular beam mass spectrometry: new tools to investigate wood tissues. Wood Science and Technology, 39, 61-76.

Lee, K. J., Marcus, S. E., & Knox, J. P. (2011). Cell wall biology: perspectives from cell wall imaging. Molecular Plant, 4, 212-219.

Liu, Q., Luo, L., & Zheng, L. (2018). Lignins: Biosynthesis and biological functions in plants. International Journal of Molecular Sciences, 19, 335e, doi:10.3390/ijms19020335.

López, C. J., Caleja, C., Prieto, M. A., Barreiro, M. F., Barros, L., & Ferreira, I. C. (2018). Optimization and comparison of heat and ultrasound assisted extraction techniques to obtain anthocyanin compounds from *Arbutus unedo* L. fruits. Food Chemistry, 264, 81-91.

Louro, R. P., Dos Santos, A. V., & Machado, R. D. (1999). Ultrastructure of *Eucalyptus grandis*× *Eucalyptus urophylla*. I. Shoots cultivated *in vitro* in multiplication and elongation-rooting media. International Journal of Plant Sciences, 160, 217-227.

Lupoi, J. S., Singh, S., Parthasarathi, R., Simmons, B. A., & Henry, R. J. (2015). Recent innovations in analytical methods for the qualitative and quantitative assessment of lignin. Renewable and Sustainable Energy Reviews, 49, 871-906.

Malheiro, R., Sá, O., Pereira, E., Aguiar, C., Baptista, P., & Pereira, J. A. (2012). *Arbutus unedo* L. leaves as source of phytochemicals with bioactive properties. Industrial Crops and Products, *37*, 473-478.

Mandal, A., & Chakrabarty, D. (2011). Isolation of nanocellulose from waste sugarcane bagasse (SCB) and its characterization. Carbohydrate Polymers, 86, 1291-1299.

Martins, J. F. D. S. (2012). Estudos de cultura in vitro em medronheiro (*Arbutus unedo* L.) aplicados ao seu melhoramento. Master Dissertation, University of Coimbra, Coimbra

Martins, J. F., Correia, S., Correia, B., Pinto, G., & Canhoto, J. M. (2019). Shoot proliferation and organogenesis on *Arbutus unedo*: physiological analysis under water stress. Biologia Plantarum, 63, 278-286

Masuko, T., Minami, A., Iwasaki, N., Majima, T., Nishimura, S. I., & Lee, Y. C. (2005). Carbohydrate analysis by a phenol–sulfuric acid method in microplate format. Analytical Biochemistry, 339, 69-72.

McCann, M. C., Bush, M., Milioni, D., Sado, P., Stacey, N. J., Catchpole, G., & Wilson, R. H. (2001). Approaches to understanding the functional architecture of the plant cell wall. Phytochemistry, 57, 811-821.

McFarlane, H. E., Gendre, D., & Western, T. L. (2013). Seed coat ruthenium red staining assay. The Plant Cell.

Mendes, L., de Freitas, V., Baptista, P., & Carvalho, M. (2011). Comparative antihemolytic and radical scavenging activities of strawberry tree (*Arbutus unedo* L.) leaf and fruit. Food and Chemical Toxicology, 49, 2285-2291.

Miguel, M., Faleiro, M., Guerreiro, A., & Antunes, M. (2014). *Arbutus unedo* L.: chemical and biological properties. Molecules, 19, 15799-15823.

Mohnen, D. (2008). Pectin structure and biosynthesis. Current Opinion in Plant Biology, 11, 266-277.

Molina, M., Pardo-de-Santayana, M., Aceituno, L., Morales, R., & Tardío, J. (2011). Fruit production of strawberry tree (*Arbutus unedo* L.) in two Spanish forests. Forestry, 84, 419-429.

Monties, B. (1989). Lignins. In: Dey, P. M. & Harborne, J. B. (eds.) Methods in Plant Biochemistry. New York: Academic Press.

Moore, J. P., Fangel, J. U., Willats, W. G., & Vivier, M. A. (2014). Pectic-β (1, 4)-galactan, extensin and arabinogalactan–protein epitopes differentiate ripening stages in wine and table grape cell walls. Annals of Botany, 114, 1279-1294.

Moreira-Vilar, F. C., de Cássia Siqueira-Soares, R., Finger-Teixeira, A., de Oliveira, D. M., Ferro, A. P., da Rocha, G. J., & Ferrarese-Filho, O. (2014). The acetyl bromide method is faster, simpler and presents best recovery of lignin in different herbaceous tissues than Klason and thioglycolic acid methods. PloS one, 9, e110000, doi: 10.1371/journal.pone.0110000.

Moubayidin, L., Di Mambro, R., & Sabatini, S. (2009). Cytokinin–auxin crosstalk. Trends in Plant Science, 14, 557-562.

Nixon, B. T., Mansouri, K., Singh, A., Du, J., Davis, J. K., Lee, J. G., & Roberts, A. W. (2016). Comparative structural and computational analysis supports eighteen cellulose synthases in the plant cellulose synthesis complex. Scientific Reports, 6, 86-96.

Oliveira, I. (2010). Caracterização fitoquímica de folhas e frutos de *Arbutus unedo* L. Master Dissertation, ESAB, Bragança.

Oliveira, I., Baptista, P., Malheiro, R., Casal, S., Bento, A., & Pereira, J. (2011). Influence of strawberry tree (*Arbutus unedo* L.) fruit ripening stage on chemical composition and antioxidant activity. Food Research International, 44, 1401-1407.

Özcan, M. M., & Hacıseferoğulları, H. (2007). The strawberry (*Arbutus unedo* L.) fruits: chemical composition, physical properties and mineral contents. Journal of Food Engineering, 78, 1022-1028.

Park, J., Meng, J., Lim, K. H., Rojas, O. J., & Park, S. (2013). Transformation of lignocellulosic biomass during torrefaction. Journal of Analytical and Applied Pyrolysis, 100, 199-206.

Pawlowska, A. M., De Leo, M., & Braca, A. (2006). Phenolics of *Arbutus unedo* L. (Ericaceae) fruits: Identification of anthocyanins and gallic acid derivatives. Journal of Agricultural and Food Chemistry, 54, 10234-10238.

Pedro, J. (1994). Carta da distribuição de figueira e medronheiro - Notícia Explicativa. Ministério do Ambiente e Recursos Naturais, Direcção Geral do Ambiente. Lisboa.

Picoli, E. A., Otoni, W. C., Figueira, M. L., Carolino, S. M., Almeida, R. S., Silva, E. A., & Fontes, E. P. (2001). Hyperhydricity in in vitro eggplant regenerated plants: structural characteristics and involvement of BiP (Binding Protein). Plant Science, 160, 857-868.

Piotto, B., Piccini, C., & Arcadu, P. (2001). La ripresa della vegetazione dopo gli incendi nella regione mediterrânea. Propagazione per seme di alberi e arbusti della flora mediterranea. Roma: Dipartimento Prevenzione e Risanamento Ambientali, 32-38.

Prada, M. A., & Arizpe, D. (2008). Riparian Tree and Shrub Propagation Handbook: An Aid to Riverine Restoration in the Mediterranean Region. Generalitat Valenciana, 27-29.

Quevedo, L., Arnan, X., & Rodrigo, A. (2013). Selective thinning of *Arbutus unedo* coppices following fire: Effects on growth at the individual and plot level. Forest Ecology and Management, 292, 56-63.

Quoirin, M., & Lepoivre, P. H. (1977). Improved media for in vitro culture of *Prunus* sp. In Symposium on Tissue Culture for Horticultural Purposes 78 , 437- 442.

Rotondi, A., Rossi, F., Asunis, C., & Cesaraccio, C. (2003). Leaf xeromorphic adaptations of some plants of a coastal Mediterranean macchia ecosystem. Journal of Mediterranean Ecology, 4, 25-36.

Ruiz-Rodríguez, B. M., Morales, P., Fernández-Ruiz, V., Sánchez-Mata, M. C., Camara, M., Díez-Marqués, C., Pardo-de-Santayana, M., Molina, M., & Tardío, J. (2011).

Valorization of wild strawberry-tree fruits (*Arbutus unedo* L.) through nutritional assessment and natural production data. Food Research International, 44, 1244-1253.

Saeman, J. F., Moore, W. E., & Millett, M. A. (1963). Sugar units present. Hydrolysis and quantitative paper chromatography. Methods in Carbohydrate Chemistry, 3, 54-69.

Saffer, A. M. (2018). Expanding roles for pectins in plant development. Journal of Integrative Plant Biology, 60, 910-923.

Saher, S., Piqueras, A., Hellin, E., & Olmos, E. (2005). Pectin methyl esterases and pectins in normal and hyperhydric shoots of carnation cultured in vitro. Plant Physiology and Biochemistry, 43, 155-159.

Sain, M., & Panthapulakkal, S. (2006). Bioprocess preparation of wheat straw fibers and their characterization. Industrial Crops and Products, 23, 1-8.

Salem, I. B., Ouesleti, S., Mabrouk, Y., Landolsi, A., Saidi, M., & Boulilla, A. (2018). Exploring the nutraceutical potential and biological activities of *Arbutus unedo* L. (Ericaceae) fruits. Industrial Crops and Products, 122, 726-731.

Scheller, H. V., & Ulvskov, P. (2010). Hemicelluloses. Annual Review of Plant Biology, 61, 89-263.

Schulz, H., & Baranska, M. (2007). Identification and quantification of valuable plant substances by IR and Raman spectroscopy. Vibrational Spectroscopy, 43, 13-25.

Schwanninger, M., Rodrigues, J. C., Pereira, H., & Hinterstoisser, B. (2004). Effects of short-time vibratory ball milling on the shape of FT-IR spectra of wood and cellulose. Vibrational Spectroscopy, 36, 23-40.

Schweingruber, F. H., Börner, A., & Schulze, E. D. (2011). Atlas of stem anatomy in herbs, shrubs and trees (Vol. 1). Springer Science & Business Media, Berlin.

Silva, J. S. (2007). Árvores e Florestas de Portugal Vol. 7, Floresta e Sociedade - Uma história em comum.

Steele, N. M., McCann, M. C., & Roberts, K. (1997). Pectin modification in cell walls of ripening tomatoes occurs in distinct domains. Plant Physiology, 114, 373-381.

Sills, D. L., & Gossett, J. M. (2012). Using FTIR to predict saccharification from enzymatic hydrolysis of alkali-pretreated biomasses. Biotechnology and Bioengineering, 109, 353-362.

Sluiter, A. (2012). Determination of structural carbohydrates and lignin in biomass: laboratory analytical procedure (LAP): Issue Date, April 2008, Revision Date: August 2012 (Version 08-03-2012). National Renewable Energy Laboratory.

Souci, S. W., Fachmann, W., & Kraut, H. (2000). Food composition and nutrition tables (No. Ed. 6). Medpharm GmbH Scientific Publishers, Stuttgart.

Spurr, A. R. (1969). A low-viscosity epoxy resin embedding medium for electron microscopy. Journal of Ultrastructure Research, 26, 31-43.

Srivastava, V., McKee, L. S., & Bulone, V. (2017). Plant Cell Walls. In: eLS. John Wiley & Sons, Ltd, 1-17.

Sulusoglu, M., Cavusoglu, A., & Erkal, S. (2011). *Arbutus unedo* L. (Strawberry tree) selection in Turkey Samanli mountain locations. Journal of Medicinal Plants Research, 5, 3545-3551.

Sun, X., Yang, Q., Guo, W., Dai, L., & Chen, W. (2013). Modification of cell wall polysaccharide during ripening of Chinese bayberry fruit. Scientia Horticulturae, 160, 155-162.

Szymanska-Chargot, M., & Zdunek, A. (2013). Use of FT-IR spectra and PCA to the bulk characterization of cell wall residues of fruits and vegetables along a fraction process. Food Biophysics, 8, 29-42.

Szymanska-Chargot, M., Chylinska, M., Kruk, B., & Zdunek, A. (2015). Combining FT-IR spectroscopy and multivariate analysis for qualitative and quantitative analysis of the cell wall composition changes during apples development. Carbohydrate Polymers, 115, 93-103.

Sørensen, P. (1987). *Arbutus tessellata* (Ericaceae), new from Mexico. Brittonia, 39, 263-267.

Taiz L, Zeiger E, Møller I. M. & Murphy A (2015). Plant physiology and development. 6th edition, Sinauer Associates. Sunderland, Massachusetts, USA.

Takrouni, M., & Boussaid, M. (2010). Genetic diversity and population's structure in Tunisian strawberry tree (*Arbutus unedo* L.). Scientia Horticulturae, 126, 330-337.

Torres, J., Valle, F., Pinto, C., García-Fuentes, A., Salazar, C., & Cano, E. (2002). *Arbutus unedo* L. communities in southern Iberian Peninsula mountains. Plant Ecology, 160, 207-223.

Tuberoso, C., Bifulco, E., Caboni, P., Cottiglia, F., Cabras, P., & Floris, I. (2009). Floral markers of strawberry tree (*Arbutus unedo* L.) honey. Journal of Agricultural and Food Chemistry, 58, 384-389.

Ursache, R., Andersen, T. G., Marhavý, P., & Geldner, N. (2018). A protocol for combining fluorescent proteins with histological stains for diverse cell wall components. The Plant Journal, 93, 399-412.

van den Dries, N., Giannì, S., Czerednik, A., Krens, F. A., & de Klerk, G. J. M. (2013). Flooding of the apoplast is a key factor in the development of hyperhydricity. Journal of Experimental Botany, 64, 5221-5230.

Vasques, A., Vallejo, V., Santos, M., & Keizer, J. (2014). The role of cold storage and seed source in the germination of three Mediterranean shrub species with contrasting dormancy types. Annals of Forest Science, 71, 863-872.

Vicente, A. R., Ortugno, C., Rosli, H., Powell, A. L., Greve, L. C., & Labavitch, J. M. (2007). Temporal sequence of cell wall disassembly events in developing fruits. 2. Analysis of blueberry (*Vaccinium* species). Journal of Agricultural and Food Chemistry, 55, 4125-4130.

Vidrih, R., Hribar, J., Prgomet, Ž., & Poklar Ulrih, N. (2013). The physico-chemical properties of strawberry tree (*Arbutus unedo* L.) fruits. Croatian Journal of Food Science and Technology, 5, 29-33.

Wang, D., Yeats, T. H., Uluisik, S., Rose, J. K., & Seymour, G. B. (2018). Fruit softening: revisiting the role of pectin. Trends in Plant Science, 23, 302-310.

Wilson, R. H., Smith, A. C., Kačuráková, M., Saunders, P. K., Wellner, N., & Waldron, K. W. (2000). The mechanical properties and molecular dynamics of plant cell wall polysaccharides studied by Fourier-transform infrared spectroscopy. Plant Physiology, 124, 397-406.

Yadav, R. K. P., Bosabalidis, A. M., & Vokou, D. E. S. P. I. N. A. (2004). Leaf structural features of Mediterranean perennial species: plasticity and life form specificity. Journal of Biology Research, 2, 21-34.

Xu, F., Yu, J., Tesso, T., Dowell, F., & Wang, D. (2013). Qualitative and quantitative analysis of lignocellulosic biomass using infrared techniques: a mini-review. Applied Energy, 104, 801-809.

Ziv, M. (1991). Quality of micropropagated plants - vitrification. *In Vitro* Cellular & Developmental Biology-Plant, 27, 64-69.

Ziv M, Chen J (2008) The anatomy and morphology of tissue cultured plants. In: George EF, Hall MA, de Klerk G-J (eds) Plant propagation by tissue culture, 3rd edn. Springer, The Netherlands, 465–479.

Zhang, S. J., Song, X. Q., Yu, B. S., Zhang, B. C., Sun, C. Q., Knox, J. P., & Zhou, Y. H. (2012). Identification of quantitative trait loci affecting hemicellulose characteristics based on cell wall composition in a wild and cultivated rice species. Molecular Plant, 5, 162-175.

Zhao, Q. (2016). Lignification: flexibility, biosynthesis and regulation. Trends in Plant Acience, 21, 713-721.

Zhou, H., Li, G., & Zhao, X. (2016). Comparative analysis of pectate lyase in relation to softening in strawberry fruits. Canadian Journal of Plant Science, 96, 604-612.

Zobayed, S. A., Armstrong, J., & Armstrong, W. (2001). Leaf anatomy of in vitro tobacco and cauliflower plantlets as affected by different types of ventilation. Plant Science, 161, 537-548.